MICRODRILLING OF BIOCOMPATIBLE MATERIALS

A Thesis

by

SANKALP MOHANTY

Submitted to the Office of Graduate Studies of
Texas A&M University
in partial fulfillment of the requirements for the degree of

MASTER OF SCIENCE

December 2011

Major Subject: Industrial Engineering

Microdrilling of Biocompatible Materials

MICRODRILLING OF BIOCOMPATIBLE MATERIALS

A Thesis

by

SANKALP MOHANTY

Submitted to the Office of Graduate Studies of
Texas A&M University
in partial fulfillment of the requirements for the degree of

MASTER OF SCIENCE

Approved by:

Co-Chairs of Committee,	V. Jorge Leon
	Wayne N.P. Hung
Committee Member,	Amarnath Banerjee
Head of Department,	César O. Malavé

December 2011

Major Subject: Industrial Engineering

ABSTRACT

Microdrilling of Biocompatible Materials. (December 2011)

Sankalp Mohanty, B.Tech, National Institute of Technology, Tiruchirappalli, India

Co-Chairs of Advisory Committee: Dr. V. Jorge Leon
Dr. Wayne N.P. Hung

This research studies microdrilling of biocompatible materials including commercially pure titanium, 316L stainless steel, polyether ether ketone (PEEK) and aluminum 6061-T6. A microdrilling technique that uses progressive pecking and micromist coolant is developed that allows drilling of 127 μm diameter microholes with an aspect ratio of 10:1. The drilling parameters, dominant wear pattern, hole positioning accuracy and effect of AlTiN tool coating are experimentally determined. The experimental data trend agrees with classical Taylor's machining equation. Despite of fragile and long microdrills, the progressive pecking cycle and micromist allowed deep hole drilling on all the tested materials. Drill wear is more pronounced at outer cutting edge due to higher cutting speeds. However, when drilling 316L stainless steel attrition wear at chisel edge is dominant. Hole quality degradation due to formation of built up edge at the drill tip is observed. Coated drill improves tool life by 122% and enhances hole quality when drilling 316L stainless steel. The hole positioning accuracy is improved by 115% and total hole diameter variation decreased from 0.11% to 0.003% per mm of drilling distance.

DEDICATION

I would like to dedicate this work to my mother Mrs. Rajashree Mohanty, father Dr. Sibaram Mohanty and brother Mr. Ankit Mohanty for their continuous support and encouragement on every path of my life. I owe a lot to my family for the numerous sacrifices they have made to give me the best education and environment where I can learn and better myself as a human being.

ACKNOWLEDGEMENTS

I would like to thank Dr. Hung for giving me this wonderful opportunity to pursue research under his guidance. He provided an excellent learning and research environment. I am thankful for his invaluable guidance and advice throughout the course of this research. I would also like to thank Dr. Leon and Dr. Banerjee for their guidance and support throughout the course of the research.

I would like to thank Mr. Adam Farmer, Mr. Stephen Wells, Ms. Manasa Velamati, and Mr. Dominic Shioshaki at Texas A&M University for their help and cooperation for carrying out experiments.

I would like to extend my gratitude to all the sponsors i.e. PMT Corporation for providing microdrills, Swiss Tek for coating microdrills, Haas Automation Inc. for providing CNC machines and UNIST for providing micro-mist lubrication system. I am grateful to ETID department at Texas A&M University for covering my tuition and insurance thus making me financially secure.

TABLE OF CONTENTS

Page

LIST OF FIGURES

Page

Page

Page

Page

LIST OF TABLES

Page

1. INTRODUCTION

There has been a rapid increase in demand of medical devices which are used in medicine, dentistry and biotechnology. As these devices interact with biological systems the material used for manufacturing these devices must be biocompatible or biomaterials. According to a study the total market for biomaterials in United States is $9 billion USD in the year 2000 (Ratner, 2004). With the increase in emphasis on healthcare, the market for biomaterials is bound to increase in coming years. Moreover, the global market also holds a promising future for the usage of biomaterials.

Manufacturing of medical devices needs utmost precision and state of the art quality control. These devices need to pass stringent norms set forth by various agencies. Many of the medical devices like catheter tubes, needles have a functional requirement for small holes in the range of few hundred microns with high aspect ratios. Product miniaturization is becoming key aspect of modern design which demands micro manufacturing techniques. Micromachining technologies play an important role in manufacturing of these devices. Micromachining is the next generation of precision material removal at the micro-scale level. It has numerous advantageous in terms of energy saving, minimum lubrication, easier control of waste and pollution. The applications of this technology extend anywhere from electronics to microscale medical

---

This thesis follows the style of *Machining Science and Technology.*

implants. Micromilling and microdrilling have the potential to be the most cost effective and efficient material removal process due to ease of use and accessibility of the tools, which make research in the field very valuable. While of most of the work in micromachining is done in micromilling, few people have done extensive research on high aspect ratio microdrilling. Also, limited study has been done on microdrilling of difficult to drill materials like CP titanium and 316L stainless steel.

The scope of this research is limited to biomaterials namely commercially pure (CP) titanium, 316 L stainless steel, aluminum 6061-T6, and PolyEther Ether Ketone (PEEK) plastic. Microdrilling with an aspect ratio of 10:1 is performed at high rotational speeds using micromist as a coolant in all the cases. The main objectives of present research are to:

- Analyze wear pattern of microtools
- Model tool wear under different cutting conditions
- Analyze hole quality

Information about tool wear pattern for tested materials can be found in sections 4.2 to 4.5; tool wear model is described in section 4.6, and hole quality is discussed in section 4.7. The subsequent sections discuss about literature review of microdrilling and properties of biocompatible materials, experimental set up and design, results and discussions followed by conclusions and recommendations.

2. LITERATURE REVIEW

2.1 Materials for biomedical applications

Biomaterial is defined as a nonviable material used in a medical device, intended to interact with biological systems (Williams, 1987). Biomaterials can include metals, polymers, glasses, carbons, and composite materials. It is generally integrated with a medical device or used as an implant. It is extensively used in biotechnology, dentistry, and medicine. It encompasses different fields of science like medicine, biology, chemistry and material science. Until recently its application was limited due to biocompatibility issues but with technological advancement and better knowledge of human body, it is now used successfully for making implants and medical devices. There is a huge demand for biocompatible materials due to increase in healthcare spending. TABLE 1 highlights the market figures for biomaterials and healthcare.

The application of biomaterials in human body dates back to early civilizations. Though there was a little knowledge of material science, biology and medicine but still the success of these implants shows the drive to address the need to replace vital body parts with an implant. Similarly linen sutures were used by early Egyptians, catguts were used in middle ages in Europe and metallic sutures were mentioned in Greek literature (Ratner, 2004).

TABLE 1 The Biomaterials and Healthcare Market - Facts and Figures (per year) (U.S numbers- Global numbers are typically 2-3 times the U.S numbers) (Ratner, 2004)

Total U.S. health care expenditures (2000)	$1,400,000,000,000
Total U.S. health research and development (2001)	$82,000,000,000
Number of employees in the medical device industry (2003)	300,000
Registered U.S. medical device manufacturers (2003)	13,000
Total U.S. medical device market (2002)	$77,000,000,000
U.S. market for disposable medical supplies (2003)	$48,600,000,000
U.S. market for biomaterials (2000)	$9,000,000,000
Individual medical device sales:	
Diabetes management products (1999)	$4,000,000,000
Cardiovascular Devices (2002)	$6,000,000,000
Orthopedic-Musculoskeletal Surgery U.S. market (1998)	$4,700,000,000
Wound care U.S. market (1998)	$3,700,000,000
In Vitro diagnostics (1998)	$10,000,000,000
Numbers of devices (U.S.):	
Intraocular lenses (2003)	2,500,000
Contact lenses (2000)	30,000,000
Vascular grafts	300,000
Heart valves	100,000
Pacemakers	400,000
Blood bags	40,000,000
Breast prostheses	250,000
Catheters	200,000,000
Heart-Lung (Oxygenators)	300,000
Coronary stents	1,500,000
Renal dialysis (number of patients, 2001)	320,000
Hip prostheses (2002)	250,000
Knee prostheses (2002)	250,000
Dental implants (2000)	910,000

Due to its sensitive application a biomaterial must possess certain properties. A biomaterial should not be toxic unless and otherwise it is intended (e.g. smart drug delivery system that kills cancer cells) (Ratner, 2004).

Biocompatibility is defined as ability of a material to perform with an appropriate host response in a specific application (Williams, 1987). The implant material should be inert to inflammatory reactions which can vary in intensity and duration. The mechanical

properties of implant materials vary according to their application; for example a hip prosthesis must be strong and rigid where as a tendon implant must be strong and flexible (Ratner, 2004). Medical devices are designed and manufactured under strict quality control norms.

TABLE 2 Some Applications of Synthetic Materials and Modified Natural Materials in Medicine (Ratner, 2004)

Application	Types of materials
Skeletal system	
Joint replacements (hip, knee)	Titanium, Ti–Al–V alloy, stainless steel, polyethylene
Bone plate for fracture fixation	Stainless steel, cobalt–chromium alloy
Bone cement	Poly(methyl methacrylate)
Bony defect repair	Hydroxylapatite
Artificial tendon and ligament	Teflon, Dacron
Dental implant for tooth fixation	Titanium, Ti–Al–V alloy, stainless steel, polyethylene
	Titanium, alumina, calcium phosphate
Cardiovascular system	
Blood vessel prosthesis	Dacron, Teflon, polyurethane
Heart valve	Reprocessed tissue, stainless steel, carbon
Catheter	Silicone rubber, Teflon, polyurethane
Organs	
Artificial heart	Polyurethane
Skin repair template	Silicone–collagen composite
Artificial kidney (hemodialyzer)	Cellulose, polyacrylonitrile
Heart–lung machine	Silicone rubber
Senses	
Cochlear replacement	Platinum electrodes
Intraocular lens	Poly(methyl methacrylate), silicone rubber, hydrogel
Contact lens	Silicone-acrylate, hydrogel
Corneal bandage	Collagen, hydrogel

These norms and regulations are set by Food and Drug Administration (FDA) in USA and similar bodies worldwide. The biomaterials must comply with these regulations before they can be used for making implants. Application of some of the materials in medicine is listed in TABLE 2.

2.1.1 Titanium alloys

Commercially available pure titanium and Ti-6Al-4V are the most common type of titanium used for medical implants. Mechanical and physical properties of CP titanium grade 2 are given in TABLE 3 and TABLE 4.The Ti alloy Ti-6Al-4V is an alpha-beta alloy of titanium and its microstructure is dependent on the type of heat treatment cycle and mechanical working. The material composition of CP titanium grade 2 for implants is given in TABLE 5.

It has excellent biocompatibility because of its high corrosion resistance and inert nature. It can be used in direct contact with tissue or bone. Ti alloy machining usually encounters the problems of high tool wear rate, high machining cost, and low productivity. There is a crucial need for cost-effective machining processes applicable to Ti alloy. It has a poor surface wear characteristic and hence cannot be used in direct contact with another metal. It has lower density compared to iron, low modulus and very stable oxide layer. It has better corrosion resistance compared to stainless steel and cobalt when contact with body fluid. It is used in widely in biomedical implants and aerospace industry. Some of the applications in medical implant are joint replacement

arthroplasty, femoral hip stem, fracture fixation plate, spinal component, orthopedic implants, and pacemaker case. However, Ti alloys have poor machinability due to several reasons. One of the reasons is poor thermal conductivity of Ti alloy which leads to high temperature of the cutting edge (approximately 1000°C). At this high temperature the tools wear is accelerated.

TABLE 3 Mechanical Properties of Commercially Pure Titanium Grade 2 (ASTM B348-11, 2011)

Mechanical Properties	**Min.**
Tensile Strength, MPa	345
Yield Strength, MPa	275
Elongation, %	20
Reduction in area, %	30

TABLE 4 Physical Properties of Commercially Pure Titanium Grade 2 (Boyer et al., 1994)

Density	4.51 g/cc
Specific Heat Capacity	0.54 J/g-°C
Thermal Conductivity	16.3 W/m-K
Melting Point	1662-1692 °C

TABLE 5 Material Composition of Commercially Pure Titanium Grade 2 (ASTM B348-11, 2011)

Elements	**Percentage composition max.**
Carbon	0.08
Oxygen	0.25
Nitrogen	0.03
Hydrogen	0.015
Iron	0.3

The second reason is its strong affinity to many tool materials (especially at high temperatures) (Dornfeld et al., 1999). This will also cause rapid tool wear. Furthermore,

because Ti alloy can retain its hardness and strength at high temperatures, the force and stress on the cutting edge will be higher (Thornes, 2001). This can potentially cause some tools to fail.

2.1.2 Stainless steels

Stainless steel is chemically inert to many products, easy to clean and sanitize to eliminate bacteria and residues. It can be machined, formed and welded. Due to its inert nature and ease of manufacturability it is widely used in making medical devices and implants. Based on medical application stainless steel can be divided into commercial grade and implantable grade. Commercial grade is used for non-implant devices subjected to transient body fluid contact, e.g. scissors, trays, forceps, scalpels. Implantable grade is suitable for long term contact with the body tissue and fluids and hence have high corrosion resistance. Impurity refining is done using vacuum melting and electro-slag process.

Stainless steel can also be classified by their crystalline structure as martensitic, ferritic austenitic, duplex and precipitation hardenable. Martensitic stainless steel has body centered tetragonal structure. It is ferromagnetic, heat-treatable and has high hardness. Ferritic stainless steel has body centered cubic structure. It is softer compared to martensitic steel. Austenitic stainless steel is non-heat treatable, non-magnetic, and can maintain high strength at cryogenic as well as at high temperature. It has excellent corrosion resistance property. Duplex contains 2 phase alloys e.g. ferrite and austenite. It

has improved mechanical strength, superior stress corrosion resistance and pitting resistance. Precipitation hardenable alloys can be adjusted for ductility and hardness.

Stainless steel 316L has a wide variety of application in industry and has unique material properties. Another version of the 316 stainless steel is 316L having less carbon content. The composition and mechanical properties of stainless steel 316L are shown in TABLE 6 and TABLE 7 respectively. It is an austenitic stainless steel with iron, chromium, nickel, molybdenum and manganese. The main purpose of addition of chromium is to form a surface oxide layer which is resistant to corrosion. The disadvantage of adding Cr is that it stabilizes the ferritic phase of iron and steel which is weaker compared to austenitic phase. Moreover, molybdenum and silicon are also ferritic stabilizers and hence nickel is added to stabilize stronger austenitic phase. Low carbon content in 316L helps in improving corrosion resistance by diminishing the formation of carbides in the grain boundaries which ultimately hamper the formation of protective oxide formation (Ratner, 2004).

Some of the typical application of stainless steel in medical implants and devices are bone screws, bone plate for fracture fixation, joint replacement (knee, hip), forceps, scissors, needles, braces, scalpels etc.

TABLE 6 Physical Properties of 316L Stainless Steel (Azom, 2009)

Grade	Density (kg/m^3)	Elastic Modulus (GPa)	Mean coefficient of Thermal Expansion (µm/m/°C)			Thermal Conductivity (W/m.K)	
			0-100 °C	0-315°C	0-538°C	At 100°C	At 500°C
316L	8,000	193	15.9	16.2	17.5	16.3	21.5

TABLE 7 Grade Specification Comparison of 316L Stainless Steel (Azom, 2009)

Grade	UNS No	Old British		Euronorm		Swedish SS	Japanese JIS
		BS	En	No.	Name		
316L	S31603	316S11		1.4404	X2CrNiMo17-12-2	2348	SUS316L

2.1.3 Aluminum alloy

Aluminum is one of the most abundant metals on earth and has wide application in engineering field. There are two types of aluminum alloys namely wrought alloy and cast alloys. The properties that make aluminum favorable for many applications are light weight, appearance, mechanical properties, physical properties and corrosion resistance. Aluminum has a density of only 2.7 g/cm^3, approximately one-third as much as steel (7.83 g/cm^3). It has excellent corrosion resistance in most environments, including atmosphere, water (including salt water), petrochemicals, and many chemical systems. There are different families of wrought alloys of aluminum depending on the type of alloying element starting from 1xxx to 9xxx.

Aluminum 6061 is the most widely used alloy in 6000 series. It is a precipitation hardening alloy containing magnesium and silicon as its major alloying elements. The mechanical and physical properties of aluminum 6061 are listed in TABLE 8 and TABLE 9 respectively. It exhibits excellent formability and good weldability. It is available in pre-tempered grades such as, 6061-O (solutionized), 6061-T6 (solutionized and artificially aged), 6061-T651 (solutionized, stress-relieved stretched and artificially aged).

TABLE 8 Typical Mechanical Properties of Alloy 6061 (ASM Handbook Volume 1: Properties and Selection: Irons, Steels, and High-Performance Alloys, 1990)

Temper	Tensile strength MPa	Tensile strength ksi	Yield strength MPa	Yield strength ksi	Elongation, % 1.6 mm (1/16 in.) thick specimen	Elongation, % 13 mm (1/2 in.) diam specimen	Shear strength MPa	Shear strength ksi
Bare 6061								
O	124	18	55	8	25	30	83	12
T4, T451	241	35	145	21	22	25	165	24
T6, T651	310	45	276	40	12	17	207	30
Alclad 6061								
O	117	17	48	7	25	...	76	11
T4, T451	228	33	131	19	22	...	152	22
T6, T651	290	42	255	37	12	...	186	27

TABLE 9 Physical Properties of Alloy 6061 (ASM Handbook Volume 1: Properties and Selection: Irons, Steels, and High-Performance Alloys, 1990)

Density	2.7 g/cc
Specific Heat Capacity	0.896 J/g-°C
Thermal Conductivity	167 W/m-K
Melting Point	582-652 °C
Solidus	582 °C
Liquidus	652 °C

However, aluminum is not used as an implant material as it is not biocompatible but it has a wide application in manufacturing of medical equipment. It is used for making trays, crutches, hospital beds, wheel chairs and other medical devices.

2.1.4 Polymers

Many types of polymers are widely used in medical implants including orthopedic, cardiovascular, dental and soft tissue. They represent the largest class of biomaterials. They can be derived from natural sources or synthetic processes. Both natural and synthetic polymers are long chain molecules that consist of a large number of small repeating units. They can be classified on the basis of their structure as thermoplastic, thermoset and elastomer. Thermoplastic is a linear or branched polymer widely used in medical field. Thermoset is a cross-linked polymer which is rigid and cannot be recycled. Elastomers are highly elastic. Thermoplastic, thermoset and elastomers are widely used to make medical devices. Some of the applications of polymers include artificial teeth, membrane for dialysis, contact lenses, and drug delivery systems. Biodegradable polymers are used in making implants. Body cellular fluids, lipids and protein interact with polymers. These implants need not be removed surgically and can be used as temporary implants. Some of the examples include polylactide, lactide copolymers, biodegradable stitches. The applications of biodegradable polymers include vascular graft prostheses, heart patch, and non-absorbable sutures.

PolyEther Ether Ketone (PEEK) is one of the most mechanically robust and high temperature thermoplastics. Mechanical and physical properties of PEEK are given in TABLE 10 and TABLE 11 respectively. It is resistant to solvent, radiation, bases and to some acids. It exhibits high strength and toughness over a wide range of temperatures. It has excellent friction and wear properties.

TABLE 10 Mechanical Properties of PEEK, standard viscosity grade for injection molding (Platt, 2003)

Ultimate Tensile Strength	100 MPa
Yield Strength	89.6 MPa
Shear Strength	52.4 MPa
Compressive Strength	118 MPa
Ductility	50% elongation at break
Flexural Strength	170 MPa
Hardness	126 Rockwell R
Poisson's Ratio	0.39

TABLE 11 Physical Properties of PEEK, standard viscosity grade for injection molding (Platt, 2003)

Density	1320 kg/m^3
Specific Heat Capacity	1700 J/kg-K
Thermal Conductivity	0.2 W/m-K
Melting Point	343 °C

2.2 Microdrilling

2.2.1 Definition

Microdrilling of hole diameter less than 0.5 mm with aspect ratio larger than 10 is becoming increasingly popular (Lin et al., 1995). FIGURE 1 shows size comparison of microdrill of diameter 0.050 mm with an ant's leg. It is a challenging task to produce good quality hole consistently without damaging the parent material. Microhole drilling is becoming increasingly more important due to its application in various industries like medical engineering (FIGURE 2), aeronautics, electronics, optics, and automotive.

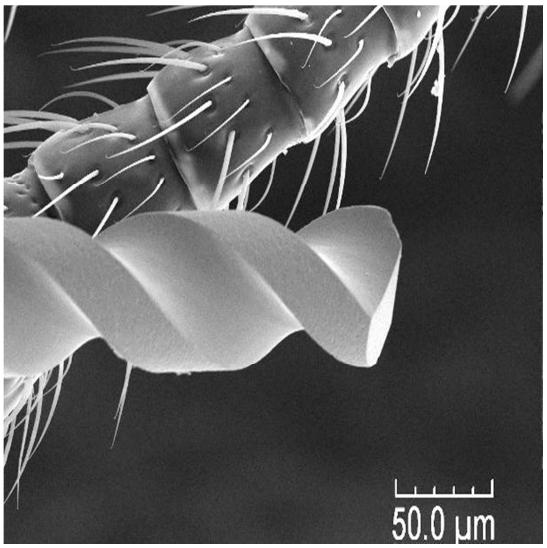

FIGURE 1 Microdrill of diameter 0.050 mm compared to an ant's leg.

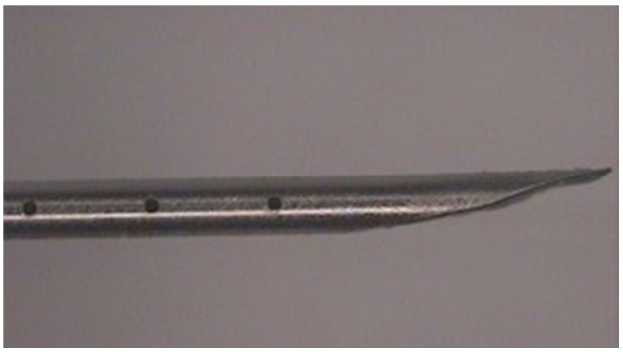

FIGURE 2 160μm hole in stainless steel needle (after POTOMAC, 2011).

2.2.2 Overview of microdrilling technologies

Manufacturing processes to produce micro-holes include electro discharged machining (EDM), energy beam (laser, electron), chemical etching, and lithography. Previous attempts have been made to drill small holes using EDM. This could cause subsurface damages and give a rough surface finish due to repeated sparks. Also, the electrode gets consumed with time which affects both the form and dimension of the part. Laser drilling is another technology used in microdrilling applications. It is a complex and expensive process in which the laser thermally interacts with the material that causes change in material property in the heat affected zone. Electron beam drilling is also used to drill miniature holes where a highly concentrated electron beam is focused on the workpiece in high vacuum. Upon impact, the release of kinetic energy of the electrons causes thermal damage and vaporizes the workpiece. There is need for a process which is cost effective and can address these problems. Etching is also used for micro-hole fabrication in which many chemical solutions including acids and bases are used to remove layers from the workpiece surface. Depth of hole can be controlled by etching

time and etching rate. The major drawback associated with etching is undercut of cavity that produces sloping walls. Lithography is capable of producing micro features and is commonly used for fabricating MEMS devices. Photolithography transfers patterns and shapes on the substrate by optical and chemical means. Electron beam lithography uses concentrated electron beam to form shapes and patterns on the substrate by selectively exposing it. Both processes are expensive and involve complex steps.

Although, micro EDM and laser microdrilling can compete against traditional micro-hole drilling, there are concerns about surface integrity, hole quality, aspect ratio, product contamination and cost. Thus when micro holes are required, the traditional microdrilling has the potential to achieve superior roundness, smoother surfaces, and better lead times (Allen et al., 2000). Although the technology is promising, there is lack of information on traditional microdrilling of biomaterials.

2.2.3 Challenges in traditional microdrilling

Drilling is a complex material removal process whose performance depends on many interacting factors. Drilling is more challenging than turning and milling because of the complexity involved in removing chips from the hole. Microdrilling poses a greater challenge than macrodrilling in many aspects:

- Microdrills are subjected to severe skidding motion during initial penetration into the workpiece. A very small radial force during skidding can lead to fracture of the tool in the first hole itself (Imran et al., 2008)

- Heat dissipation in microdrilling especially while drilling holes with high aspect ratio is a major concern. High temperature may arise due to inefficient supply of coolant and can eventually break the tool. Most of the research presently discusses microdrilling with an aspect ratio of 5:1 and below. Deep hole drilling with aspect ratio of 10:1 or more demand special cooling techniques (Imran et al., 2008).
- Chip removal is another major concern in deep hole microdrilling. The inability of the cutting fluid to reach cutting zone and remove chips effectively can lead to tool breakage.
- Entry burr formation in microdrilling severely affects the hole quality.
- Although there are similarities between macro and micromachining but the cutting parameters of macro machining, like cutting speed, feed and depth of cut, cannot be offhand downscaled into the micro range due to size effects. Presently there is a lack of literature for selecting these cutting parameters for a given material.
- Microdrills can fracture even with by a small impact as they are very weak in bending due to their slender shape. Handling these tools to carry out various experiments also poses difficulty.
- Work hardening of certain materials like austenitic stainless steel makes microdrilling even more challenging. Rubbing of tool against work hardened zone leads to rapid tool wear.

2.2.4 Microdrill life and failure modes

Usually the microdrill life is very short. In most of the practical condition the life of microdrills is randomly distributed from 1- 100 holes (Tansel, 1998). Typically the drills fail due to gradual wear of cutting edge or too high cutting temperature. However, majority of the failure is due to excessive cutting force at the tip of the tool causing it to fail suddenly by brittle fracture (Ueng et al., 2006). This kind of failure is unpredictable and difficult to observe with unaided eye. Even a slight damage may lead to total breakage of the tool in a few seconds. Secondly, monitoring microdrilling operation is more difficult than monitoring macro-scale conventional operations. The cutting forces in microdrilling are very small and hence to identify the signals of cutting forces and torque is quite difficult due to poor signal to noise ratio. Also there is no simple correlation between tool wear and cutting forces (Ueng et al., 2006).

Kudla (2011) studied the behavior of microdrills in bending, compression and torsion under static condition. Torsion is applied along with compression and the values of deflections, forces, and torques are measured. The formation of micro cracks and their propagation is observed.

During drilling the tool is exposed to the action of torque M (torsion moment), thrust F (axial feed force) and radial force R (FIGURE 3). The microdrill with diameter d is rotating at n rpm. Torque M generates shear stress in the drill, thrust F causes compression and buckling and radial force R causes bending of microdrill. The friction force f is generated from the chips clogged in the flute.

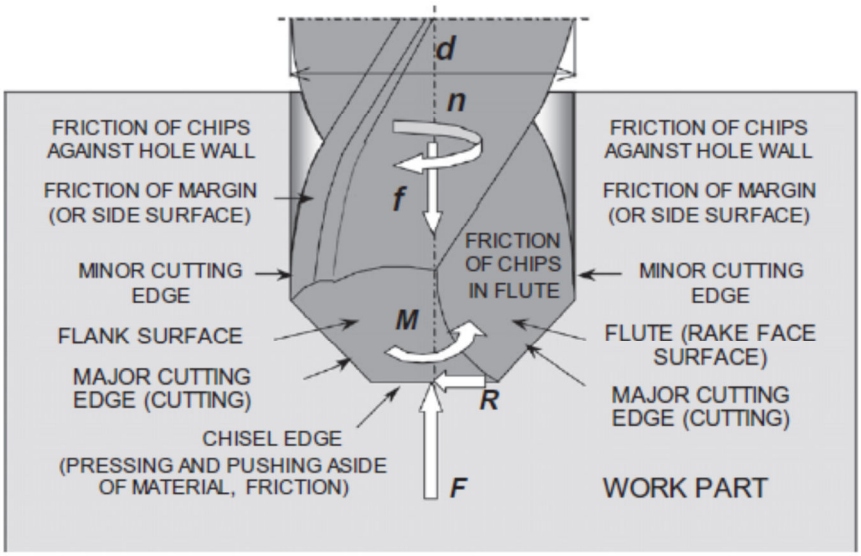

FIGURE 3 Motions, basic phenomena and resulting cutting forces in drilling process (after Kudla, 2011).

The entry of the drill tip plays a very important role. The surface irregularities on the work part cause the drill tip to be pushed aside and change of its axial position (FIGURE 4). Excessive stress from cutting forces is one of the main reasons for drill failure.

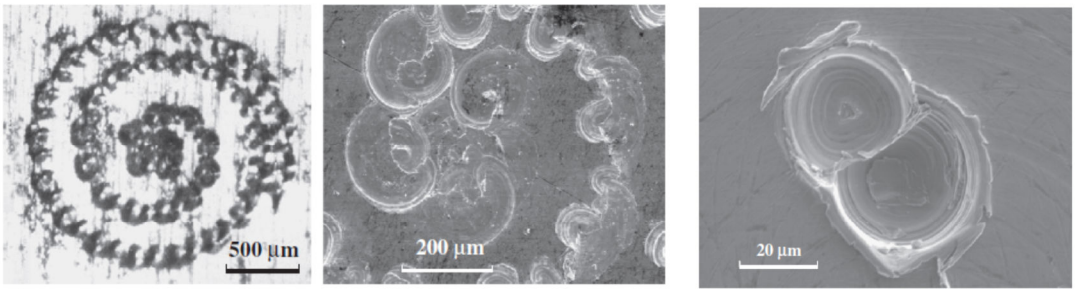

(a) (b)

FIGURE 4 a) Spiral marks made by twist drills on plain carbon steel b) Double start drill spot in stainless steel specimen (after Kudla, 2011).

Some of the important observations from the experiment are:

- In steel microdrills the breakage followed elastic and then plastic deformation of the cutting part whereas sintered carbide microdrills showed only elastic strains and brittle fracture sections.
- The first crack took place on the drill periphery due to maximum stress value.
- Under dynamic condition start of the drilling is very important to minimize drill tip wandering and reduce radial force.
- Under dynamic condition drill breakage is a sudden and complex phenomenon.

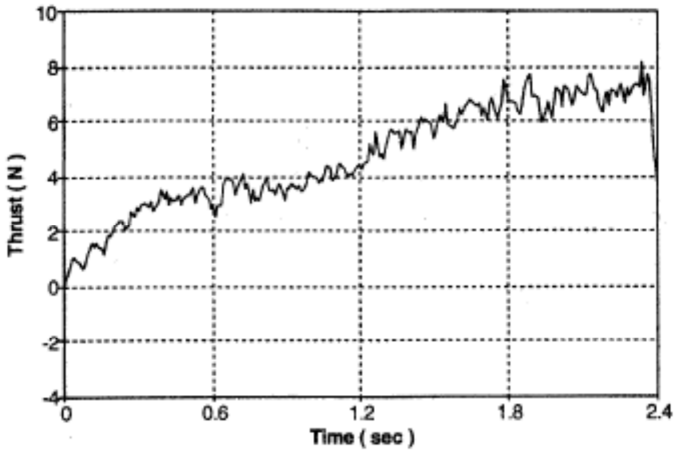

(a) Thrust variation

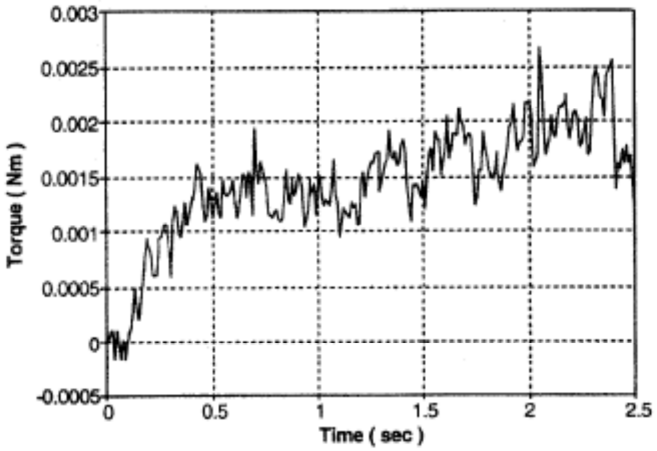

(b) Torque variation

FIGURE 5 Cutting force variation as drill depth increases continuously. Frequency: 750 Hz, feed rate: 0.32 mm/s, diameter: 0.5 mm (after Cheong et al., 1999).

Cheong et al. (1999) proposed a method to regulate the cutting force to achieve continuous drilling instead of peck drilling in microdrilling applications. They also discussed two important problems given as under:

- Force increasing: For drilling holes which have high aspect ratio, the cutting forces increase with the drill depth (FIGURE 5).

- It can be seen that as the drill depth increases (a function of drill time) both thrust and torque increase. This is due to the chip produced during drilling which increases the friction between the tool and the job leading to wear.
- Drill wandering: The wandering motion of the drill is more likely to take place during the inlet stage of drilling. Torque and thrust variation during initial wandering motion is shown in the FIGURE 6. It can be seen that torque has a much higher degree of variation than thrust. The paper also discusses the four boundary conditions for drilling which is shown in FIGURE 7. Wandering motion is most likely to occur in for the boundary condition shown in FIGURE 7(b) where lateral motion is possible as drill bit motion is not stabilized. When the drill feed velocity is large or the drill is drilling through the workpiece, the boundary condition changes to FIGURE 7(c). After the drill has completely penetrated into the workpiece the condition changes to FIGURE 7(d).It is found that in order to minimize the effect of wandering motion it is desirable to change the boundary condition. This can be achieved by lower initial drill rotation speed to feed rate ratio compared to later stages of penetration.

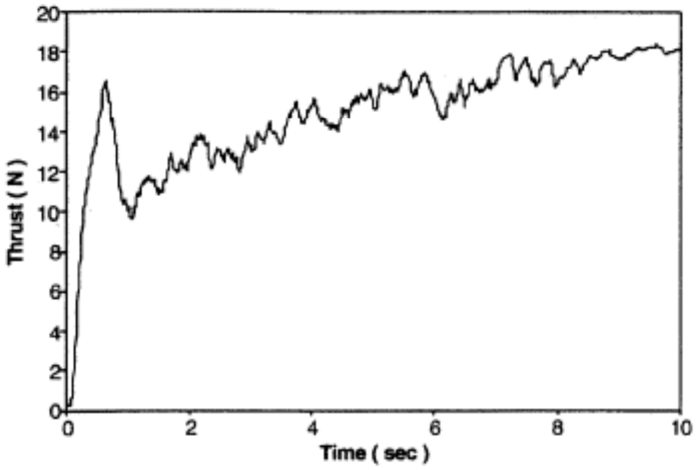

(a) Thrust

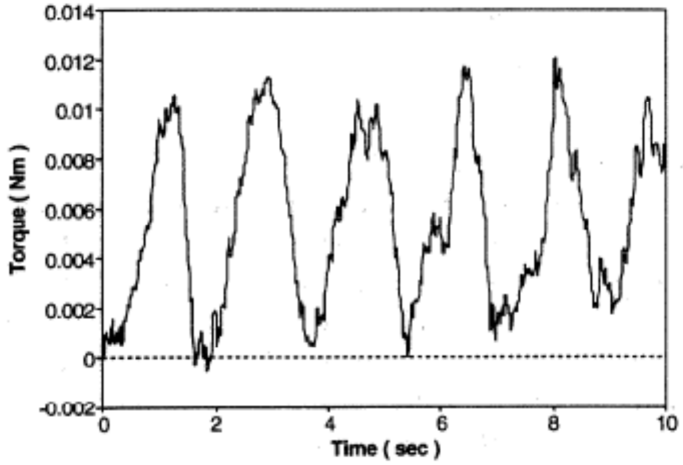

(b) Torque

FIGURE 6 Cutting force variation during wandering motion. Frequency: 750 Hz, feed rate: 0.18 mm/s, diameter: 0.9 mm (after Cheong et al., 1999).

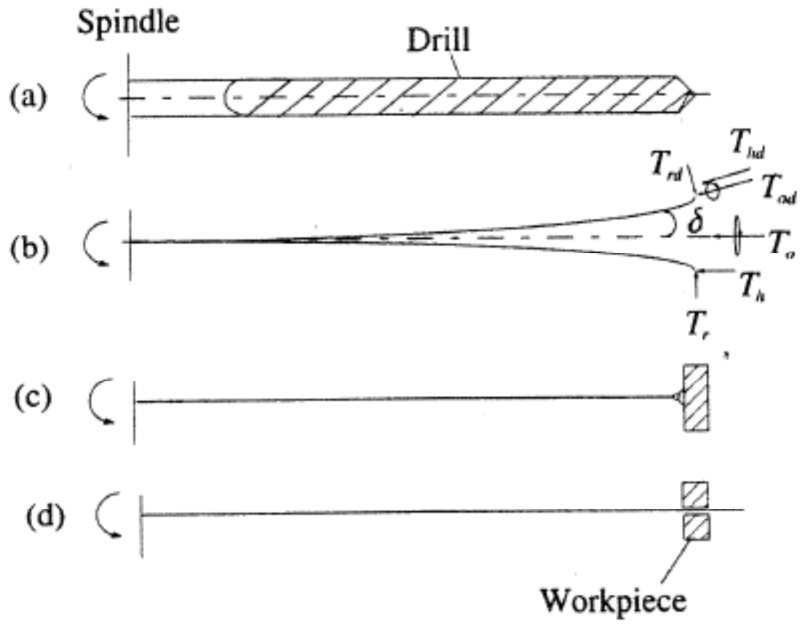

FIGURE 7 Drill wandering motion and variation of boundary conditions: (a) Drill clamped in the spindle, (b) end point free, (c) end point pin joint, (d) end point fixed (after Cheong et al., 1999).

Classical Taylor's equation gives a good approximation of tool life. It uses cutting speed, feed rate, and depth of cut to predict tool life. Tool life can be predicted under different cutting conditions for a single tool using the same equation. If a tool is used at an initial condition and then altered, tool life can still be predicted by taking all the cutting conditions into consideration. Hung and Zhong (1996) proposed cumulative wear models to predict tool life progressively as the tool is used under different cutting conditions. Equations (1) and (2) represent the cumulative tool wear models.

$$T_c = \sum_{j=1}^{k} \Delta t_j \tag{1}$$

$$V_c^{1/n} = \frac{\sum_{j=1}^{k} \Delta t_j V_{cj}^{1/n}}{Q \sum_{j=1}^{k} \Delta t_j} \tag{2}$$

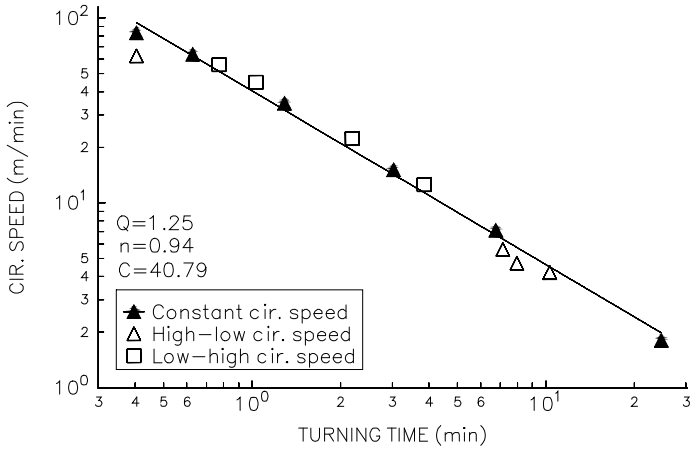

FIGURE 8 Cumulative wear model with transition from high to low speed and low to high speed (after Hung, 1996).

where T_c and V_c represent the cumulative tool life and the cumulative average of the cutting speeds for the tool life, respectively; k is the number of machining experiments done using the tool, Δt_j is the time at each experiment, Q is the cumulative wear on the tool in micrometers, n is the constant based on tool wear rate, and V_{cj} is the cutting speed of the tool at each experiment.

The order of experiments was negligible as predicted in Equation (2). High speeds could be used first with rapid wear then switched to low speeds or low speeds first with lower

wear rates, the models still held consistent and accurate in determining the tool wear (Hung and Zhong, 1996). FIGURE 8 shows data plots of the cumulative wear model.

2.2.3 Machine tool and requirement

Microdrilling requires precision equipment for consistent quality of holes. (Iwata et al., 1981) used both vertical and horizontal drilling machine for conducting experiments (TABLE 12).

TABLE 12 Machine Specifications for Microdrilling (Iwata et al., 1981)

Nomenclature	Spindle 1	Spindle 2
Maximum spindle speed, rpm	180,000	50,000
Radial error load free condition, µm	< 1	
Feed rate, mm/min	30-800	
Feed per step	10 µm - 99.99 mm	

Chern and Lee (2005) studied the effect of vibration on drilling quality of aluminum alloy and steel alloy. They used machining center MC-1050P, Mitsubishi-520AM controller with spindle speed range of 45 rpm to 6000 rpm for carrying out microdrilling. Laser displacement meter (Keyence LC-2430) was used to measure the vibration amplitude of the workpiece. Toolmakers' microscope (Olympus-STM) was used for measuring the hole diameter and tool wear measurement. It had a maximum magnification of 600 times. Klocke et al., (2009) conducted microdrilling experiments without cooling on the ultra-precision CNC Machining center KERN Evolution. It had a

position accuracy of ± 0.5 μm, maximum spindle speed of 160,000 rpm. It also featured non-contact measurement of the microdrills with a laser beam.

Imran et al. (2008) conducted microdrilling tests using a Mikron HSM 400 high speed machining center. The tests were carried out using HOCUT 3830 water based coolant. The tool edge radius was measured using scanning electron microscopy (SEM) and BSE microscopy studies were carried out on Hitachi 3400 scanning electron microscope.

2.2.5 Process parameters and case studies

The cutting parameters of conventional machining, like cutting speed, feed and depth of cut, cannot be offhand downscaled into the micro range. When the uncut chip thickness is on the same order as the material grain size, the workpiece material cannot any more be assumed as homogeneous and isotropic. Furthermore, the tool edge radius significantly influences the cutting mechanism in micro machining with regard to the effective rake angle and the ploughing effect (Dornfeld et al., 1999).

In a study the relation between drill geometry parameters, cutting conditions and tool wear shows that an increase in feed increases both thrust force and torque but an increase in spindle speed only increases thrust force and decreases torque (Chen and Ehmann, 1994). Also the effect of point angle on the thrust force is much more significant than the torque.

Klocke et al. (2009) investigated the size effects by down scaling the twist drill process into the micro range (Ø 50-1000 µm). The drill used in this study is made up of ultra-fine grained carbide with point angle 118°, front clearance angle 10°, and helix angle 35°. Experimental microdrilling tests are conducted on steel AISI 1045 (normalized and full-annealed) under different cutting conditions (drill diameter, feed, cutting speed) and compared with data obtained from conventional drilling. Due to different mechanical loading capacities of the drills and to ensure the comparability of the micro and conventional drilling results, the feed is selected as 0.012 times drill diameter and the drilling depth amounted to 2 times drill diameter for all drilling tests.

An increase in the cutting speed decreases the feed force until it reaches a minimum value after which the feed force again starts to increase (FIGURE 9). At higher cutting speeds the temperature between the tool and metal interface starts to increase causing thermal softening. However, at very high speeds there is a formation of built up edge contrary to the conventional machining.

Hoshi et al. (1981) studied high speed micro deep drilling in two types of drilling machine i.e. horizontal drilling and vertical drilling. In horizontal drilling relative rotary motion is applied to both workpiece and the drill. Three types of drills are used in their study, details of which are given in TABLE 13. Also the cutting conditions are listed in TABLE 14 for all the drills.

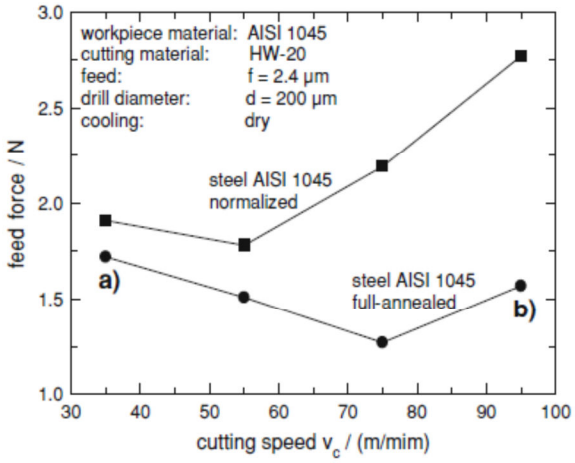

FIGURE 9 Effect of cutting speed on feed force in steel AISI 4015 (after Klocke et al., 2009).

TABLE 13 Dimension of Twist Drills (Hoshi et al., 1981)

Nomenclature	#1 drill	#2 drill	#3 drill
Material	Carbide	Carbide	HSS
Drill diameter, mm	0.45	0.35	0.1
Drill length, mm	5.0	4.0	0.7
Helix angle, deg	30	30	20
Point angle, deg	120	120	11.8
Diameter of shank, mm	3.175	3.175	1.0
Overall length, mm	38.1	38.1	17.0
Note	Applicable to #2 spindle only		—

TABLE 14 Cutting Conditions (Hoshi et al., 1981)

Nomenclature	#1 drill	#2 drill	#3 drill	
Work material	Stainless steel	Stainless steel	Stainless steel	Brass
Spindle speed, 10^3 rpm	10-50	10-50	10-140	10-140
Feed rate, mm/min*	100-750	50-750	30-120	30-120
Feed per step, µm	110-230	10-180	10	10
Depth of hole, mm	2.5	2.5	0.4	0.4

Effect on cutting forces and temperature under different lubricating conditions like dry cutting, air blow, direct application of oil and oil mist is studied. Oil mist is found to give the best result in terms of cutting forces and torque (FIGURE 10).

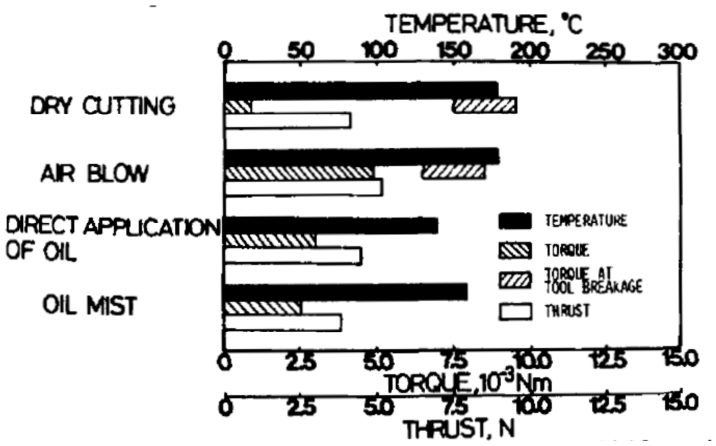

FIGURE 10 Cutting forces, torque and temperature under different lubricating conditions (after Hoshi et al., 1981).

They made following observations based on experimental data:

- Holes of diameter 0.1 mm can be drilled efficiently with spindle speed of 100,000 rpm, feed rate of 11.5 mm/min, feed increment of 10 μm with oil mist lubrication.
- At higher spindle speeds there is a decrease in both torque and thrust force due to reduced chip load (FIGURE 11). However, outer corner wear and flank wear are more at higher spindle speed.
- Worn out drills lead to burr formation.

Imran et al. (2008) investigated the feasibility of deep hole microdrilling of Ni based super alloy. Poor machinability of these alloys made it a challenging task. Two drills are used in the experiment; center drill to make a pilot hole and then a twist drill for actual drilling.

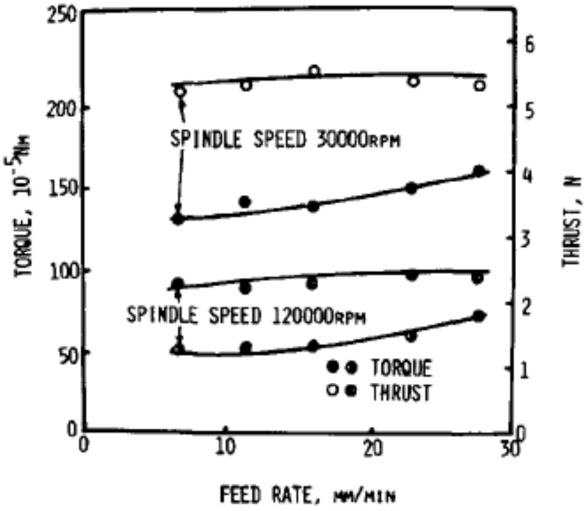

FIGURE 11 Effect of spindle speed on torque and thrust in stainless steel (after Hoshi et al., 1981).

Specifications of the drills are given as under:

- Pilot drill: Point angle 120°, helix angle 30°
- Twist drill: Diameter 0.5 mm, point angle 150°, helix angle 30°

Drill is made up of tungsten carbide which is coated with TiAlN. All machining trials are conducted on Micron HSM-400 machine and BLASOCUT BC 25-MD is used as a coolant. Cutting conditions of the tools are given in TABLE 15 and TABLE 16.

TABLE 15 Cutting Conditions for Pilot Hole (Imran et al., 2008)

Parameter	Value
Cutting speed (m/min)	4.7
Spindle speed (r/min)	3000
Feed (mm/rev)	0.005
Peck depth (mm)	0.1
Blind hole depth (mm)	0.13
Coolant	Flood

TABLE 16 Cutting Conditions for Actual Hole (Imran et al., 2008)

Parameter	Value(s)
Drill diameter (mm)	0.5
Cutting speed (m/min)	1.6–17.3
Spindle speed (r/min)	1000–11 000
Feed (mm/rev)	0.001–0.008
Peck depth (mm)	0.005–0.2
Blind hole depth (mm)	5
Coolant	Flood

Some of the important results and observations from their research are:

- Tool life decreases on either side of cutting range of 3000 rpm to 5000 rpm. Higher cutting speeds cause hardening which leads to tool wear (FIGURE 12)
- Higher feed rate can cause drill fracture due to higher mechanical load and disturbances at the beginning of the hole (FIGURE 13)
- Peck depth also has an effect on tool life. Tool life decreases on either side of the nominal value of 0.1mm (FIGURE 14)
- It is possible to drill 80 holes of 0.5 mm diameter with an aspect ratio of 10 times the hole diameter.
- As number of holes increases, hole diameter decreases (FIGURE 15).

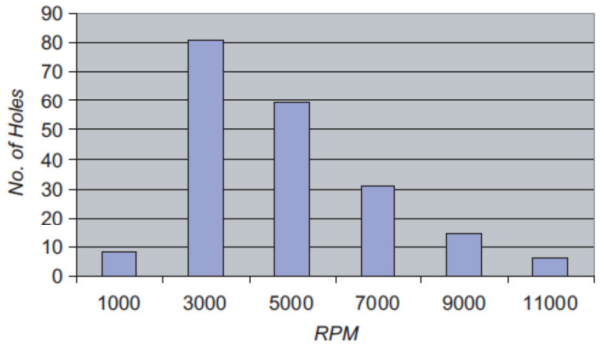

FIGURE 12 Effect of spindle speed on drill life (after Imran et al., 2008).

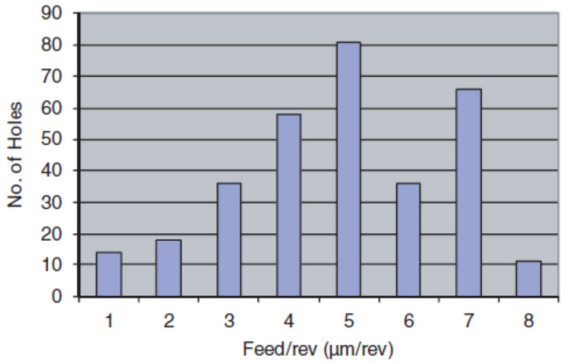

FIGURE 13 Effect of feed rate on drill life (after Imran et al., 2008).

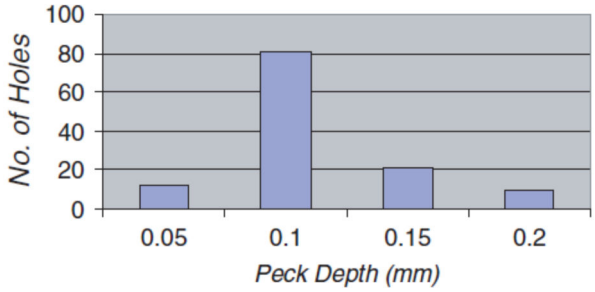

FIGURE 14 Effect of peck depth on drill life (after Imran et al., 2008).

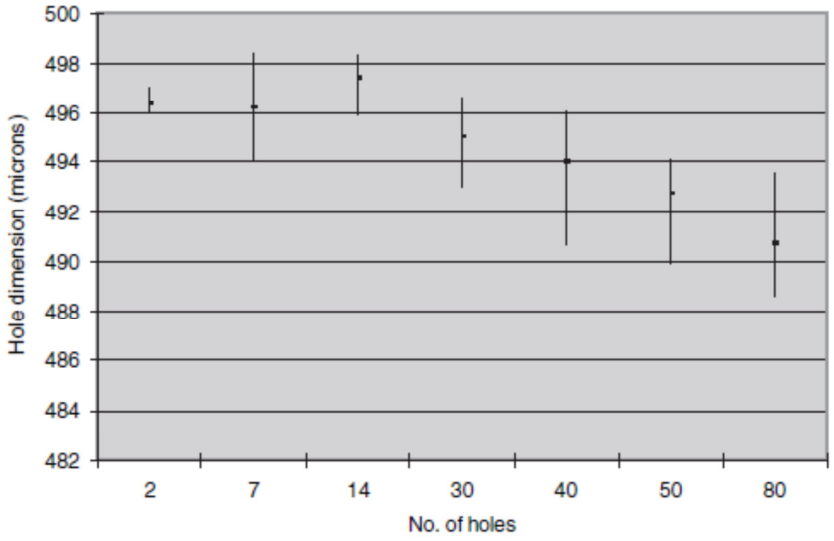

FIGURE 15 Variation of hole diameter (after Imran et al., 2008).

2.2.6 Hole quality

Lee et al. (2002) studied burr formation in microdrilling where they investigated the factors which significantly influence the burr formation process. The primary factors in their analysis are diameter, feedrate, cutting speed, and mechanics of burr formation. Experiment is carried out in two types of materials namely 6061-T6 aluminum and 25MoCrS4 steel using speed and feed combination listed in TABLE 17. Three different cutting tool diameters are 130 µm, 250 µm, and 500 µm. A microdrill is attached to Mori Seiki CNC drilling center TV-30 or Cameron Microdrill Press MD-90. The height and thickness of the burr are measured using SEM pictures. The tendency of increasing height with increase in feed rate is observed in aluminum micro burr (FIGURE 16).

The effect of cutting speed is not clear from the experiment. Increase in feed rate also increases the thickness of the micro burr whereas the effect of speed is not consistent with burr formation.

In case of steel, feed rate shows the same trend for thickness as well as the height of the burr as that of aluminum (FIGURE 17). Cutting speed again has no significant effect on the thickness of the burr. Also it is observed that there is a uniform burr formation at lower feed rates but at higher feed rates there is a formation of crown burr.

TABLE 17 Experimental Cutting Condition (Stirn et al., 2002)

Parameter	Aluminum	Steel
Diameter	130µm, 250µm, 500µm	
feed/diameter	0.00625 – 0.1	0.005 – 0.08
feed/rev [µm]	0.81 – 50	0.65 – 40
RPM	6000 – 19500	4000 – 7600
Cutting speed [m/min]	2.5 – 30.6	1.6 – 11.9

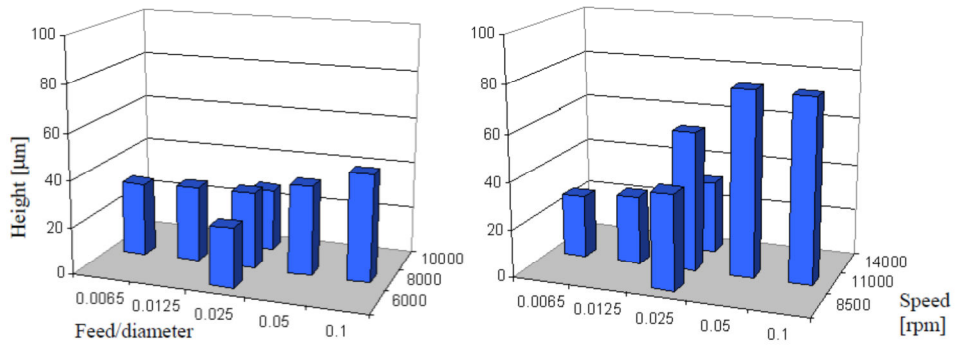

FIGURE 16 Burr height of aluminum in 130 micron drill (left) and 250 micron drill (right) (after Stirn et al., 2002).

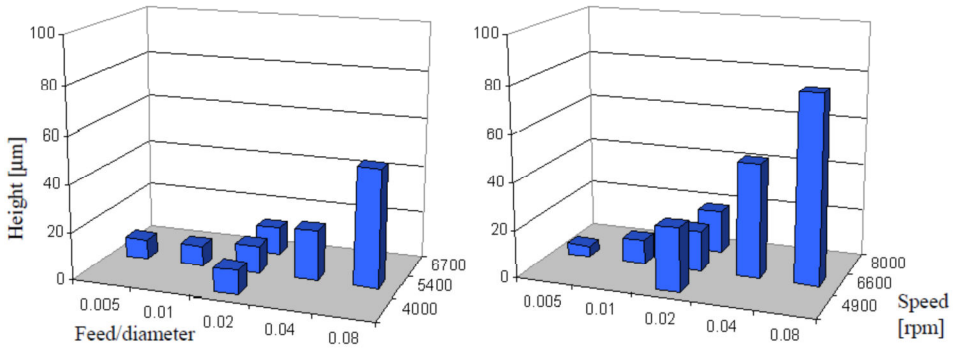

FIGURE 17 Burr height of steel in 130 micron drill (left) and 250 micron drill (right) (after Stirn et al., 2002).

Imran et al. (2010) investigated the effect of tool geometry in microdrilling of Ni based super alloy. Factorial design is used to find the effect of drill point angle and helix angle on tool wear and burr size. Burr formation and surface integrity is also studied in terms of surface and subsurface alterations.

A two factorial design with three levels is used in which the two factors are drill point angle and helix angle (TABLE 18) Inconel 718 alloy is used for conducting the experiments. Drills of diameter 500 µm coated with TiAlN and base material made with fine tungsten carbide is used. All tests are conducted on Mikron HSM 400 high speed machining center. HOCUT 3830 is used as water based coolant. A fixed feed of 7 µm/rev and speed of 7000 rpm is used for all the experiments.

TABLE 18 Factors and their Levels (Imran et al. 2010)

	Level 1	Level 2	Level 3
Point angle (θ)	130°	150°	170°
Helix angle (θ)	25°	30°	40°

Some of the important outcomes of the experiment are:

- Tool wear is strongly influenced by interaction of helix angle and drill point angle. An optimum value of 150° point angle and 40° helix angle results in reduced drill wear rate, reduced burr height and subsurface plastic deformation for microdrilling of nickel based super alloy.
- Increase in burr size is influenced by increase in tool wear which increases the plastic deformation and more material is extruded in the form of burr.
- The angle of burr cap is smaller than the drill point angle showing evidence that the material experiences spring back when pushed out.
- For 130° and 150° drill point angle, the thickness of deformation reduces with increase in drill helix angle as shown in FIGURE 18.

Sugawara and Inagaki (1982) attempted to investigate the phenomena in which burr size was reduced and cutting ability was improved as the drill diameter went down in workpieces which were granular in structure and had relatively large crystals. They performed the experiment with various materials and different diameters of the drill. The cutting conditions are given below in TABLE 19.

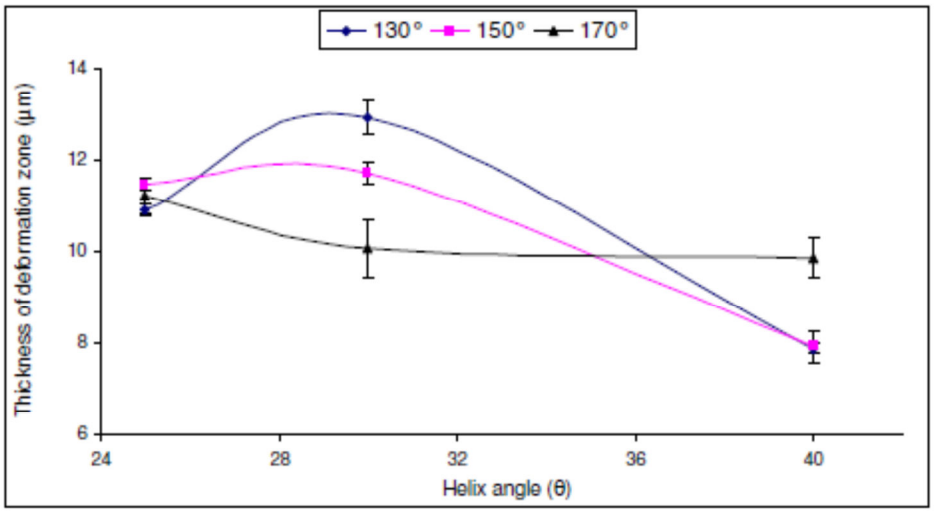

FIGURE 18 Variation of deformation zone at various points and helix angles (after Imran et al. 2010).

In a single crystal structure the grain boundary is far away from the drilling point and therefore range of plastic flow can be large. Due to this reason the quantity of burr formation is large. In polycrystals with large grains, the number of grains in the drilling area is small. Hence working area supports the plastic flow but the grain boundaries impede it. This is also illustrated in FIGURE 19.

TABLE 19 Working Conditions in Drilling (Sugawara and Inagaki, 1982)

Drill diameter, mm			Speed, r/min	Feed speed, mm/min	Workpiece (Corresponding to drill diameter)
2.5	2.0	1.8	2000	11.58	[Fe(R),Fe(H)] , SUS, Fe(S)
1.5	1.1	1.0	2400	7.68	Fe(S), [Fe(R), Fe(H)] , SUS
1.0		0.5	2800	4.26	Fe(S), [Fe(R), Fe(H), SUS]
	0.41		880	4.26	Ag
	0.32		1130	0.1074	Ag
0.3	0.25	0.2	3800	0.1074	Fe(S), SUS, [Fe(R), Fe(H), Ag]
0.41	0.32	0.17	3800	0.1074	Ag
0.1		0.05	3800	0.1074	Ag
	0.17		2120	0.1074	Ag
	0.1		3800	0.1074	Ag
	0.1		4800	0.0702	Fe(S), Fe(R), Fe(H), SUS
0.06		0.05	6000	0.0386	[SUS, Fe(R), Fe(H)] , Fe(S), Ag

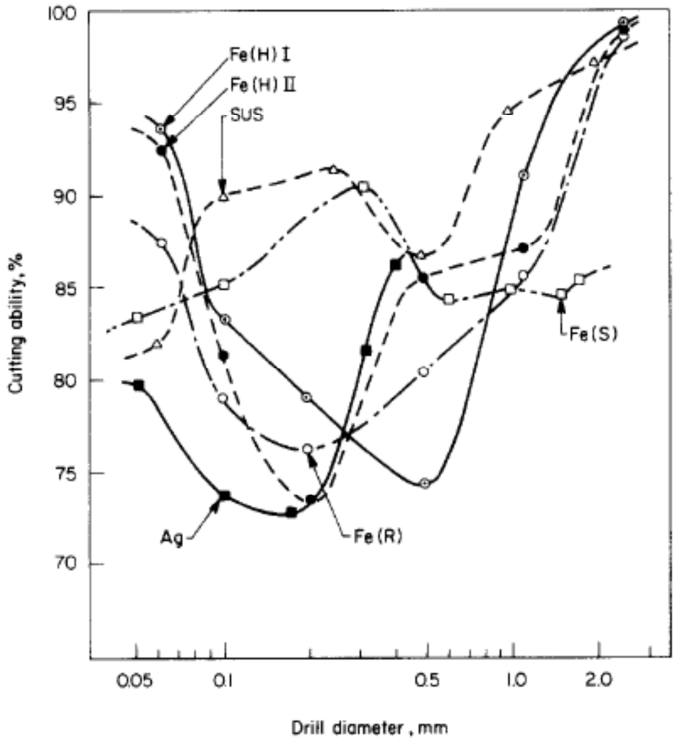

FIGURE 19 Variation of workpiece cutting ability with drill diameter (after Sugawara and Inagaki, 1982).

3. EXPERIMENTS

The objective of the experiment was to successfully drill microholes and build a tool wear model. Proper selection of cutting parameters was important to get useful results. Although parameters for macro-scale drilling drills are available, little information about microdrilling made it a challenging task. Several experiments were performed under different cutting conditions to understand the effect of cutting speed and chip load. Also, machine runout analysis was performed to understand the effect of tool deflection.

3.1 Materials

Commercially pure titanium, 316 L stainless steel, 6061-T6 aluminum and PEEK plastic were used. Initially the Ti samples were machined to the dimension of 12 mm X 8 mm X 90 mm using milling machine and edges were deburred.

It was decided to grind the sample step by step moving from 200 to 600 grit sandpapers followed by polishing. This helped in improving the surface finish without work hardening. Parallelism of the sample was measured with respect to the clamp base using a dial indicator (FIGURE 20). The measured values along the length and the width of the workpiece were 0.076 mm and 0.025 mm respectively. Sample preparation process for stainless steel was on the same lines as Ti alloy.

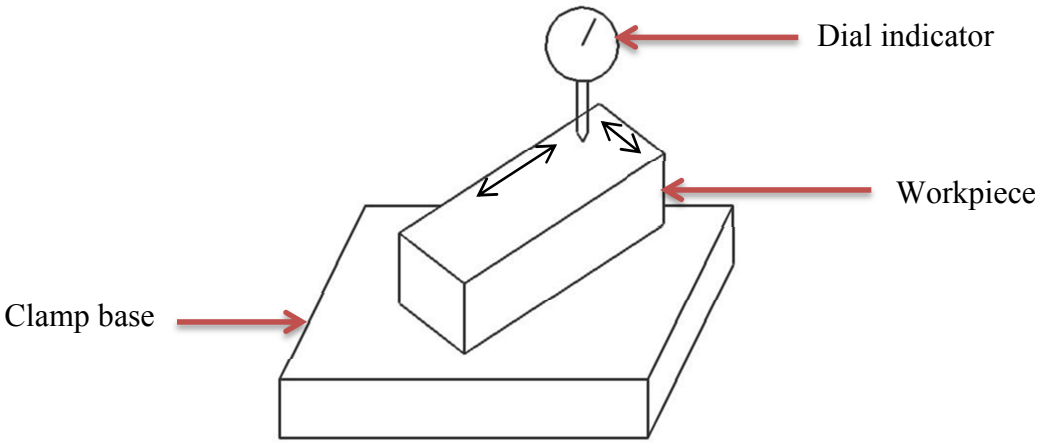

FIGURE 20 Parallelism measurement of the workpiece.

3.2 Tooling and machine

- Microdrills

  The tools used in these experiments were provided by Performance Micro Tools. The corresponding part numbers for the tools were KT-0050-R and KT-0040-R. The specifications of the tools are listed in TABLE 20 Cemented carbide is one of the most widely used cutting tool material. Its properties are given in TABLE 21.

TABLE 20 Specifications of Microdrills (Performance Micro Tools, 2011)

Nomenclature	KT-0050-R	KT-0040-R
Diameter, mm	0.127	0.100
Material	Micrograin Tungsten Carbide (WC)	Micrograin Tungsten Carbide (WC)
Coating	Uncoated and AlTiN coated	Uncoated
Point angle, degree	135°	135°
Rake angle, degree	30°	30°
Helix angle, degree	44°	40°
Number of flutes	2	2
Flute length, mm	2.286	1.778
Overall length, mm	38.1	38.1
Shank diameter, mm	3.175	3.175

TABLE 21 Properties of Tungsten Carbide (Mitsubishi Materials Corporation, 2011)

Hard Materials	Hardness (HV)	Thermal conductivity (W/m.k)	Thermal Expansion (x 10^{-6}/k)	Tool Material
WC	2100	121	5.2	Cemented Carbide

- HAAS OM 2 CNC Machine

  It is a vertical CNC machine that was used for conducting all the experiments. The workpiece was clamped on the table which had 4 degrees of freedom. The drill was mounted using a collet. The spindle could move up and down along the Z-axis. Machine specifications are given in TABLE 22 and additional details about the machine are given in appendix A1.The CNC code for microdrilling is given in appendix A4.

TABLE 22 HAAS OM 2 Machine Specification (High Point Precision Products, 2011)

Characteristics	**Specifications**
Spindle	
Max rpm	50,000
Min rpm	1000
Feed rate	
Max cutting	12.7 m/min
Max thrust	5111 N
Accuracy	
Positioning	±0.005 mm
Repeatability	±0.003 mm

- UNIST cool lubricator system

  It was used to supply micromist lubrication during drilling to enhance tool life by using minimum quantity of coolant. The micro fluidization system consisted of a variable rate pulse generator which produced infinite cycles of metering pump. Lubricant output was controlled by a knob on each metering pump. The pulse generator was set at 4 pulses per minute. The lubricant used for the experiments was Coolube 2210 EP which was supplied by UNIST.

- Mistbuster 850 Air Cleaner

  It is an electronic mist collector that was used for cleaning oil mist and smoke from metal working application to maintain healthy mist free environment in the workplace. It is equipped with a variable motor which can be set at high and low settings. During the experiments it was set at high setting.

3.3 Metrology

- Olympus STM 6 Optical Microscope

  It was used for measuring tool wear throughout the experiment. It is equipped with the DP 70 12.5 megapixel camera. It has a resolution of 0.1μm. It is a 3-axis measuring microscope having objective lens from 1.25x to 50x. Co-axial knobs are provided for movement of the 3-axis stage. Different stages on these knobs provide coarse and fine movement.

- Keyence LK-G1577 Laser Displacement Sensor

  It was used to measure and set offset in z-direction. The measurement accuracies required for micromachining is in the range of microns. This called for the use of ultra-precision measuring instruments that are stable and reliable. As the tool was susceptible to break easily even with slightest contact with workpiece hence it was difficult to measure the tool offset in z direction. In order to overcome this difficulty, a sponge was mounted on top of a flat metal piece. This arrangement was placed on top of the workpiece and z-offset was measured by touching the sponge face with the drill. The height of sponge metal piece assembly was

subtracted from the z offset to get the actual tool offset from the workpiece. The laser system was used for measuring the height of the sponge and metal assembly accurately.

- Ultrasonic cleaner Metason 200

  It was used to clean dirt, oil and small chips of metal attached to the microdrills before observing them under microscope. It required a cleaning agent to effectively clean the workpiece which in present case was Isopropyl alcohol. An ultrasonic transducer produces compression waves through the cleaning agent. This results in the formation of large number of minute vacuum bubbles. These bubbles collapse, release high energy and pressure which helps in removing the contaminants from the surface.

- JEOL JSM-6400 Scanning Electron Microscope (SEM)

  To study the minute details of the holes and the tool requires a Scanning Electron Microscope. A JEOL JSM-6400 SEM is used for studying the wear and quality of the holes. It has a tungsten source SEM having secondary electrons (SE), backscattered electrons (BSE). It has a magnification range from 10X to 300,000X with a resolution of 3.5nm. The accelerating voltage can be varied from 0.2 to 40kV. The sample to be studied is placed in the SEM chamber after ultrasonically cleaned in alcohol and blew dry.

- GF AgieCharmilles Cut 20P Wire Electro Discharge Machining (EDM)

  It was used to cut the drilled sample without damaging the surface details. It was important to observe the section of the hole to verify depth of hole and to extract information from microstructure deformation near the hole. As the holes were very small it was difficult to cut a section through the holes. Wire EDM was used to cut a section close to the holes and later this section was ground and polished to get the required detail.

3.4 Machine runout

Machine runout was measured and analyzed to confirm the adequacy of the machine to perform the experiments. High runout would affect the quality of the hole. The runout data was analyzed from previous data collected using a Keyence LK-G157 displacement laser system. TABLE 23 and TABLE 24 show the test parameters used in the experiment.

The experiments were conducted on HAAS OM2 machine. The end milling tools were provided by MA Ford. Micro milling was performed on 316 L stainless steel along a straight line using constant axial and radial depth of cut.

TABLE 23 Conditions for Measuring Spindle Runout (Chittipolu, 2009)

Microcutting tool	Gauge pin, diameter: 3.175 mm
Spindle speed	0 rpm (stationary), 6000 rpm (19.15 m/min), 10,000 rpm (31.92 m/min)

TABLE 24 Process Parameters for Measuring Tool Deflection when Machining (Chittipolu, 2009)

Microcutting tool	Diameter: 1.016 mm, 2 flute
Workpiece material	316L Stainless Steel
Chip load	10 μm/tooth
Axial depth of cut	0.35 mm
Radial depth of cut	0.56 mm
Spindle speed	6,000 (19.15 m/min), 15,000 (47.88 m/min) and 25,000 rpm (79.80 m/min)
Coolant	Unist mist spray

3.5 Tool workpiece positioning

The tool was mounted in the collet carefully without causing any damage to the cutting edge. The work coordinate system for the workpiece is shown in FIGURE 21. The back left corner of the workpiece was set as programming reference point for all the experiments (FIGURE 21). The x, y position of the tool was set by using an ocular lens. Very precise positioning in x, y direction was not necessary as a clearance of at least twice the diameter of the tool was provided between the holes in both x and y directions. The procedure for determining the z height is as follows (FIGURE 22):

1) A central point was marked on the surface of the foam block and the height of the block was measured at that marked location using Keyence LK-G1577 Laser

Displacement Sensor (FIGURE 23). This process was repeated multiple times, each time moving the block to a slightly different location. These heights were averaged to find the height of the foam block which was 30.092 mm.

2) The work surface of the CNC machine and tip of the tool was cleaned using ultrasonic cleaner with rubbing alcohol.
3) The sponge block was placed on the work surface, and the tip of the tool was adjusted so that it was directly above the central marked point on the sponge block surface.
4) The laser on the vice clamp was mounted at an angle so that the laser spot was 1-2 mm away from the marked point.
5) The tool was slowly lowered until it contacted the sponge block. This was indicated by a sudden change in laser values. When the tool contacted the sponge block, the value on the laser jumped suddenly.
6) The z coordinate displayed on the CNC work co-ordinate display screen combined with the average height of the sponge block indicated the height of the tool above the work surface.

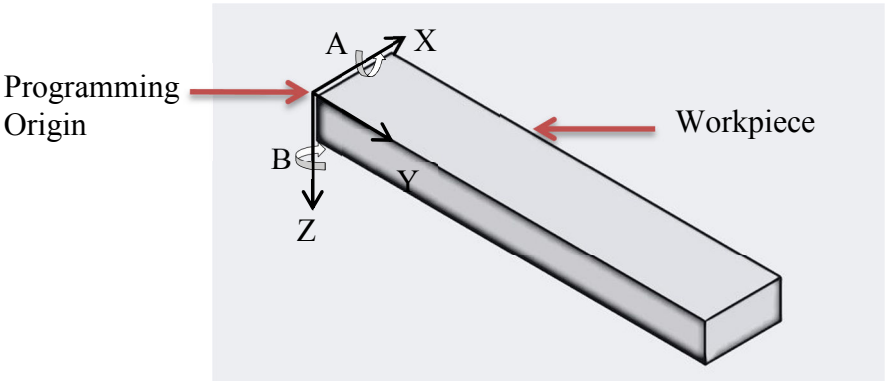

FIGURE 21 Coordinate frame of the workpiece.

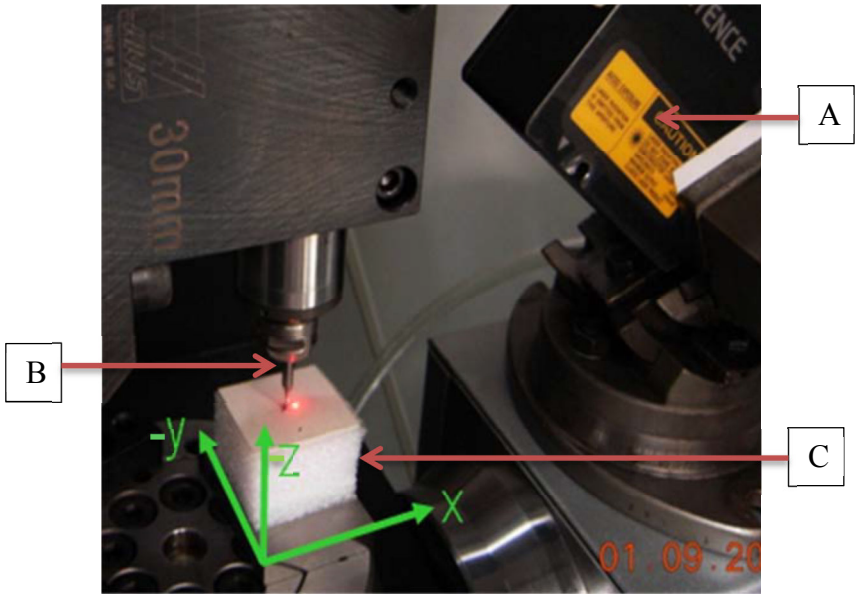

FIGURE 22 Setup showing the Keyence laser and cutting tool for tool positioning in z-direction. A: Keyence laser, B: Microdrill, C: Foam block (after Kajaria, 2009).

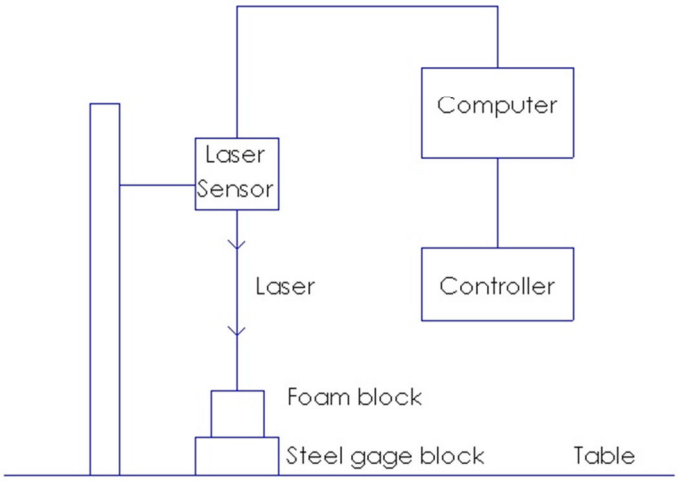

FIGURE 23 Schematic layout to measure height of the foam block with laser displacement sensor.

3.6 Nozzle orientation

Nozzle angle is set based on the research for optimization of coolant spray direction to maximize surface contact. Spray angle played a crucial role to maximize the effectiveness of micro-mist coolant. The nozzle position was set with respect to the tip of the tool, being the origin. The coordinates were (r, θ, Ø) = (30 mm, 60°, 55°). 'r' is the radial distance from the tool tip; 'Ø' is the angle between the y-axis on the machine coordinate system and the mist nozzle direction, and 'θ' is the angle between the tool axis and the mist nozzle direction. FIGURE 24 and FIGURE 25 show the orientation of the tool.

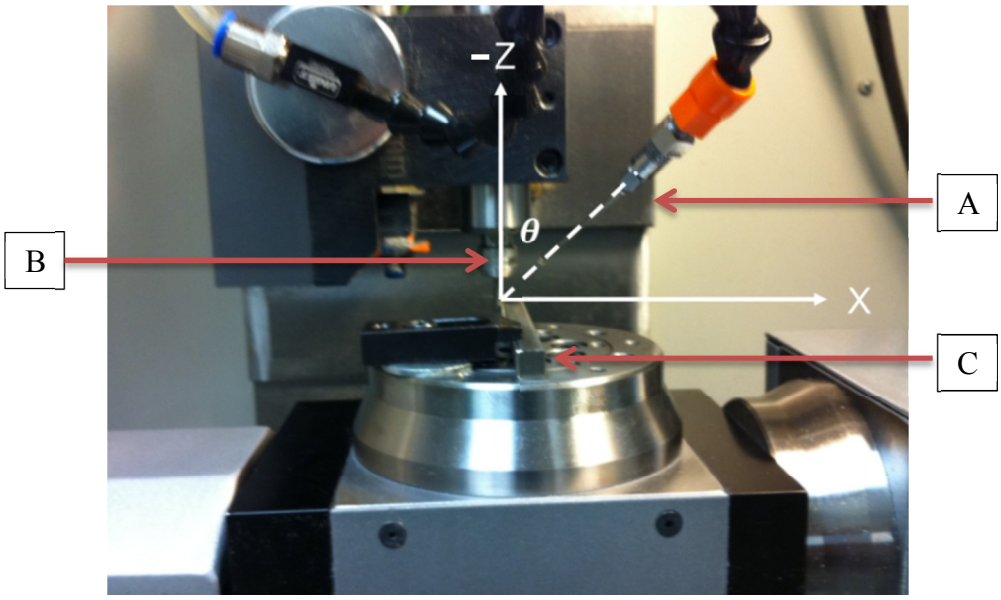

FIGURE 24 Coolant nozzle angle setup for θ (front view). A: Nozzle, B: Spindle, C: Workpiece (after Kajaria, 2009).

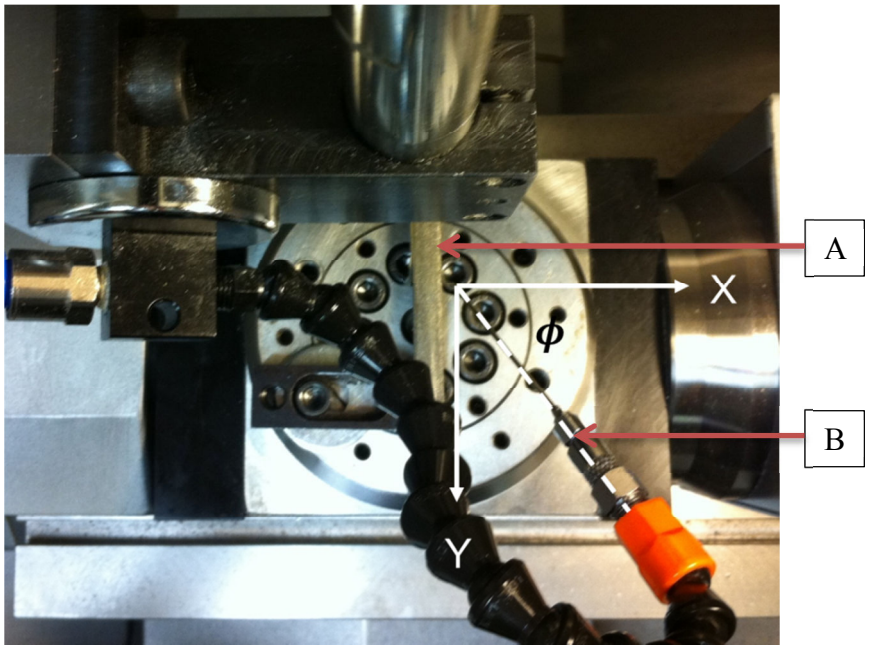

FIGURE 25 Coolant nozzle angle setup for Ø (top view). A: Workpiece, B: Nozzle (after Kajaria, 2009).

3.7 Experimental procedure

All the tools were numbered for easy identification and tracking. Each drill was inspected in the optical microscope for any defects or irregularities before starting the experiment. In case any impurity was found attached to the tool, it was cleaned using ultrasonic cleaning.

The collet was cleaned using compressed air and then the tool was tightened in the collet. The workpiece and nozzle were positioned as described in section 3.4 and 3.5 respectively. Before running the actual CNC program a warm up program was run if the machine was idle for more than two hours. This helped in minimizing wear and tear of the spindle. The warm up program is given in APPENDIX B.

The drilling program was written with pecking cycle incorporated as a macro in the main program (see APPENDIX B). Variable peck cycle was used instead of using constant peck to save time and resources. The pecking depth was deep in the beginning, but was reduced as we drilled deeper. We started with an initial pecking depth of 2*diameter and gradually reduced it to 0.5*diameter at the depth of 10*diameter (TABLE 25). Pecking depth and pecking cycles was calculated from:

$$\frac{P}{D} = \frac{1}{9(-1.5R + 19.5)} \quad for\ R \leq 10 \tag{3}$$

$$\frac{P}{D} = 0.5 \quad for\ R > 10 \tag{4}$$

where

P = incremental pecking depth (mm)

D = drill diameter (mm)

R = intermediate drill aspect ratio

TABLE 25 Pecking cycle for drill diameter 0.127 mm with an aspect ratio of 10:1

Pecking cycle Number	Hole depth (mm)	Aspect ratio	P/D	Pecking depth (mm)
1	0.254	2	1.83	0.233
2	0.487	3.83	1.53	0.194
3	0.681	5.36	1.27	0.162
4	0.843	6.63	1.06	0.135
5	0.977	7.70	0.88	0.112
6	1.090	8.58	0.74	0.094
7	1.183	9.32	0.61	0.078
8	1.261	9.93	0.51	0.065
9	1.326	10.44	0.43	0.054

The UNIST cool lubricator system was turned on before actual drilling. Normally the coolant system took some time before it started spraying the coolant. The presence of coolant was checked by placing a paper in front of the nozzle for oil trace. Mist buster air cleaner was started and drilling was performed along the width of the workpiece. Each cycle consisted of ten holes with a pitch of twice the diameter (FIGURE 26). After end of each cycle the drill was carefully removed from the collet and taken for inspection. The drill was mounted again in the collet after inspection and the next cycle of drilling was started at a distance of five times drill diameter from the previous row.

Two different cutting speeds were used for the same chip load for each material. Tool wear in Ti was studied with air blown and also with oil mist. The drilling parameters and conditions used for different materials are given in TABLE 26.

TABLE 26 Cutting Conditions for Different Materials

Material	Cutting Condition	Tool Diameter (µm)	Spindle speed (rpm)	Cutting Speed (m/min)	Chip Load (µm/flute)	Aspect ratio
CP Ti Grade 2	Oil mist	100	40,000	12.5	0.1	10:1
		127	50,000	20	0.1	
		127	30,000	12	0.05	
		127	50,000	20	0.05	
	Air blown	100	20,000	5	0.05	
		100	15,000	6	0.05	
316 L Stainless steel	Oil mist	127	35,000	14	0.02	
		127	50,000	20	0.02	
		127	35,000	14	0.035	
		127	50,000	20	0.035	
Al-6061 T6	Oil mist	127	20,000	8	1	
		127	40,000	16	1	
PEEK	Oil mist	127	10,000	4	0.06	
		127	15,000	6	0.06	

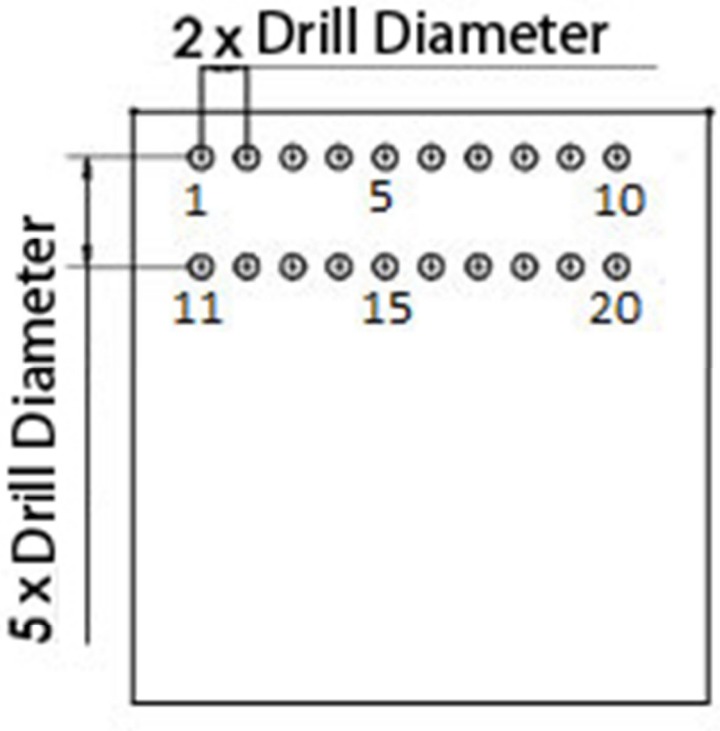

FIGURE 26 Drilling sequence.

3.8 Calibration

A standard piece was measured under microscope and picture was taken with a known scale (FIGURE 27). This picture was imported to Solidworks to measure10 µm, 30 µm, and 50 µm dimensions ten times each using Solidworks interface. Mean and standard deviation was found for each set of dimension (TABLE 27). The maximum percentage deviation was found to be 1.3%.

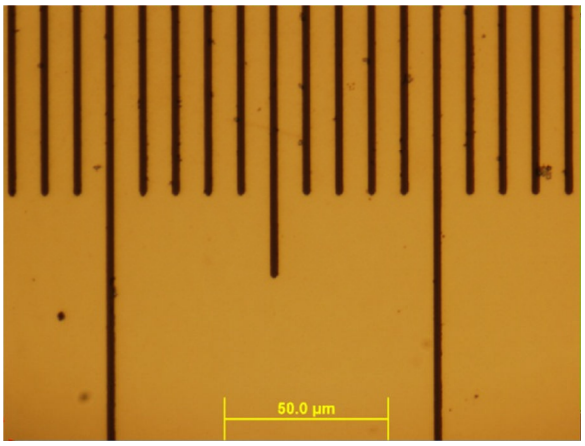

FIGURE 27 Picture of standard piece for calibration.

TABLE 27 Measured Values of Calibrated Piece using Solidworks

Observation	50 µm measured as (in µm)	30 µm measured as (in µm)	10 µm measured as (in µm)
1	50.393	30.332	10.052
2	50.481	30.201	10.009
3	50.350	30.157	10.140
4	50.393	30.288	10.140
5	50.262	30.201	10.184
6	50.393	30.245	10.140
7	50.306	30.288	10.140
8	50.393	30.288	10.096
9	50.393	30.245	10.227
10	50.393	30.201	10.140
11	50.393	30.245	10.052
12	50.306	30.201	10.096
13	50.350	30.288	10.140
14	50.481	30.332	10.140
15	50.350	30.288	10.184
16	50.393	30.288	10.140
17	50.481	30.376	10.096
18	50.350	30.245	10.140
19	50.437	30.201	10.096
20	50.393	30.201	10.184
Mean	50.385	30.256	10.127
Standard deviation	0.058	0.056	0.051
Percentage deviation	0.008	0.009	0.013

3.9 Tool wear measurement

Micro images of the tool were taken before drilling and after every ten holes. Digital image stitching was used to obtain a final picture with deep depth of field. Tool wear was monitored on both flutes.

FIGURE 28 shows the picture of the new tool and FIGURE 29 shows picture of worn out tool. Outline of the new tool was drawn by importing the image of the new tool using SolidWorks 2011. Tool wear was measured along the vertical line as shown in FIGURE 30. Pictures of the tool after every ten holes were superimposed on the tool outline. Care was taken to align the pictures before measuring wear along the cutting edge.

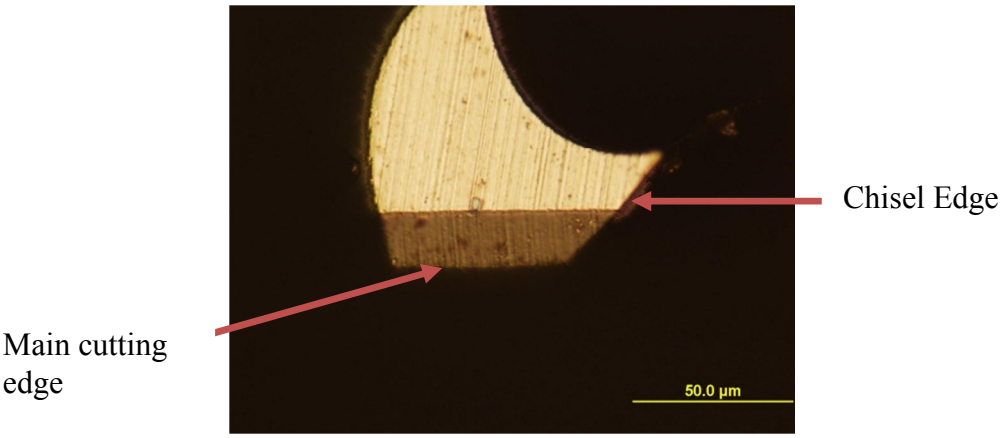

FIGURE 28 New drill as seen under microscope.

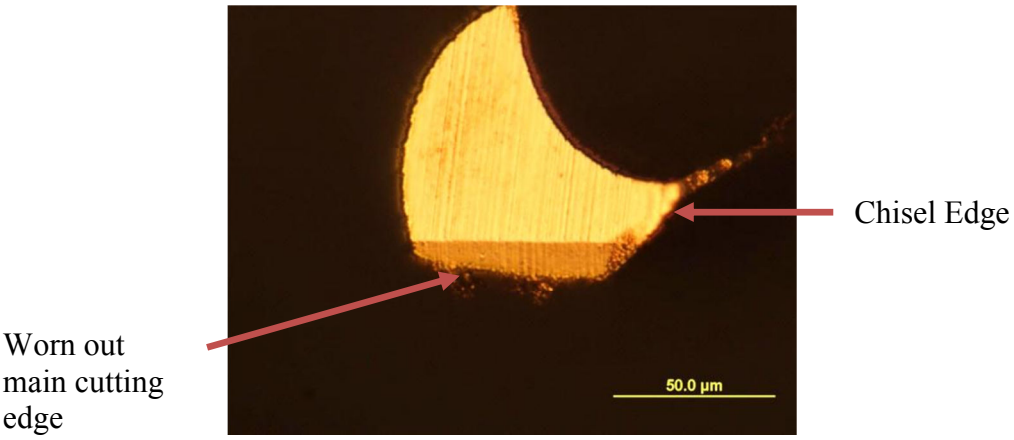

FIGURE 29 Worn out tool as seen under microscope. Workpiece: CP Ti, cutting speed: 20 m/min, chip load: 0.1 µm/flute, drilling distance: 101.6 mm, mist coolant.

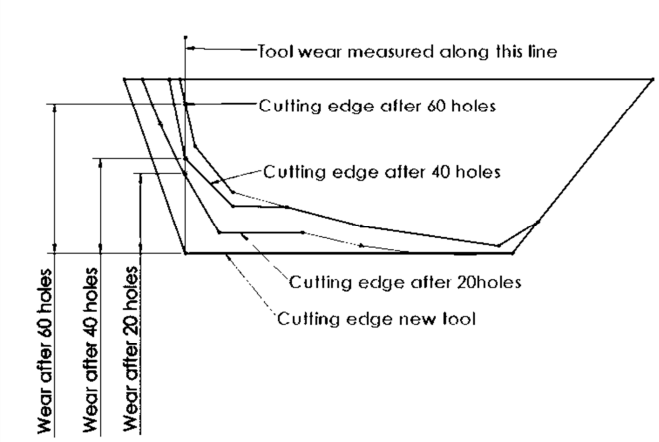

FIGURE 30 Tool wear measurement at the cutting edge. Workpiece: CP Ti, cutting speed: 20 m/min, chip load: 0.05 0.1 µm/flute, drilling distance: 76.2 mm.

3.10 Hole quality assessment

Hole position, diameter, depth and straightness were studied for hole quality assessment. A drilled sample was sectioned to measure the hole quality and to observe the microstructure. Microstructure was observed to study the effect of work hardening and grain boundary deformation.

The process of sample preparation and etching is given as under:

- Section the workpiece using wire EDM
- Mold the workpiece into a hard resin mount
- Grind
- Polish
- Chemical etching
- Observe in microscope

At first the workpiece was cut very close to the holes by using wire EDM process. Care was taken not to cut through the holes but at the same time cut as close to the holes as possible. Trials cuts were performed before cutting the actual sample to measure the erosion of the metal due to wire EDM. The cut workpiece was then placed in a silicone mold with the cut section facing down. A mixture of 15 parts of Epofix embedding resin and 2 parts of Epofix hardener was prepared in a separate container. This mixture was stirred gently using a wooden stirrer. The mixture was then poured gently into the rubber mold to avoid any formation of bubbles. The presence of bubbles might collect dirt which could scratch the surface. The mold was then left to dry overnight (FIGURE 31).After the mold was hardened it was ground to make both the top and bottom surface parallel. The mold was ground on different grits of sand paper. The sample was first ground on 200 grit paper, moving gradually to 400 and then 600 grit paper. Each time the sample was washed thoroughly before moving to the next grit of sand paper. The

sample was ground both in horizontal and vertical direction until all the machining marks were cleared.

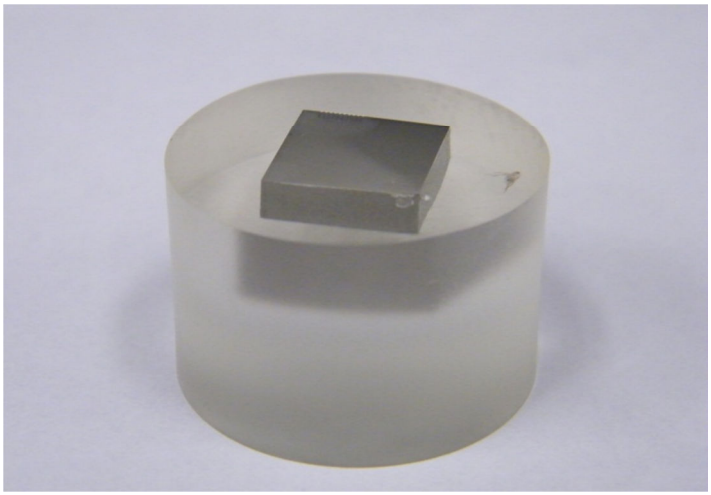

FIGURE 31 Molded workpiece.

The metal side of the mold was polished gradually from 1 micron to 0.05 micron with alumina polishing compound. To finish off the polishing stage, the side opposite to the metal side was also smoothed, while smoothing this side it was also made parallel to the reverse side by using a micrometer to check for parallelism. By making the surfaces parallel it would be easier to focus the entire face of the sample at once.

After polishing the sample was etched to reveal the microstructure. The purpose of chemical etching was to optically enhance contrast coloring of the grains in the sample. Different reagents were applied for different materials; for Ti, Kroll's reagent was used as a chemical etchant whereas for 316 L "Glyceregia" was used. The chemical

composition for Kroll's reagent and Glyceregia is shown in TABLE 28. Kroll's reagent was used by immersion whereas Glyceregia was used by swabbing on the sample. The etching time varies based on desired contrast level. The recommended range varies from 10 seconds to several minutes, with longer times resulting in more contrast but potential for oversaturation in detail.

TABLE 28 Etchants for Titanium and Stainless Steel (ASM Handbook, 1990)

Etchants	**Material**	**Chemical**	**Amount (ml)**	**Etch time (min)**
Kroll's reagent	CP Titanium	Distilled water	92	1
		Nitric acid	6	
		Hydrofluoric acid	2	
Glyceregia	316 L Stainless Steel	Hydrochloric acid	15	5
		Glycerol	10	
		Nitric acid	5	

3.11 Microhardness

Microhardness testing was done on the sectioned sample to determine the work hardening zone. The Leco LM-21 microhardness indenter was used. In the test, a

Vickers micro-indenter with a 136º pyramidal tip was indented into the material. The indenter was pressed into the material with a small mass of 0.05 kg with a dwell time of 13 s to form a square impression into the material. The first indentation was made close to the hole edge progressively moving away from the edge as shown in FIGURE 32.

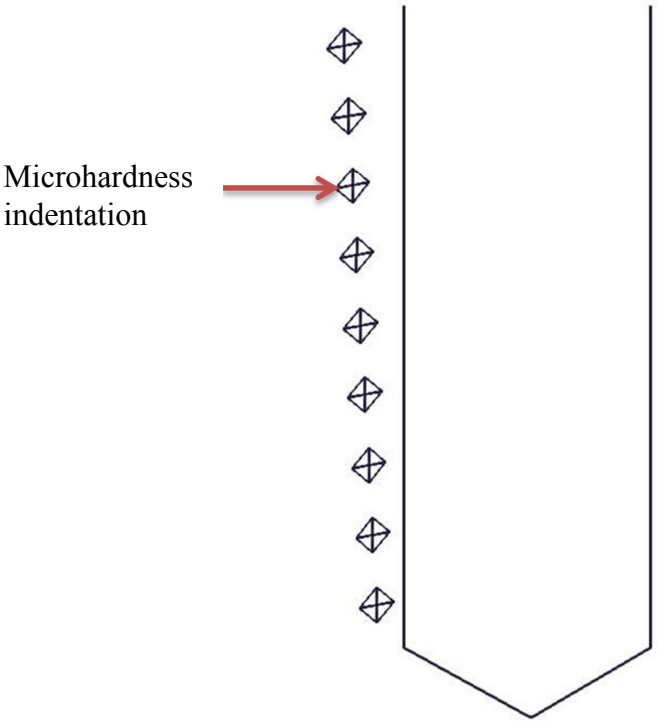

FIGURE 32 Microhardness location near a drilled edge.

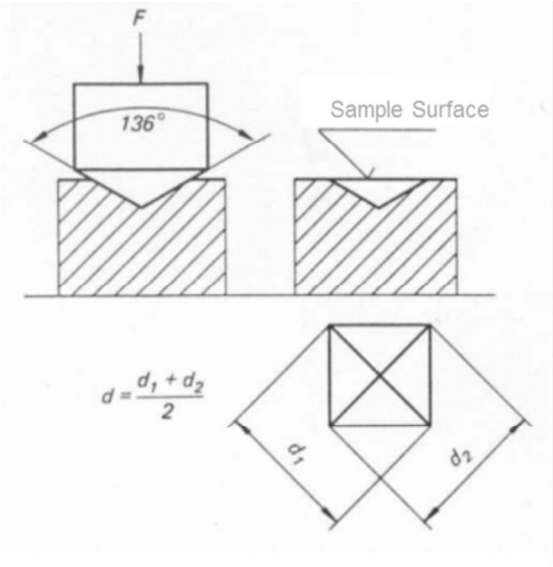

FIGURE 33 Vickers microhardness test (after BAM, 2011).

Then the diagonals of the square were measured and averaged using the optical microscope. FIGURE 33 shows the method of indenture and process of measuring the diagonals. Then by having used a static load, constant dwell time, and knowing the average length of the diagonals, equation (5) was used to determine the hardness of the material. Micro hardness was then plotted against the distance of indentation from the hole edge.

$$Hardness = \frac{1.8544 * F_i}{d^2} \tag{5}$$

4. RESULTS AND DISCUSSIONS

4.1 Machine runout analysis

The Keyence displacement laser recoded deflections of the tool under three different conditions:

- Stationary tool
- Running tool at 6000 rpm without cutting any material
- Running tool at 6000 rpm while machining under different conditions

It can be seen that when the spindle was stationary there was still some displacement of the tool (FIGURE 34). When the spindle was running at 6000 rpm without cutting any material the displacement increased. The displacement of the tool increased further as soon as the machining started.

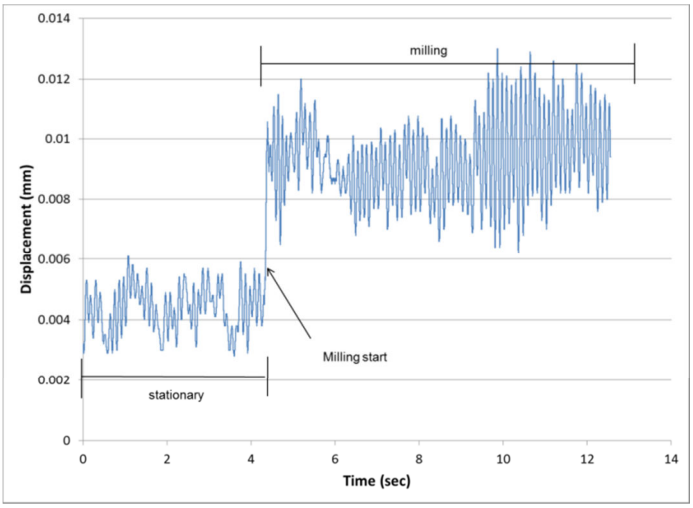

FIGURE 34 Keyence laser raw data from tool runout/displacement during machining at 6000 rpm (after Chittipolu, 2011).

To get further insight into the data Fast Fourier analysis was performed by Shioshaki (2011) and then placed in a power spectrum graph for above conditions (FIGURE 35). It can be seen that during stationary condition noise level had a thin scatter of data with a small peak at 127 Hz. At 6000 rpm before machining, there were two peaks at 127 Hz and 32 Hz which could be explained by noise and spindle runout respectively. While machining, the peaks were observed at the same frequencies but the amplitude was more due to tool deflection. The scatter of data also increased after machining. As there was no peak in amplitude other than the noise and the spindle runout, it could be concluded that the runout due to tool was negligible and tool was good for conducting experiments. Spindle runout also contributed to the increase in diameter of the drilled hole.

4.2 Microdrilling of CP titanium

Major wear in drilling Ti was observed in the main cutting edge towards the outer corner. Cutting speed is a function of tool radius which is maximum at outer corner of the cutting edge hence resulting in maximum wear (FIGURE 36 (c)). Chisel edge wear was negligible compared to outer corner wear.

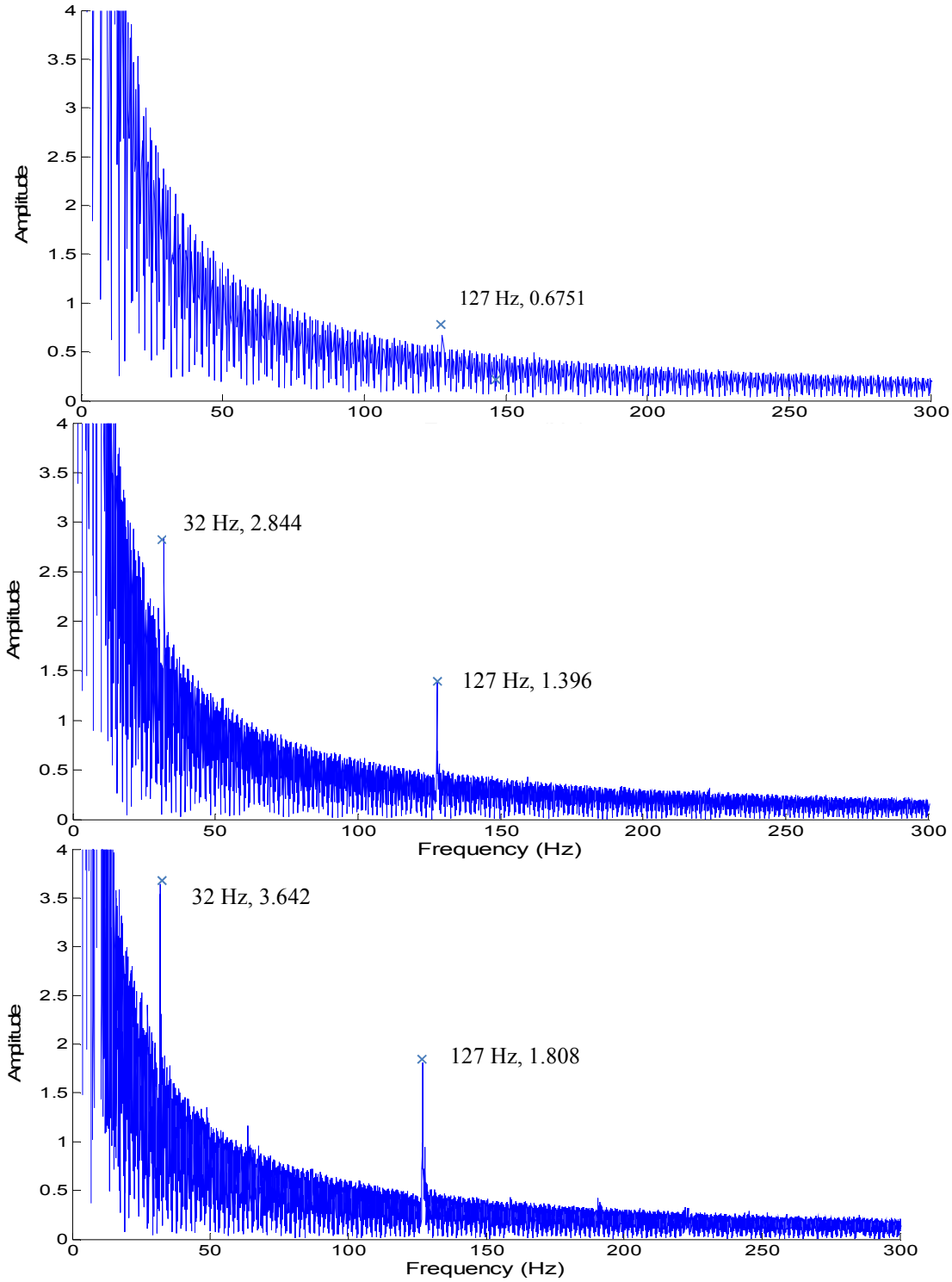

FIGURE 35 Frequency spectrum of tool runout: (top) laser noise; (middle) spindle at 6000 rpm; (bottom) machining at 6000 rpm (after Shioshaki, 2011).

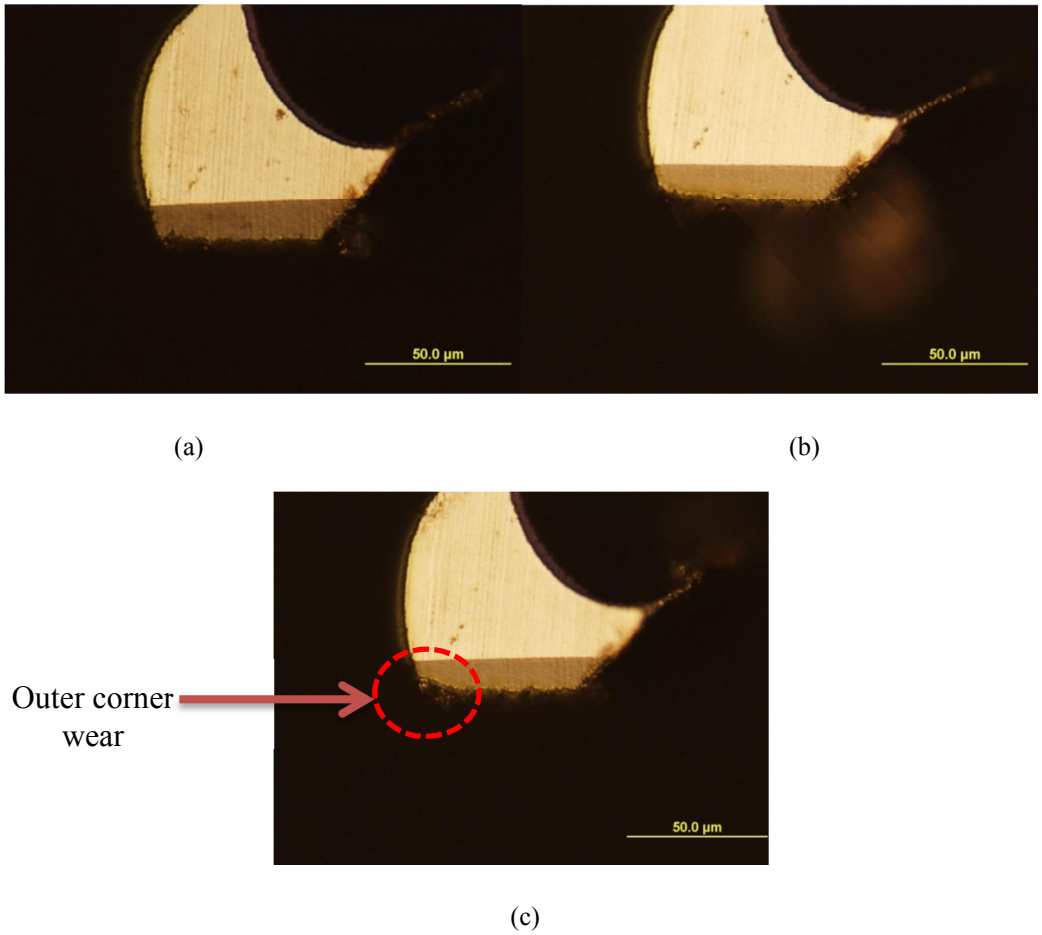

FIGURE 36 Progressive wear of drill. Drilling CP Ti at cutting speed 20 m/min., chip load 0.1 µm/flute, and mist coolant. Tool cutting edge after drill depth of (a) 2.54 mm (b) 3.08 mm (c) 7.62 mm respectively.

Workpiece material was adhered to the chisel edge and main cutting edges forming built up edge (BUE) even after ultrasonic cleaning with rubbing alcohol (FIGURE 37). This was evident in SEM image which showed brightness contrast between tool and workpiece material.

Chemical etching with aquaregia dissolved most of the BUE on the microdrill and hence gave a clearer image of the tool however some remaining BUE can still be seen after chemical etching (FIGURE 38).

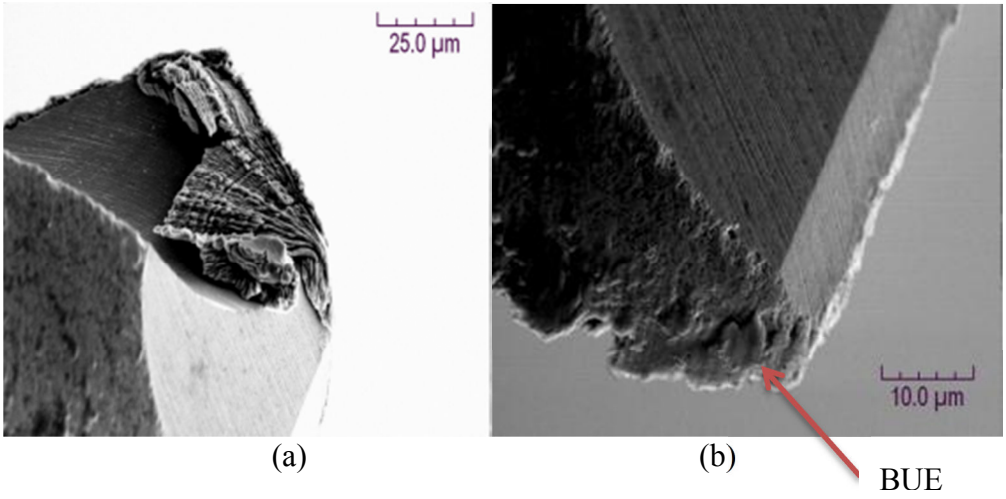

FIGURE 37 Built up edge on microdrill after ultrasonic cleaning with rubbing alcohol. Drilling CP Ti at a cutting speed of 6 m/min, chip load 0.02 µm/flute, and mist coolant. (a) BUE on chisel and cutting edge (b) BUE on outer corner.

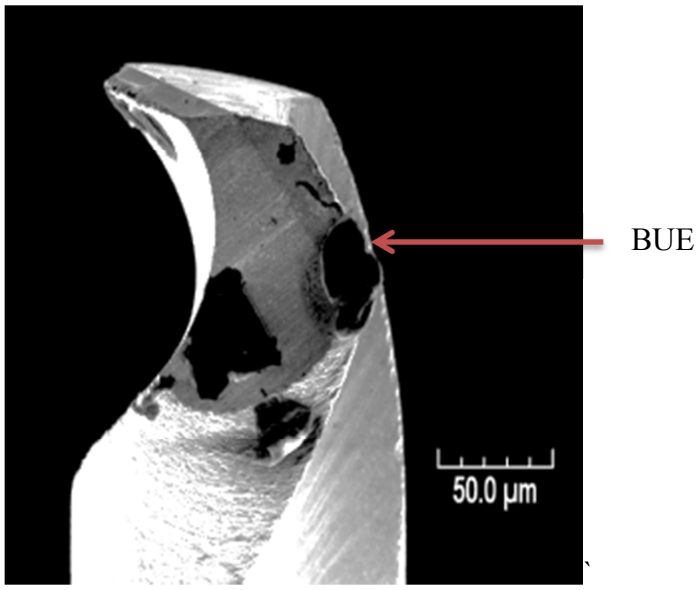

FIGURE 38 Remaining built up edge on microdrill after chemical etching followed by ultrasonic cleaning. Drilling CP Ti at cutting speed of 12 m/min, chip load 0.05 µm/flute, and mist coolant.

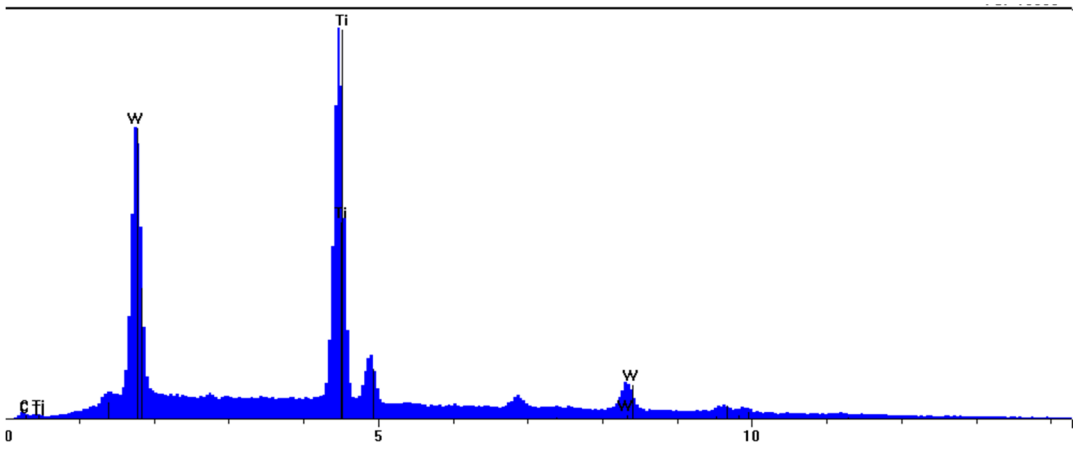

FIGURE 39 EDX of a built-up edge on the tool face. Drilling CP Ti at cutting speed of 6 m/min, chip load 0.02 µm/flute and with mist coolant.

Also, the Energy Dispersive X-ray spectroscopy (EDX) confirms the presence of Ti on tungsten carbide the tool face (FIGURE 39). During drilling, BUE was formed at lower cutting speeds with high chip load. Most of the BUE formation was seen at the chisel

edge where the cutting speed was minimum. Titanium chips are welded to the tool cutting edge due to increased temperature between the tool and the chip. Increase in temperature can be attributed to the poor thermal conductivity of Ti in which case a large amount of heat (as high as 80%) is absorbed by the tool itself (Li et al., 2007) . Also, the micro mist coolant was not very effective to lubricate the drill surface. While drilling a deep hole BUE grows until it reaches its maximum size. At higher speeds material at the tool face begins to soften and the binding force decreases thus eliminating BUE. This plucking of BUE causes tool chipping and rapid failure of the tool. Also, BUE changes the cutting geometry of the tool and hence the cutting forces.

Formation of BUE was also reported in macromachining of titanium. Komanduri (1982) found shear failure of BUE at the apex of the tool while drilling Ti alloy at low cutting speeds. The cutting speeds used ranged between 0.0212 μm/s to 5.1 m/s. Rahim and Sharif (2006) reported similar results where workpiece material adhered to the tool while drilling Ti alloy with a drill diameter of 6 mm. Drilling was performed at different cutting speeds 25, 35 and 45 m/min, constant feed 0.06 mm/rev in presence of water soluble coolant. They found non uniform flank wear and micro-chipping as the dominant wear pattern. Arrazola et al. (2009) showed EDX analysis to confirm presence of BUE on the tool cutting edge during turning of Ti alloy. The feed and depth of cut was kept constant at 0.1 mm/rev and 2 mm respectively whereas cutting speed was varied from 50 m/min to 100 m/min.

Adhesive and diffusion wear were the major wear mechanisms involved in machining Ti alloys (Muthukrishnan and Davim, 2011). Adhesive wear rate was promoted by the formation of BUE. Severe adhesive wear was characterized by welding and tearing of work material on the tool surface. In the present case, BUE formation was major reason for adhesive wear in the tool. Diffusion wear was characterized by movement of atoms from the tool material to the workpiece material.

Gradual diffusion of tool material to the workpiece led to weakened cutting edge and chipping of the cutting tool (Patil, 2010). Diffusion wear occurred at elevated temperature and required some solubility of tool material with work material phase (Patil, 2010). Simon et al. (2005) showed that Ti reacted with carbon at elevated temperatures causing diffusion of carbon. Arrazola et al. (2009) found diffusion of carbon on the tool face while drilling Ti alloy with WC/Co tool. Ginting et al. (2004) found adhesion and diffusion as the major wear mechanism while milling Ti alloy with a carbide tool. According to their study, cobalt binder material of the tool substrate also got dissolved and diffused by heat. The absence of cobalt from the tool matrix combined with interruptive mechanical loads splits the grains, finally leading to cracking, flaking, chipping and fracturing.

4.3 Microdrilling of 316L stainless steel

Unlike CP titanium where outer corner wear was predominant, severe tool wear was observed on the cutting lip close to chisel edge (FIGURE 40). Wear was also observed

on the chisel edge and outer corner of the cutting edge. Chisel wear occurs due to the rubbing action of the tool under high compressive stress acting at high temperature. The rubbing marks can be seen near the chisel edge of the tool (FIGURE 41). This rubbing action of the chisel edge increased the deformation and work hardening zone of the workpiece. Consequently, the main cutting edges faced greater resistance leading to higher temperatures and lower tool life.

Since microdrilling information is limited, data for macrodrilling of stainless steel is presented. Lin and Shyu (2000) found chisel and outer corner wear as dominant wear while drilling austenitic stainless steel which was in line with the present result. Coated drills of diameter 8 mm were used. Cutting speed employed was 25.2 m/min and feed was variable. Dolinsek (2003) reported high rubbing action at the chisel edge of the tool due to work hardening of austenitic stainless steel. The drill diameter ranged from 5 to 15 mm. Cutting parameters varied between cutting speeds of 5–15 m/min and feeds 0.08 to 0.31 mm/rev. Iwata et al. (1981) also reported outer corner wear while microdrilling of stainless steel. Drill diameter of 0.45 mm, 0.35 mm, and 0.1 mm were used to drill stainless steel. For microdrill of diameter 0.1 mm, following cutting parameters were used; spindle speed 10,000 rpm to 140,000 rpm, feedrate 30 mm/min to 120 mm/min, feed per step 10 μm, and aspect ratio 4:1.

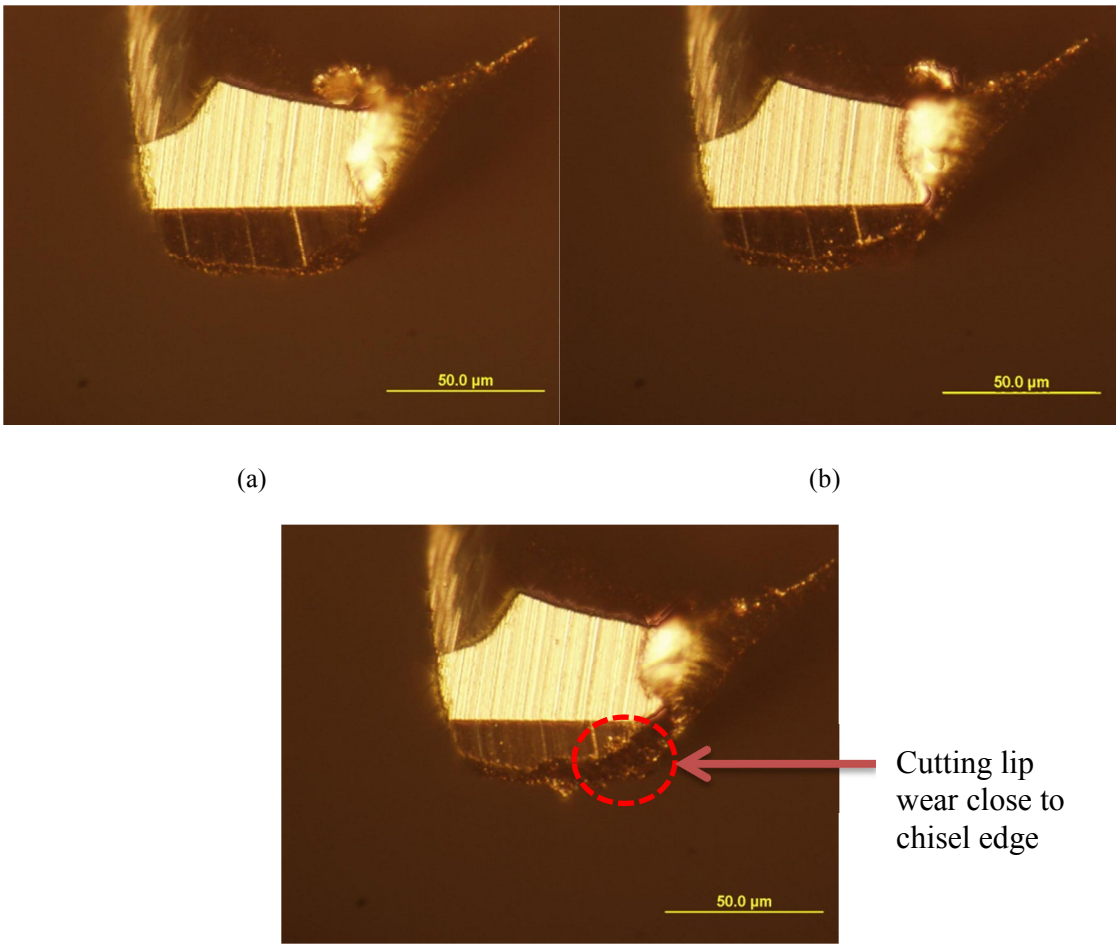

FIGURE 40 Progressive wear of cutting lip and chisel edge. Drilling 316 L stainless steel at a cutting speed 14 m/min, chip load 0.02 µm/flute, and with mist coolant. Tool cutting edge after drill depth of (a) 12.7 mm (b) 63.5 mm (c) 101.6 mm respectively.

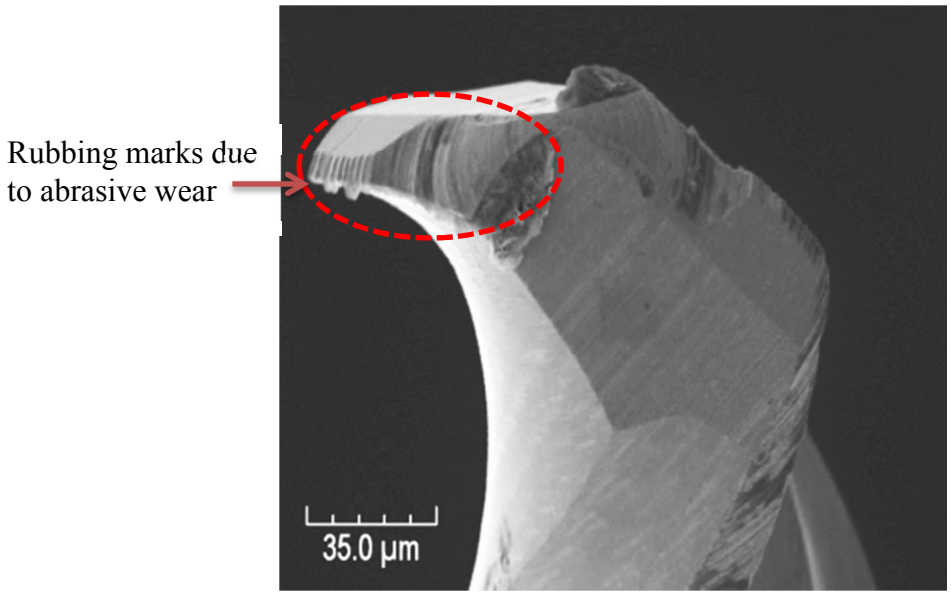

FIGURE 41 Abrasive rubbing marks on microdrill. Drilling 12.7 mm on 316 L stainless steel at a cutting speed 14 m/min, chip load 0.050 µm/flute and with mist coolant.

Although BUE was observed under all cutting conditions, severe BUE formation was observed under low cutting speeds (FIGURE 42). BUE was more prominent near the chisel edge area as the cutting speed was lowest in that region. Poor thermal conductivity leading to high cutting temperature was one of the main reasons behind BUE formation. This promoted severe adhesion to workpiece material and BUE formation. High aspect ratio (10:1) of drilling also increased the tendency to form BUE. Heat dissipation in microdrilling especially while drilling holes with high aspect ratio, was a major concern. High temperature might arise due to inefficient supply of coolant.

As information on microdrilling was limited therefore data for macrodrilling and turning of stainless steel was presented to substantiate BUE formation. Dolinsek (2003) reported

formation of BUE while drilling austenitic stainless steel. Paro et al. (2001) found the presence of BUE on the cutting tool while turning austenitic stainless steel at cutting speed 60-100 m/min, feed 0.24 mm/rev and depth of cut 1.6 mm. Rapid tool wear and chipping were the major tool failure modes. They concluded that the presence of BUE decreased the machinability and affected the surface roughness of the workpiece. Similar results were obtained by Korkut et al. (2004) who reported poor performance of tools at lower cutting speed while turning AISI 304 which was an austenitic stainless steel. This behavior was attributed to poor thermal conductivity and formation of BUE.

Notch or groove wear was observed under closer examination of the cutting lip (FIGURE 43). Notch wear was an indication of the hard abrasive surface of the workpiece which was formed due to work hardening. Chandrasekaran and Johansson (1994) found that practical tool life is limited by notch (groove) wear while machining high alloy steels (Cr 18-27% and Ni 12-30%). Notch wear is commonly observed in machining nickel based super alloys.

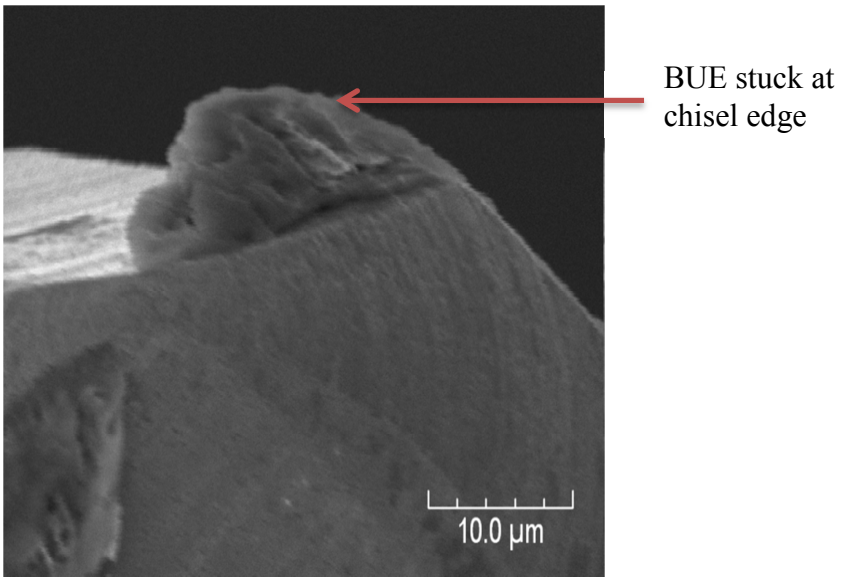

FIGURE 42 Micrograph showing BUE on tool after drilling 12.7 mm on 316 L stainless steel at a cutting speed 14 m/min., chip load 0.050 µm/flute and with mist coolant.

Shaw et al. (1966) had concluded continuous seizure and plucking of tool material as a possible wear mechanism for such alloys. Notch wear information for turning and milling of stainless steel was presented in absence of any data for microdrilling. Chandrasekaran and Johansson (1994) studied notch wear mechanism while turning austenitic stainless steels with cutting speed varying from 100-250 m/min, feed 0.08-0.3 mm/rev and depth of cut 0.5-4 mm without coolant. They reported poor machinability of austenitic stainless steel displaying different tool wear modes like flank, crater, notch and micro-chipping.

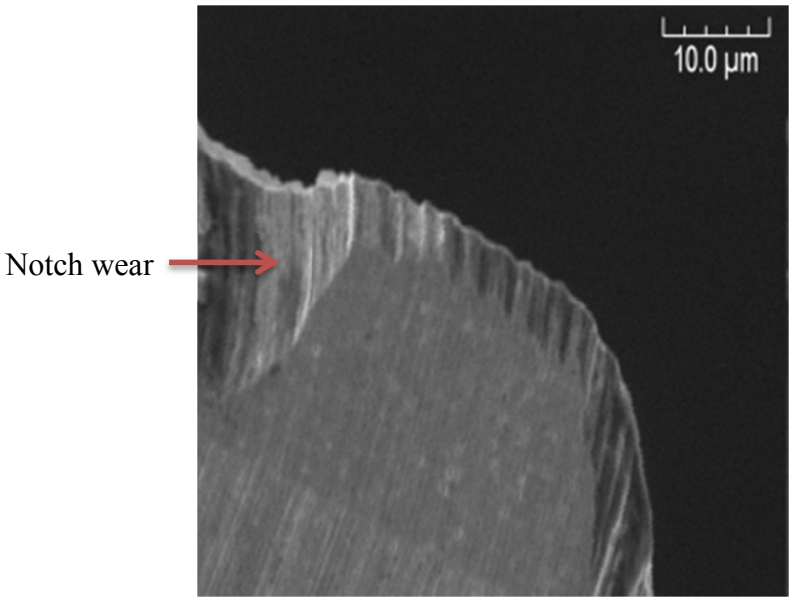

FIGURE 43 Micrograph showing notch wear at the cutting lip. Drilling 316L stainless steel, drilling distance 12.7 mm, cutting speed 14 m/min., chip load 0.050 µm/flute and with mist coolant.

Endrino et al. (2006) reported chipping of cutting edge while milling 316 austenitic stainless steel. Cutting conditions were: cutting speed of 120 m/min, feed rate of 0.05 mm, depth of cut of 10 mm and radial depth of cut of 0.5 mm in presence of coolant. The workpiece material was hot rolled Shao et al. (2007) found the basic tool wear modes while milling austenitic stainless steel are abrasive wear, adhesive wear, and diffusion wear.

Vickers microhardness was measured near a drilled surface. The microhardness test was performed on the 10^{th} hole of the workpiece (12.7mm drilling distance) to measure the effect of work hardening after the sharp edges of the drill were worn out (FIGURE 44). The overall hardness of unmachined 316 L stainless steel varied from 330-380 HV. The hardness near the drilled section was found to be 15% greater than the unmachined zone.

This increase in hardness was due to the high degree of work hardening characteristic of 316 L stainless steel. Similar work hardening was reported by Dolinsek (2003) while drilling austenitic stainless steel leading to higher resistance near the chisel edge of the drill. Work hardening was one of the major reasons for poor machinability of austenitic stainless steels (Jiang et al., 2007). It was one of the major reasons for the notch wear seen on the cutting lip of the tool. Ideally, the main cutting edges should not perform cut at the work hardened layer from the previous cut. Therefore, the feed should be greater than the depth of the work hardened zone to improve tool life. Hence it was important to find the depth of the work hardened zone to choose the best feed rate or chip load. To find the thickness of work hardened zone, hardness was plotted against distance from the hole section (FIGURE 45).

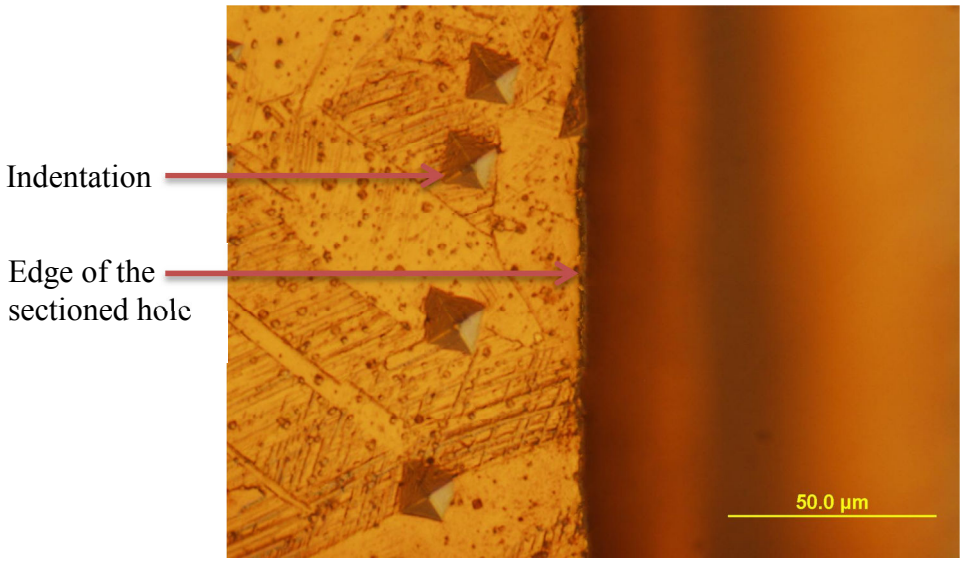

FIGURE 44 Vickers hardness test with a 50 g load, dwell time 13 s. Drilling 316 L stainless steel, 10th hole (drilling distance 12.7 mm), cutting speed 14 m/min., chip load 0.035 µm/flute and mist coolant.

It can be seen from the plot that the work hardening zone in the present scenario is approximately 30 µm from the edge of the hole section. This experiment can be repeated at different section of the holes to get an average work hardened zone. This means that the chip load required to cut this zone should exceed 30 µm for better tool life. However, it was found that increasing the chip load by a small amount (0.05 µm/flute) drastically increased the tool wear. Higher chip loads were characterized by notching of cutting lip (FIGURE 46).

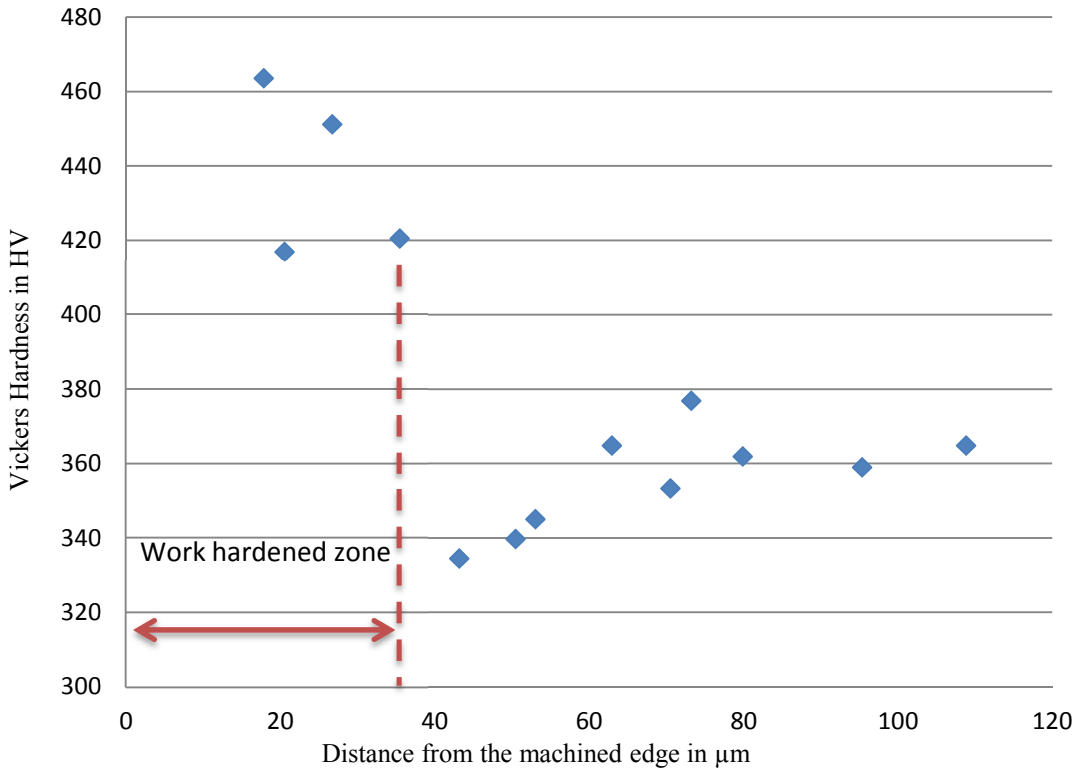

FIGURE 45 Vickers hardness of drilled 316 L stainless steel. Micro-hardness with a load of 50 g and dwell time 14 s. Drilling at cutting speed 14 m/min., chip load 0.035 µm/flute , mist coolant, and 10th hole (drilling distance 12.7 mm).

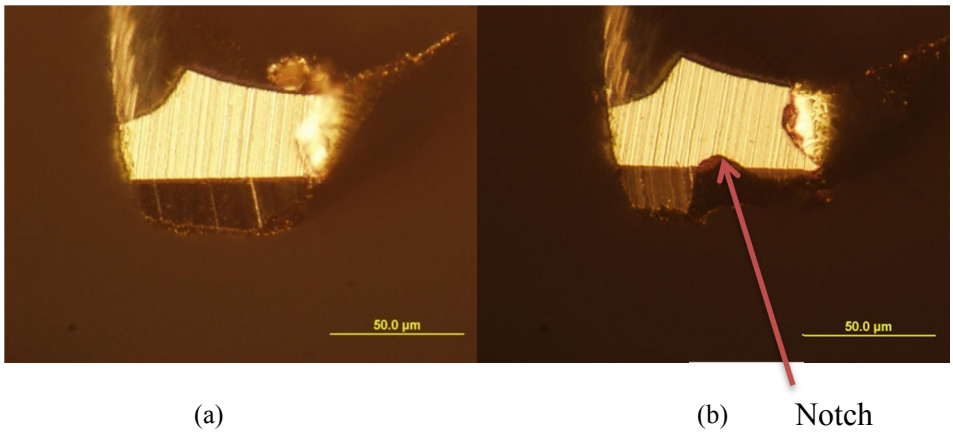

FIGURE 46 Effect of chip load on tool wear. Drilling 12.7 mm on 316 L stainless steel with micro-mist lubricant at a cutting speed of 14m/min., chip load of (a) 0.02 µm/flute and (b) 0.05 µm/flute.

As BUE formation was the reason for adhesive wear in the microdrill, it was decided to use coated drills for improved performance. A coating AlTiN had less surface adhesion tendency to austenitic stainless steel which would minimize the BUE formation on the chisel edge. The drill with diameter 0.127 mm was coated and used for drilling 316L stainless steel which showed improved performance. There was minimum BUE formation on the chisel edge even after drilling distance of 101.6 mm as compared to uncoated drill which showed significant BUE formation after drilling distance of 12.7 mm under similar condition. However, the BUE formation was significant as the drilling distance increased (FIGURE 47).

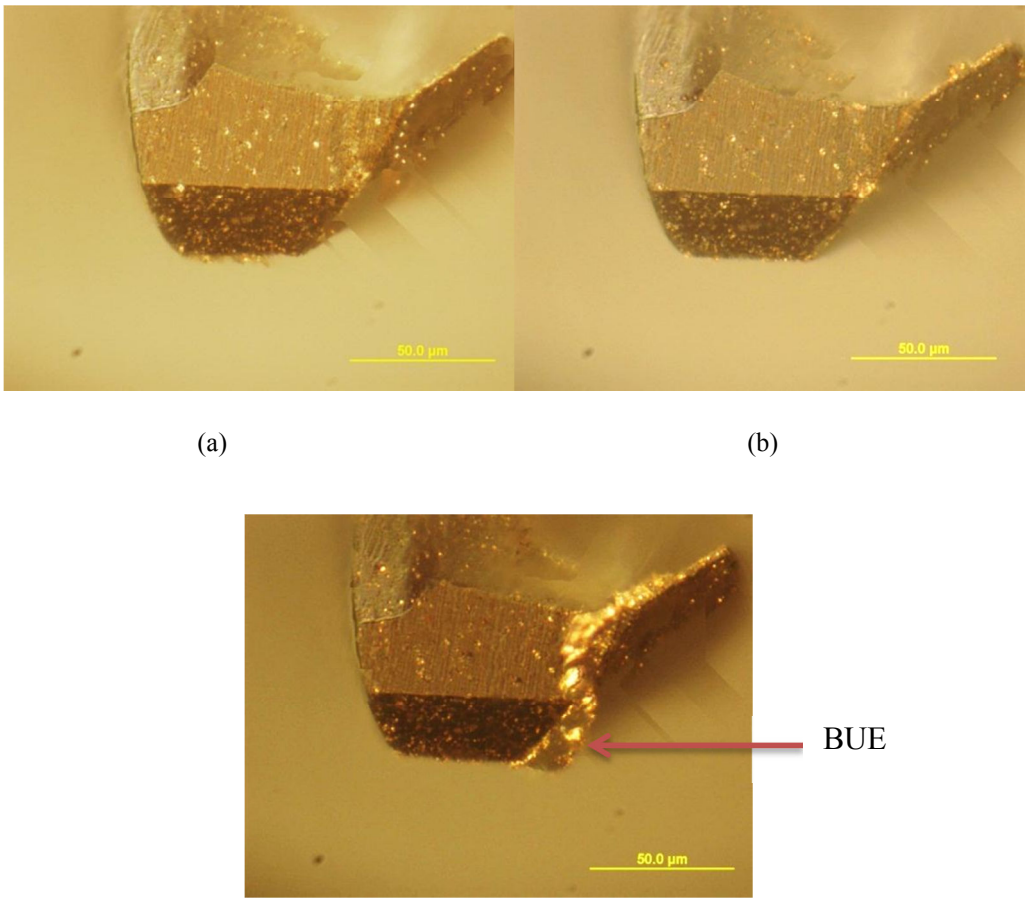

(a) (b)

(c)

FIGURE 47 Microdrill coated with AlTiN. Drilling 316 L stainless steel at a cutting speed 14 m/min., chip load 0.02 µm/flute, and with mist coolant. Tool cutting edge after drill depth of (a) 12.7 mm (b) 101.6 mm (c) 177.8 mm respectively.

4.4 Microdrilling of aluminum 6061- T6

Major wear while drilling aluminum alloy was observed in the main cutting edge towards the outer corner. Chisel edge wear was less compared to outer corner wear. There was BUE formation in later stages of the drilling near the chisel edge (FIGURE 48). This was in line with the findings of Trent (2000), who reported BUE formation in aluminum alloys at low cutting speed. There was a gradual increase in wear of the

cutting edge as we move towards the outer corner of the tool. This is because of the increase in cutting speed as we move away from the center of the tool. However, tool wear was less compared to tools after drilling CP titanium and 316 L stainless steel even at higher chip loads. This can be attributed to the fact that aluminum alloys have very good machinability due to high thermal conductivity and low cutting energy which generates a low temperature during cutting (Liu, 2004).

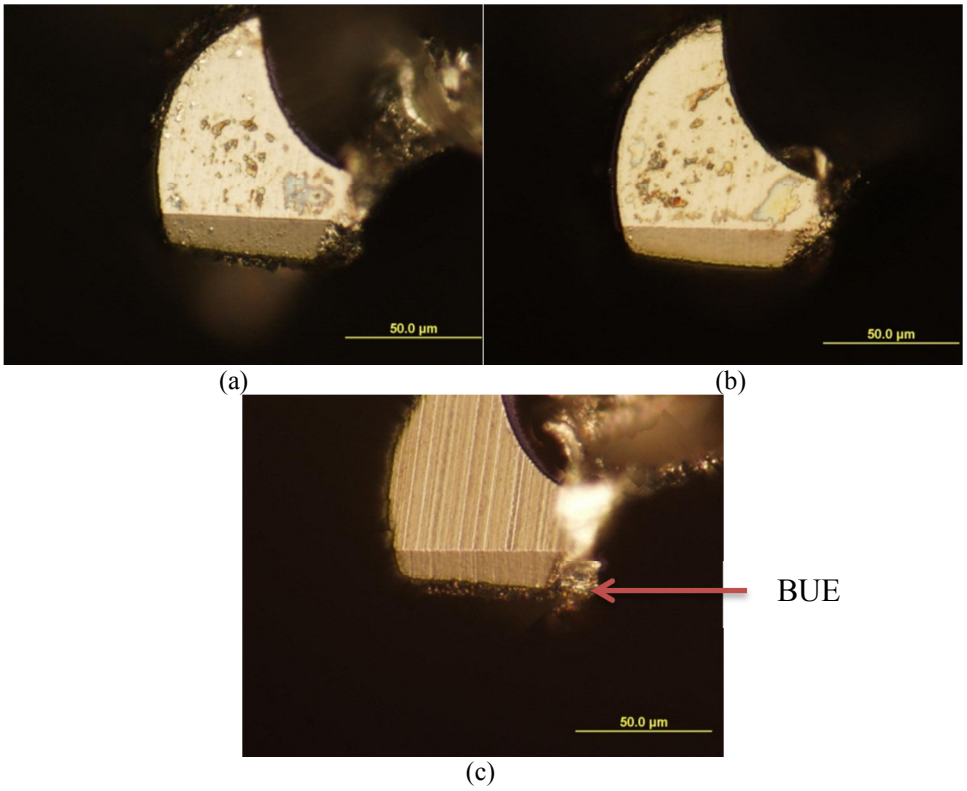

FIGURE 48 Progressive wear on cutting lip. Drilling aluminum 6061-T6 at a cutting speed 8 m/min., chip load 1 µm/flute, and with mist coolant. Tool cutting edge after drill depth of (a) 635 mm (b) 1270 mm (c) 2032 mm respectively.

4.5 Microdrilling of PEEK

Tool wear in microdrilling of PEEK was found to be minimal compared to other metals (FIGURE 49). Uniform wear was observed at the cutting lip. While cutting metals high temperatures can be reached leading to thermal softening of tool material which accelerates wear. However, in case of polymer based materials like PEEK the maximum temperature reached at high cutting speed is much lower compared to metals hence lesser tool wear (Rahman et al., 1999).

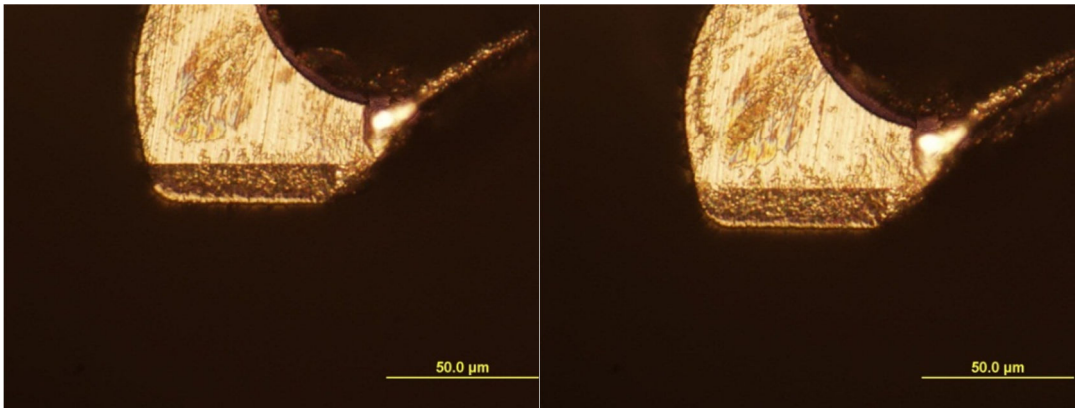

(a) (b)

FIGURE 49 Progressive wear on cutting lip. Drilling PEEK at a cutting speed 6 m/min., chip load 0.06 µm/flute, and with mist coolant. Wear after drill depth of (a) 508 mm (b) 1116 mm respectively.

4.6 Tool wear modeling

A tool wear model was required to predict tool life and to understand the effect cutting parameters. Tool wear was measured as explained in section 3.7. The cumulative tool wear was plotted against drilling distance in a log-log plot. All the tools were run until fracture or chip off. Tool life was set based on a limiting wear value for each material.

The effect of chip load and cutting speed on tool life was observed for both CP titanium and 316 L stainless steel.

4.6.1 Model for microdrilling of CP titanium

As the cutting speed was increased from 12.5 m/min to 20 m/min at a constant chip load of 0.1µm/flute, greater tool wear was observed at higher cutting speed for the same drilling distance (FIGURE 50). This increase in tool wear was because of increase in cutting temperature at the tool metal interface which led to thermal softening of the tool material. Rahim and Sharif (2006) also reported severe tool wear at higher cutting speeds while drilling titanium alloys. Ezugwu and Wang (1997) also reported cutting speed as the most influencing parameter on tool life while machining titanium alloys. They found that the tool life dramatically improved as the cutting speed was reduced. However, at lower cutting speeds (6 m/min) tendency to form BUE increases which may ultimately lead to tool failure.

Also, increase in chip load from 0.05 μm/flute to 1 μm/flute for the same cutting speed led to an increase in tool wear (FIGURE 50). However, effect of cutting speed on tool wear was more prominent compared to chip load. Tool life was sensitive to feedrate and therefore to chip load while machining titanium alloy (Ezugwu and Wang, 1997). From tool wear characteristics, maximum drilling distance of 110 mm was attained at a cutting speed of 12 m/min and chip load of 0.05μm/flute. The limiting tool wear criteria for drilling CP titanium was chosen to be 8 μm. The limiting tool wear was chosen as the minimum of the maximum tool wear values for different cutting conditions before tool failure.

Drilling distance was plotted against cutting speed in a log-log plot at constant chip loads (FIGURE 51). Tool life decreased at higher chip loads for same cutting speed as seen in the plot. This was due to higher temperature and force at higher chip load.

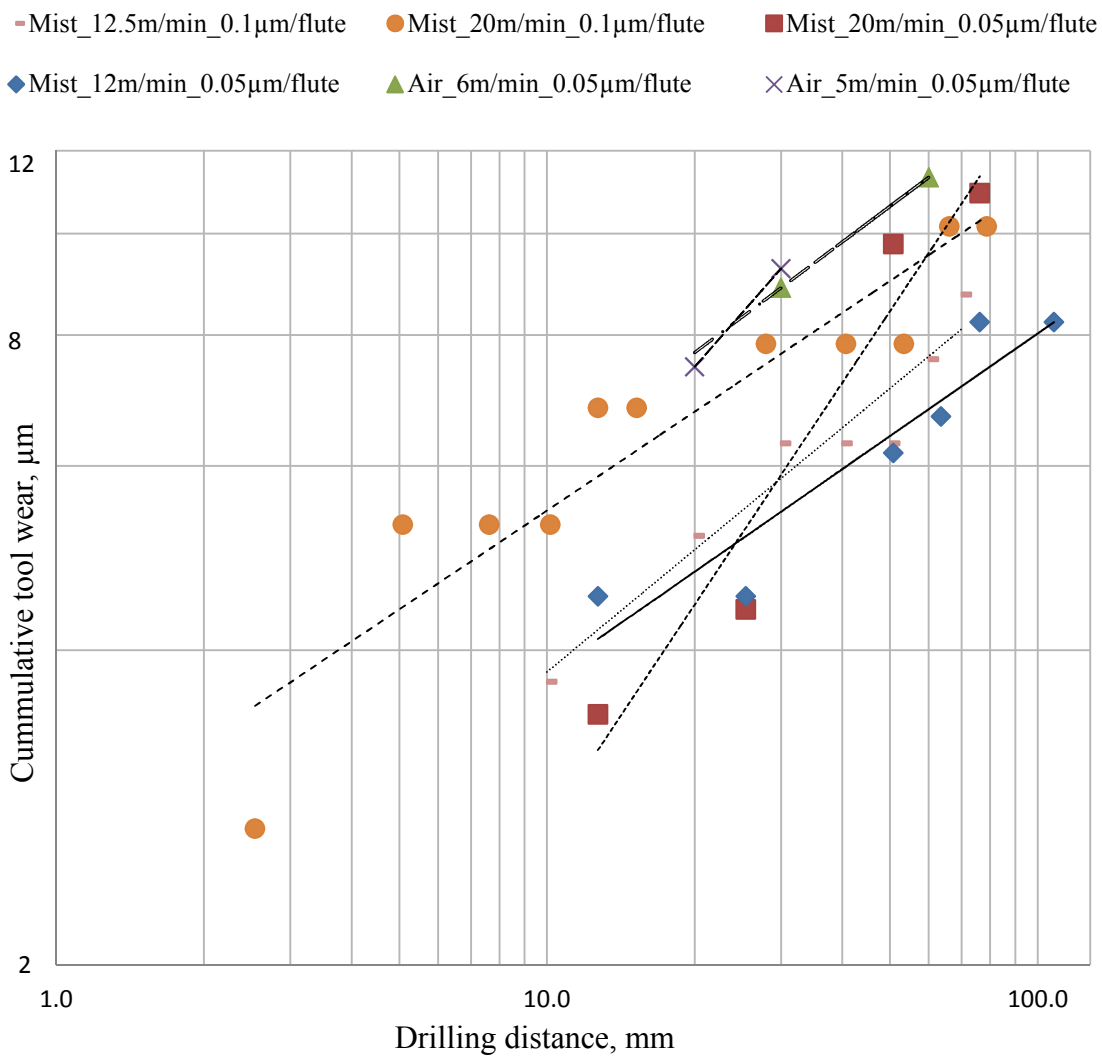

FIGURE 50 Tool wear under different cutting conditions while drilling CP titanium.

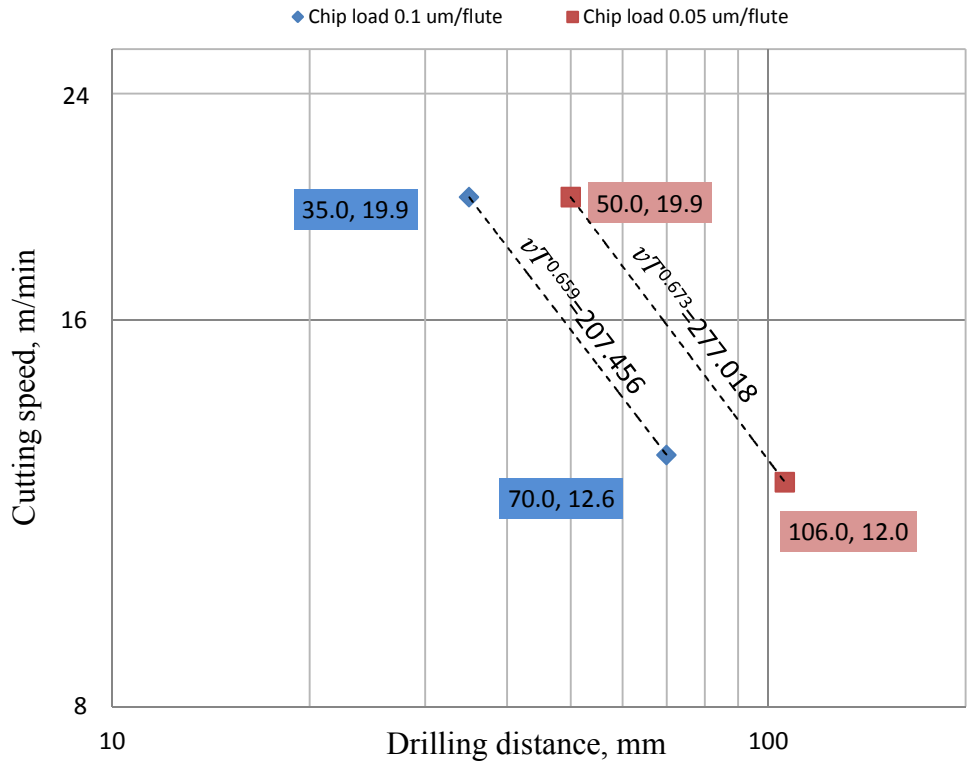

FIGURE 51 Tool life for CP titanium .Tool wear criteria of 8µm.

Taylor tool life equation is used to solve for constants that relate the tool life to a cutting speed.

$$v f_c^a T^n = C \tag{6}$$

where, v = cutting speed (m/min), f_c = chip load (µm/flute), T = tool life or drilling distance (mm), values of a, n, and C depend on workpiece, tool material and cutting conditions.

$$v T^n = C / f_c^a \tag{7}$$

$$vT^n = C' \tag{8}$$

By solving for *n* and *C'* we can calculate tool life for a particular cutting speed and chip load for a given material.

From FIGURE 51 we have two cutting speeds and corresponding tool life (in terms of drilling distance) for a given chip load which can be used to solve for constants. The calculation for finding out the constants is shown below for chip load of 0.1µm/flute.

$$19.9\ (\frac{m}{min}) * 35^n (mm)^n = C' \tag{9}$$

Similarly,

$$12.6\ (\frac{m}{min}) * 70^n (mm)^n = C' \tag{10}$$

Solving for n and C'

$$\ln 19.9 + n * \ln 35 = \ln 12.6 + n * \ln 70 \tag{11}$$

$$n = \frac{\ln 19.9 - \ln 12.6}{\ln 70 - \ln 35} \tag{12}$$

$$n = 0.659$$

$$C' = 207.456$$

The equation of the tool life for 0.1 µm/flute is

$$vT^{0.659} = 207.456 \tag{12a}$$

Once these constants are known, tool life can be found for different cutting speeds at same chip load by using Taylor's equation.

Similar calculation can be done for chip load of 0.05 µm/flute.

$$n = 0.673$$

$$C' = 277.018$$

$$vT^{0.673} = 277.018 \quad \text{(12b)}$$

4.6.2 Model for microdrilling of 316L stainless steel

Similar trends were observed in tool wear characteristics for both CP titanium and 316 L stainless steel. As the cutting speed was increased from 14 m/min to 20 m/min at a constant chip load of 0.02 µm/flute, greater tool wear was observed at 20 m/min speed for the same drilling distance (FIGURE 52). This increase in tool wear was because of increase in cutting temperature at the tool metal interface due to poor thermal conductivity of 316L stainless steel. Chip loads used were much lower compared to CP titanium as higher chip loads led to severe tool wear. Also, for the same drilling distance tool wear for 316L stainless steel was higher compared to CP titanium. This can be attributed to its tendency to work harden easily which makes it difficult to machine. Maximum drilling distance of 100 mm was obtained with cutting speed of 14 m/min and chip load of 0.02 µm/flute.

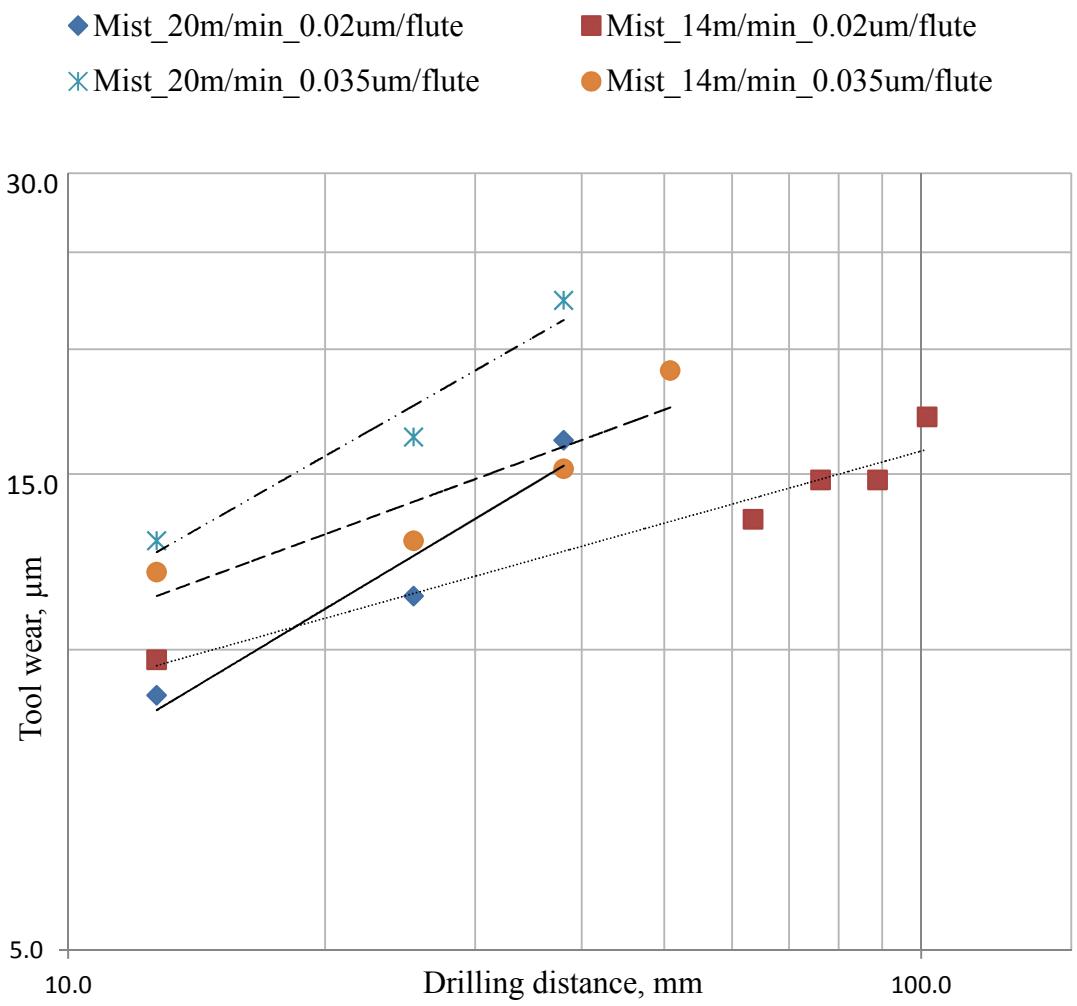

FIGURE 52 Tool wear under different cutting conditions while drilling 316L stainless steel with a limiting tool wear criteria of 15µm.

Increase in tool wear at higher cutting speed was also observed by Hoshi et al. (1981) in micro deep drilling of stainless steel. They used a grade of stainless steel for their experiments which had a lower percentage of Ni compared to 316L stainless steel. Nickel imparts work hardening property to the steel which makes 316L more difficult to machine. They measured tool wear on drill of diameter 0.350 mm and reported difficulty in measuring wear for drill of diameter 0.1 mm.

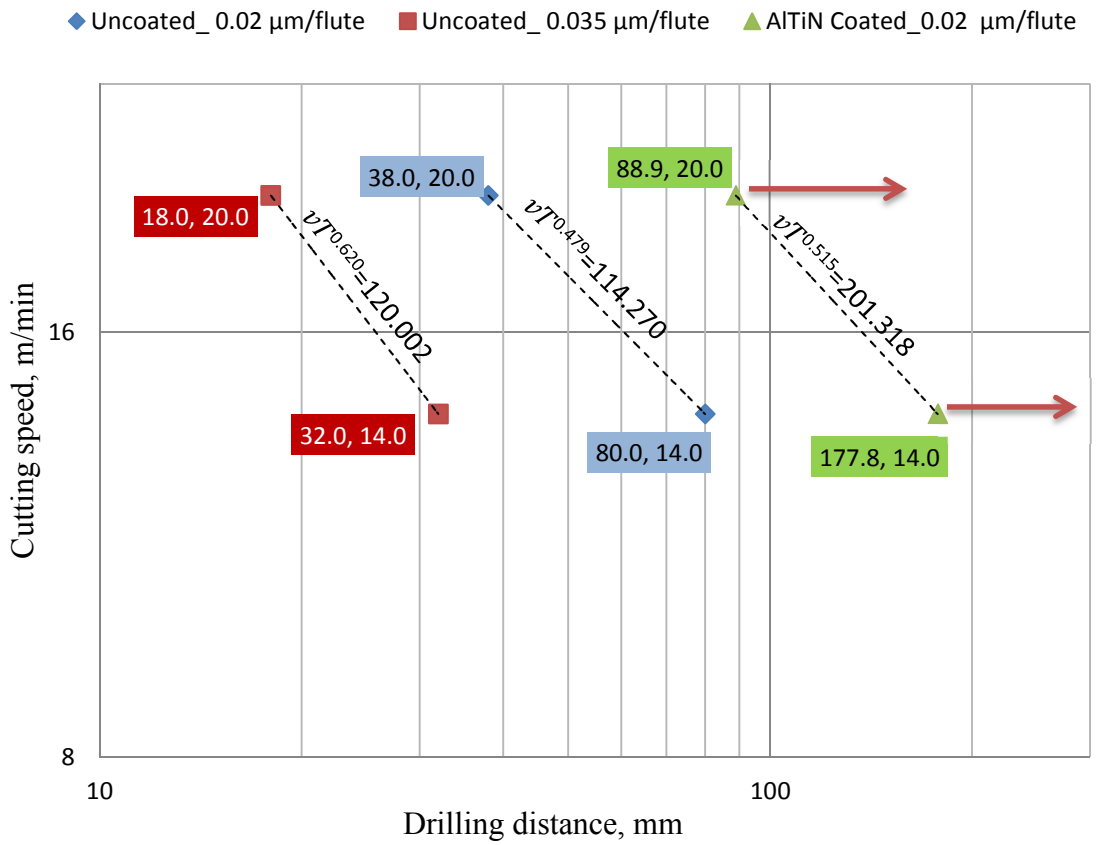

FIGURE 53 Tool life for drilling 316L stainless steel. Tool wear criteria of 15µm.

The limiting tool wear criteria for drilling 316L stainless steel was 15 µm which was shown by dotted line (FIGURE 52). The limiting tool wear was chosen as the minimum of the maximum tool wear values for different cutting conditions before tool failure. Tool life in terms of drilling distance could be found until the tool was worn out by 15 µm for each cutting speed and chip load combination from FIGURE 52. For AlTiN coated tools the limiting tool wear criteria was characterized by chipping of coating form the drill. Characteristics between cutting speed and drilling distance was plotted for

each chip load in a log-log plot (FIGURE 53). It was evident from the graph that tool life decreases with increase in cutting speed and chip load. Tool life can be found for chip loads of 0.02 µm/flute and 0.035 µm/flute and a cutting speed from the graph.

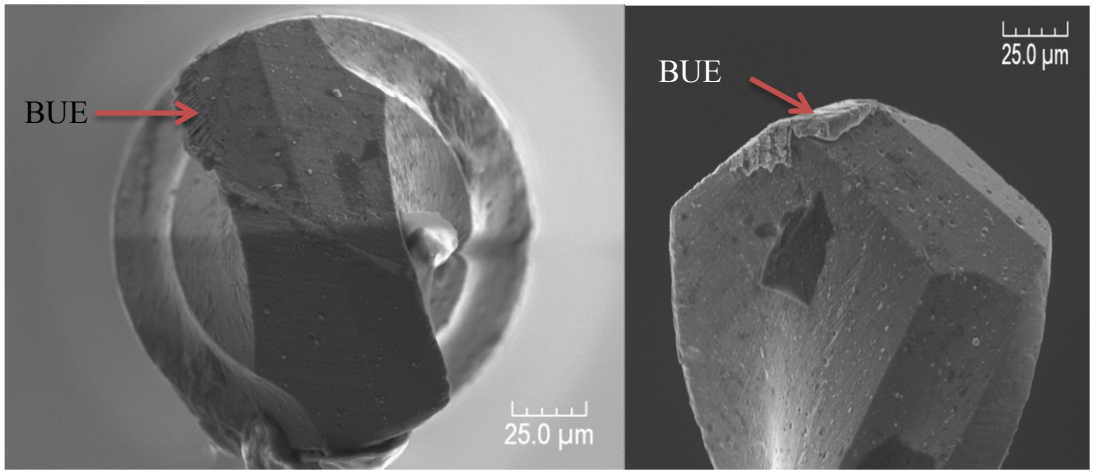

(a) (b)

FIGURE 54 Microdrill coated with AlTiN. Drilling 316 L stainless steel at a chip load 0.02 µm/flute with mist coolant. (a) cutting speed 14 m/min, drill distance of 177.8 mm (b) cutting speed 20 m/min, drilling distance 88.9 mm respectively.

It can be seen from the graph that for a cutting speed of 20 mm/min and comparable drilling distance of 35 mm, the chip load for 316L stainless steel is 0.02 μm/flute which is much lower than chip load of 0.1 μm/flute for CP titanium. This also implies that CP titanium can be microdrilled 400% faster than 316L stainless steel.

Also, for coated drill the tool life was greater than uncoated tool for the same chip load. This can be explained by less BUE formation which decreased the adhesive wear in the tool. Notch wear which was seen earlier in case of uncoated tools was absent in case of AlTiN coated tools for both cutting speeds hence the actual tool life would be greater than the result shown above. Again Taylor's equation can be used to solve for constants and tool life can be found for different cutting speeds at a constant chip load. Cutting speeds and corresponding tool life values are substituted in Equation (8) for a chip load of 0.035 μm/flute.

$$20\left(\frac{m}{min}\right) * 18^n (mm)^n = C' \tag{13}$$

Similarly,

$$14\left(\frac{m}{min}\right) * 32^n (mm)^n = C' \tag{14}$$

$$\ln 20 + n * \ln 18 = \ln 14 + n * \ln 32 \tag{15}$$

$$n = \frac{\ln 20 - \ln 14}{\ln 32 - \ln 18} \tag{16}$$

$$n = 0.620$$

$$C' = 120.002$$

$$vT^{0.620} = 120.002 \tag{16a}$$

Similar calculation can be done for a chip load of 0.02 μm/flute.

For uncoated drill,

$$n = 0.479$$

$$C' = 114.270$$

$$vT^{0.479} = 114.270 \tag{16b}$$

For AlTiN coated drill,

$$n = 0.515$$

$$C' = 201.318$$

$$vT^{0.515} = 201.318 \tag{16c}$$

4.7 Hole quality

4.7.1 Drill wandering and position accuracy

Drill wandering is one of the major problems associated with microdrilling. This could happen if the drill was not centered and drill tip started to skid. The skidding motion increased the radial force which ultimately led to tool failure while entry. It also affects the position accuracy of the hole. In microdrilling it is sometimes difficult to use a center drill to position the hole accurately due to smaller size of center drill which is difficult to manufacture.

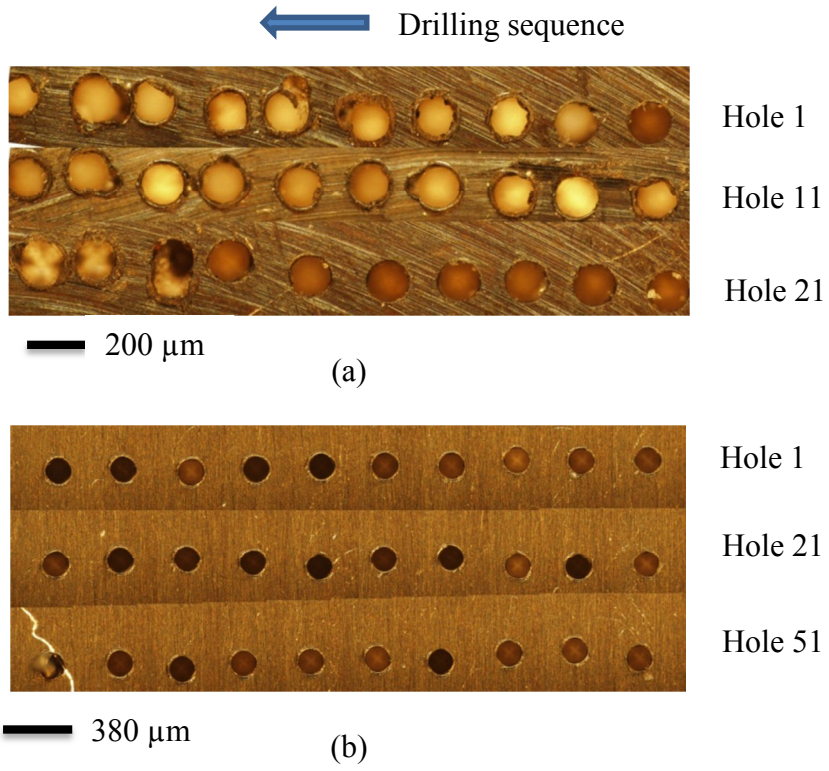

FIGURE 55 Hole wandering in drilling CP titanium. (a) Unpolished surface; cutting speed: 4 m/min, chip load: 1 µm/flute, aspect ratio: 2:1. (b) Polished surface; cutting speed 12 m/min, chip load: 0.05 µm/flute, aspect ratio: 10:1.

Wandering in microdrilling was studied by Kudla (2011). They have discussed drill tip wandering while drilling stainless steel workpiece. Cheong et al. (1999) has also discussed wandering in microdrilling and various boundary conditions to avoid drill wandering. In all the cases, rows of holes were studied for wandering motion of the drill. The deviation in hole position was plotted against number of holes.

While drilling Ti, the tool fractured after drilling first few holes. Upon closer examination of the workpiece it was found that the holes were irregular in shape due to drilling on milled surface (FIGURE 55). The surface was polished to improve hole position and minimize drill skidding.

Also, parallelism of the workpiece was ensured during grinding to avoid increase in radial force during drilling. Noticeable difference was observed in positioning accuracy after grinding and polishing the workpiece. The mean deviation in hole position was reduced by 38% (FIGURE 56). A paired t-test was performed to confirm the difference in means between two samples (TABLE 29).

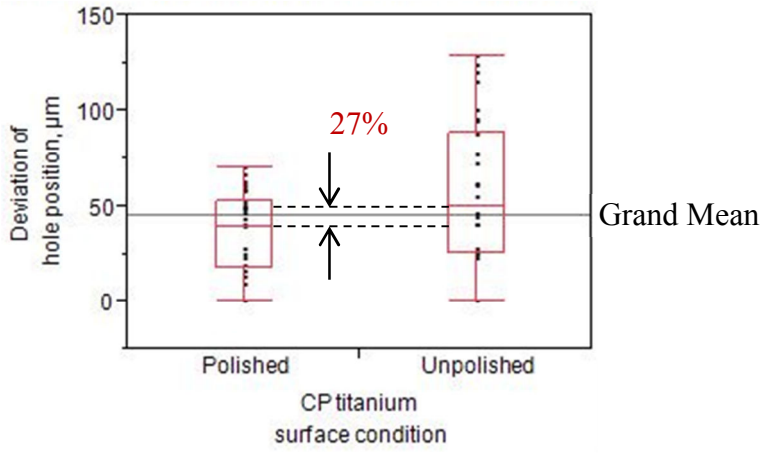

FIGURE 56 Box plot showing the deviation of hole position in polished and unpolished sample of CP titanium.

TABLE 29 Paired t-test to Compare Means of Deviation of Hole Position in Polished and Unpolished Sample of CP Titanium. Sample Size = 60, Null hypothesis, H_o: $\mu_{polished} = \mu_{unpolished}$

Statistical characteristics	Values	Statistical characteristics	Values
Difference	0.021610	t-Ratio	2.673914
Standard Error Difference	0.008082	Degree of freedom	45.86017
Upper Control Limit Difference	0.037878	Prob > |t|	0.0104
Lower Control Limit Difference	0.005341	Prob > t	0.0052
Confidence	0.95	Prob < t	0.9948

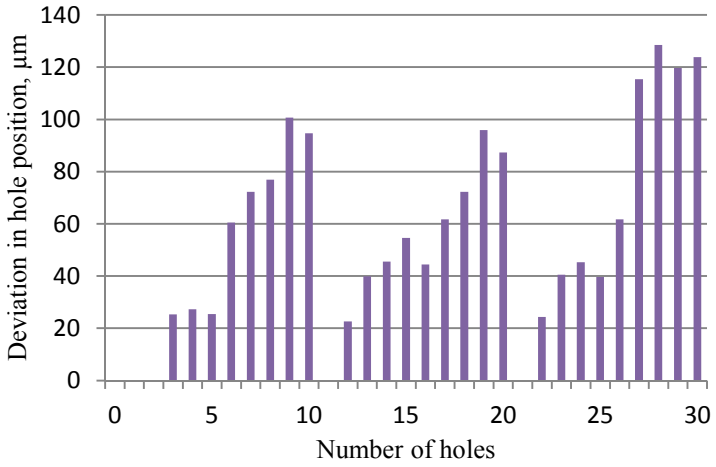

FIGURE 57 Position deviation of consecutive holes. Uncoated tool on CP titanium. Unpolished surface; cutting speed: 4 m/min, chip load: 1 µm/flute, aspect ratio: 2:1.

It was observed that the deviation in hole position increased along a row (FIGURE 57). The drop in hole position deviation between rows could be explained by ultrasonic cleaning of microdrills removing chips attached to the tool. Grinding and polishing removed surface irregularities and made the surface more even. This reduced the tendency of the drill to drift hence decreasing the deviation in hole position (FIGURE 58). This could happen due to the formation of BUE on the chisel during drilling which could lead to wandering motion. Also the position accuracy of the spindle was ±5 µm which could also affect the position of the hole.

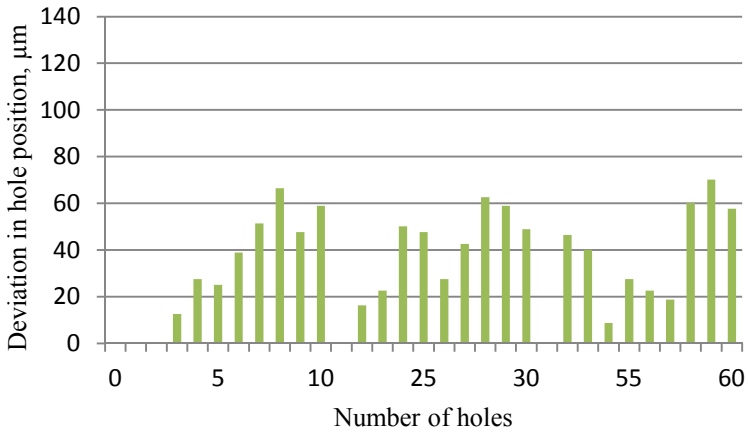

FIGURE 58 Position deviation of consecutive holes. Uncoated tool on CP titanium. Polished surface; cutting speed 12 m/min, chip load: 0.05 µm/flute, aspect ratio: 10:1.

Drill wandering when drilling 316L stainless steel was studied for both coated and uncoated drills (FIGURE 59). Deviation in hole position was higher in case of uncoated tool compared to coated (FIGURE 60). This difference could be seen in the paired t-test which verified that there was a significant difference between the samples of coated and uncoated tool (TABLE 30).

AlTiN coated tool reduced tool wear. It showed improvement in terms of less BUE formation and hence less deviation in hole position. Also there was comparatively less wear of the chisel edge in coated tool which also helped in better positioning of the tool. The bar graphs also show progressive increase in hole deviation along a row with maximum deviation being lower in case of coated tools (FIGURE 61 and FIGURE 62).

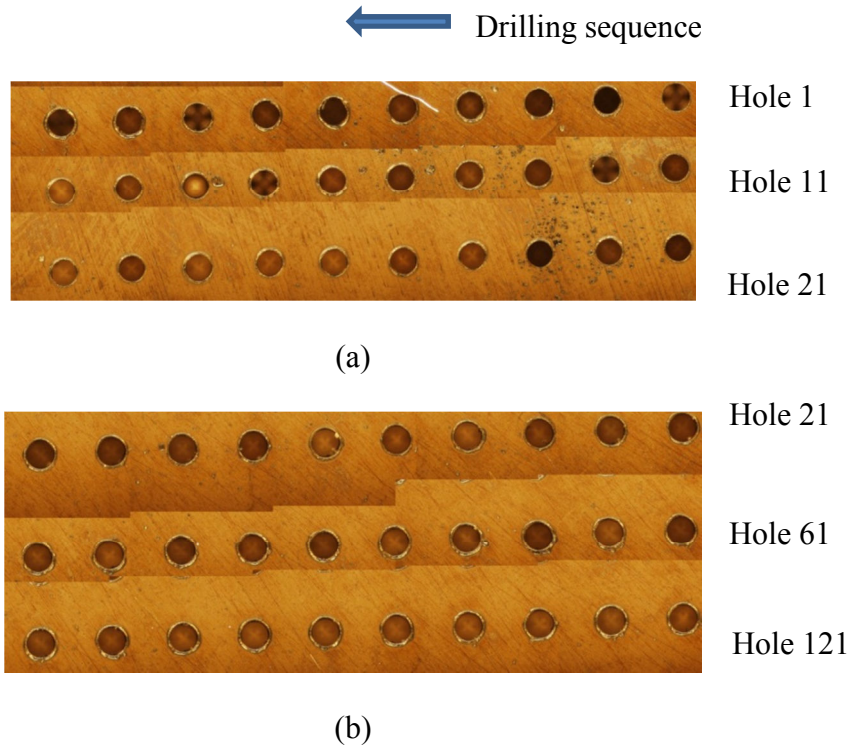

FIGURE 59 Hole wandering in drilling 316L stainless steel. (a) Uncoated tool; cutting speed: 14 m/min, chip load: 0.02 µm/flute. (b) AlTiN coated tool; cutting speed: 14 m/min, chip load: 0.02 µm/flute.

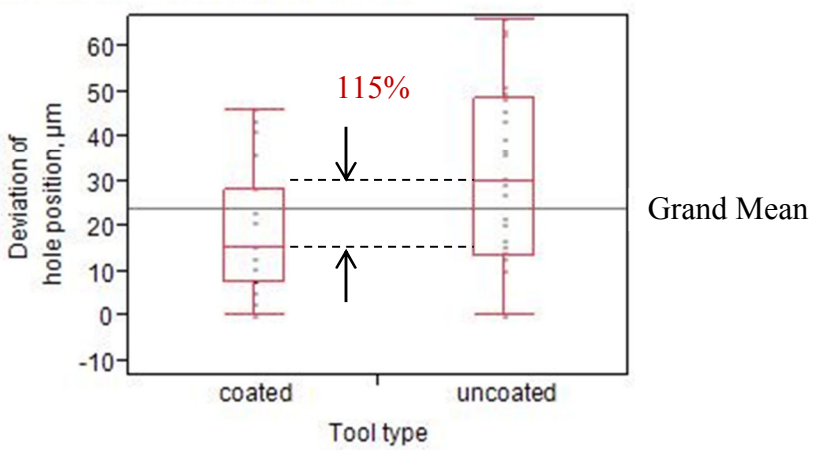

FIGURE 60 Box plot showing the deviation of hole position while drilling 316L stainless steel with coated and uncoated tool.

TABLE 30 Paired t-test to Compare Means of Deviation of Hole Position while Drilling 316L stainless steel with Coated and Uncoated Tool. Sample Size = 60, Null hypothesis, H_o: $\mu_{coated} = \mu_{uncoated}$

Statistical characteristics	Values	Statistical characteristics	Values
Difference	0.012157	t-Ratio	2.61382
Standard Error Difference	0.004651	Degree of Freedom	49.89187
Upper Control Limit Difference	0.021499	Prob > |t|	0.0118
Lower Control Limit Difference	0.002815	Prob > t	0.0059
Confidence	0.95	Prob < t	0.9941

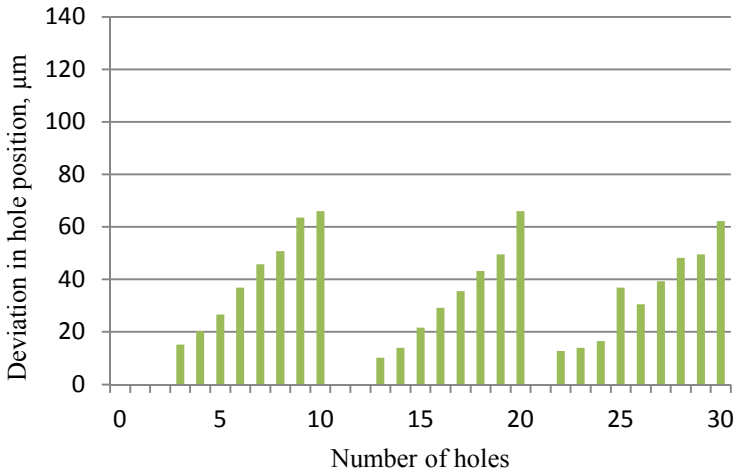

FIGURE 61 Position deviation of consecutive holes. Uncoated tool on 316L stainless steel. Cutting speed: 14 m/min, chip load: 0.02 µm/flute.

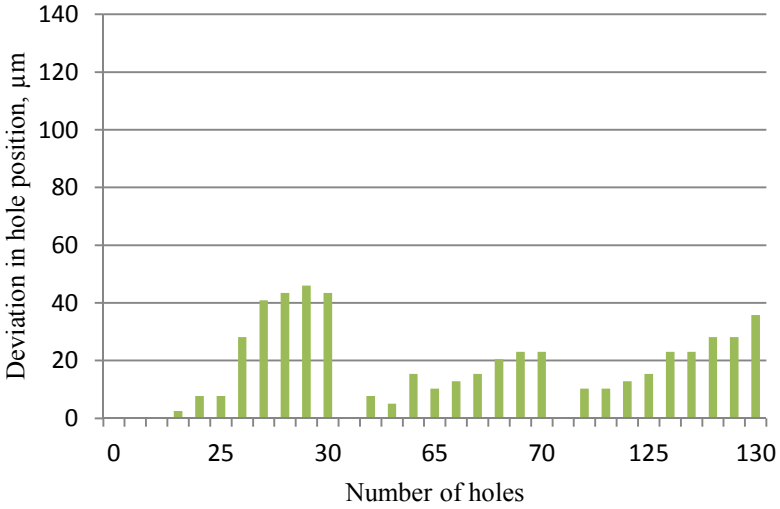

FIGURE 62 Position deviation of consecutive holes. AlTiN coated tool on 316L stainless steel. Cutting speed: 14 m/min, chip load: 0.02 µm/flute.

Aluminum alloy sample was not polished before drilling (FIGURE 63). Deviation in hole position was less than CP Ti and 316L stainless steel (FIGURE 64).

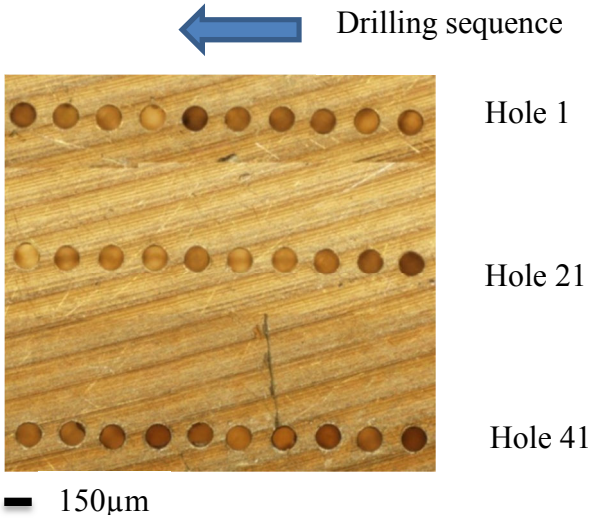

FIGURE 63 Hole wandering in drilling unpolished aluminum 6061-T6. Cutting speed: 8 m/min, chip load: 1 µm/flute.

Low tool wear when drilling aluminum alloy reduced BUE, hole position deviation, and burr formation.

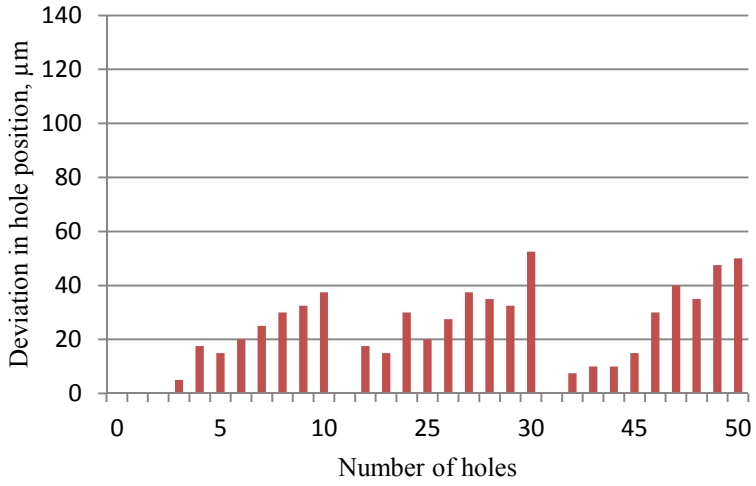

FIGURE 64 Position deviation of consecutive holes. Uncoated tool on unpolished aluminum 6061-T6. Cutting speed: 8 m/min, chip load: 1 µm/flute.

Similar analysis was done for microdrilling of PEEK. Deviation in hole position was studied before and after polishing (FIGURE 65). Significant improvement was observed after polishing the workpiece (FIGURE 66). Bar graph was plotted to show the deviation in hole position along different rows (FIGURE 67 and FIGURE 68). TABLE 31 shows the paired t-test for comparing hole position deviation in polished and unpolished sample.

However, severe burr formation was observed on the entry side. The hole circumference was not clearly visible due to burr formation which made the task of finding hole deviation very difficult. Perhaps this was the reason for high hole deviation on PEEK

compared to other metals. Also, a dark ring was formed around the periphery of the hole while drilling. This might affect the surface property of the material.

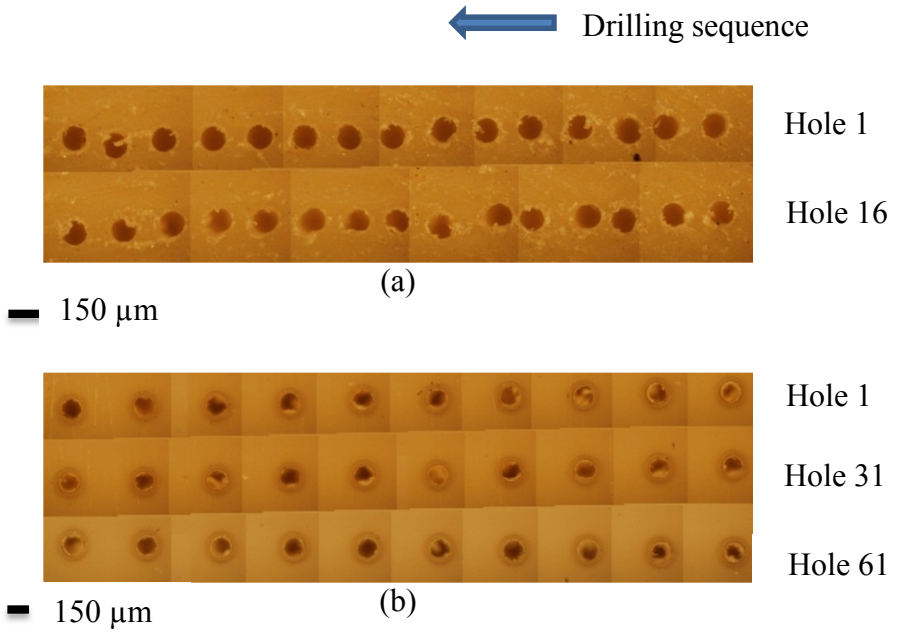

FIGURE 65 Hole wandering in drilling PEEK. (a) Unpolished; cutting speed: 4 m/min, chip load: 0.06 µm/flute. (b) Polished; cutting speed: 4 m/min, chip load: 0.06 µm/flute.

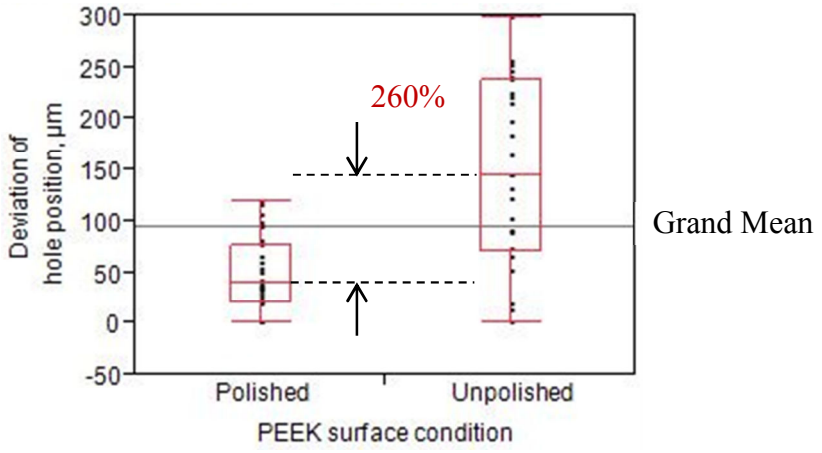

FIGURE 66 Box plot showing the deviation of hole position while drilling polished and unpolished sample of PEEK.

TABLE 31 Paired t-test to Compare Means of Deviation of Hole Position while Drilling Polished and Unpolished Sample of PEEK. Sample Size = 60, Null hypothesis, H_o: $\mu_{polished} = \mu_{unpolished}$

Statistical characteristics	Values	Statistical characteristics	Values
Difference	0.096653	t-Ratio	5.32526
Standard Error Difference	0.018150	Degree of Freedom	37.7613
Upper Control Limit Difference	0.133403	Prob > |t|	<.0001
Lower Control Limit Difference	0.059903	Prob > t	<.0001
Confidence	0.95	Prob < t	1.0000

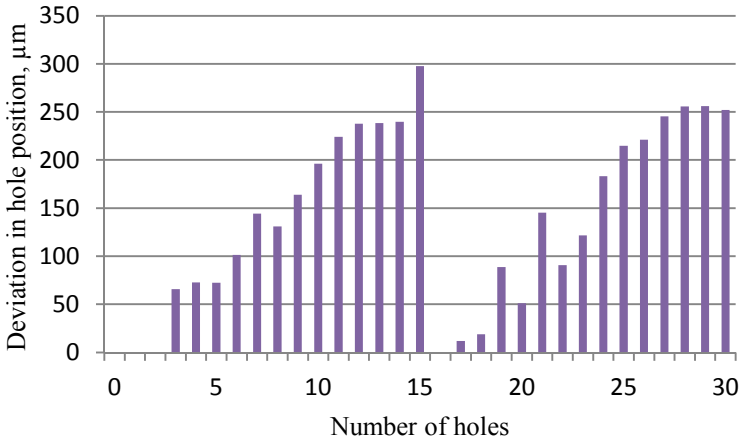

FIGURE 67 Position deviation of consecutive holes. Uncoated tool on unpolished PEEK. Cutting speed: 4 m/min, chip load: 0.06 µm/flute.

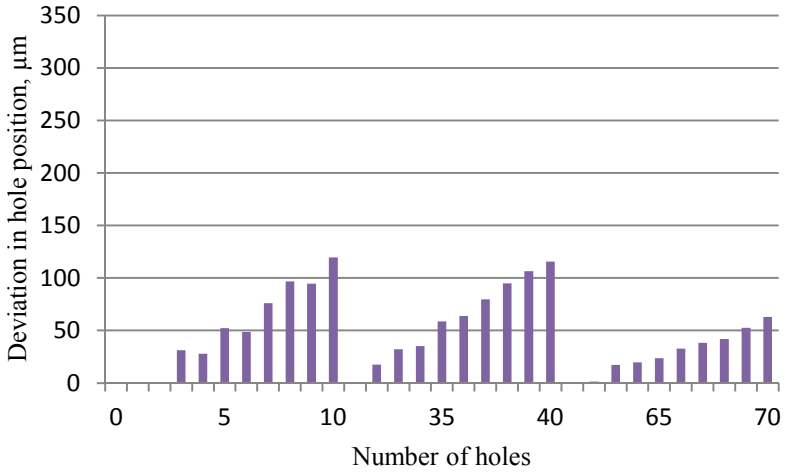

FIGURE 68 Position deviation of consecutive holes. Uncoated tool on polished PEEK. Cutting speed: 4 m/min, chip load: 0.06 µm/flute.

4.7.2 Hole diameter

Variation in hole diameter was studied for CP titanium and 316 L stainless steel. Diameter was measured along the row of holes. Analysis of variance (ANOVA) was conducted to verify the difference in means of diameter along the rows (TABLE 32, TABLE 33, TABLE 34). Significant difference between diameters was observed along the row in both the materials (FIGURE 69). Total variation in diameter was quantified as maximum percentage change in diameter per unit of drilling distance. The hole diameter reduced as we drilled more holes along the row. This could be explained by the wear in tool cutting edges as we drill more holes. In case of 316L stainless steel, hole diameter was studied for both coated and uncoated tools. The variation in diameter between rows was found to be more in case of uncoated tool as compared to coated tool (FIGURE 70

and FIGURE 71). This could be explained by less wear of coated tools as compared to uncoated one.

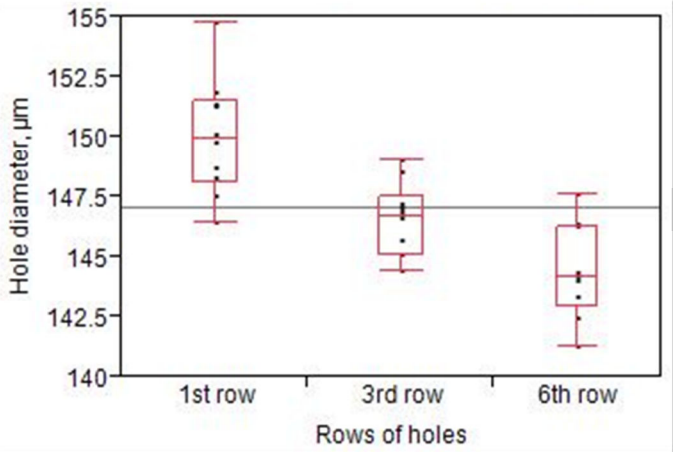

FIGURE 69 Box plot showing variation in hole diameter between rows in polished CP titanium. Total variation in diameter 0.052% per mm. Cutting speed 12 m/min, chip load: 0.05 µm/flute.

TABLE 32 Anova Comparing Means for Variation in Hole Diameter Between Rows in CP Titanium. Sample Size = 29, Null hypothesis, H_o: $\mu_{1st\ row} = \mu_{3\ rd\ row} = \mu_{6th\ row}$

Source	Degree of Freedom	Sum of Squares	Mean Square	F Ratio	Prob > F
Row of holes	2	0.00015161	0.000076	18.5038	<.0001
Error	26	0.00010652	0.000004		
Total	28	0.00025813			

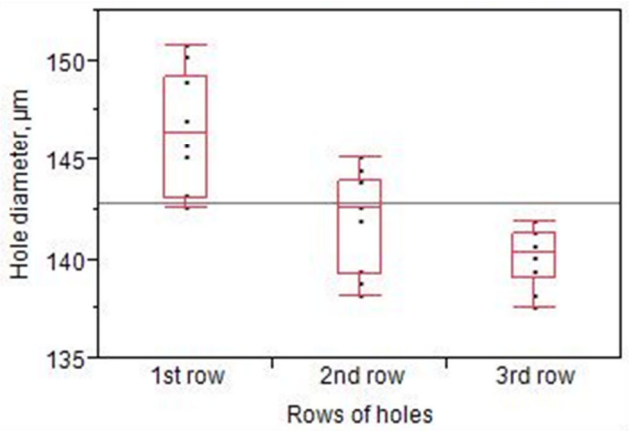

FIGURE 70 Box plot showing variation in hole diameter between rows in 316L stainless steel drilled with uncoated tool. Total variation in diameter 0.11% per mm. Cutting speed: 14 m/min, chip load: 0.02 µm/flute.

TABLE 33 Anova Comparing Means for Variation in Hole Diameter Between Rows in 316L Stainless Steel Drilling with Uncoated Tool. Sample Size = 30, Null hypothesis, H_o: $\mu_{1st\ row} = \mu_{2nd\ row} = \mu_{3rd\ row}$

Source	Degree of Freedom	Sum of Squares	Mean Square	F Ratio	Prob > F
Row of holes	2	0.00021304	0.000107	17.9754	<.0001
Error	27	0.00016000	0.000005		
Total	29	0.00037303			

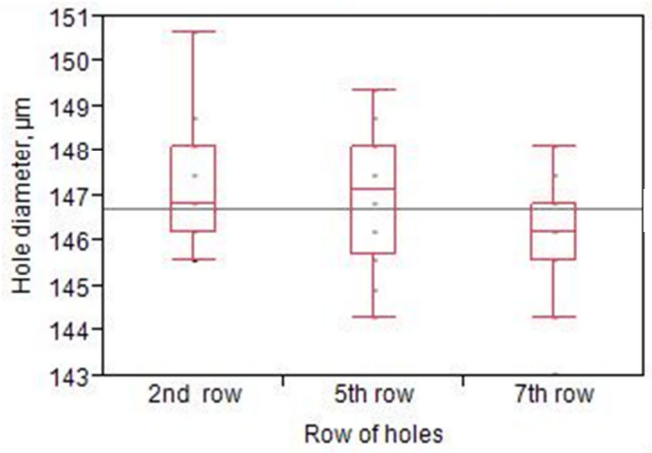

FIGURE 71 Box plot showing variation in hole diameter between rows in 316L stainless steel drilled with AlTiN coated tool. Total variation in diameter 0.003% per mm. Cutting speed: 14 m/min, chip load: 0.02 µm/flute.

TABLE 34 Anova Comparing Means for Variation in Hole Diameter Between Rows in 316L Stainless Steel Drilling with AlTiN Coated Tool. Sample Size = 60, Null hypothesis, H_o: $\mu_{2nd\ row} = \mu_{5th\ row} = \mu_{7th\ row}$

Source	Degree of Freedom	Sum of Squares	Mean Square	F Ratio	Prob > F
Row of holes	2	0.00001187	0.0000059348	3.4712	0.0378
Error	57	0.00009745	0.0000017097		
Total	59	0.00010932			

4.7.3 Hole straightness

Hole straightness was studied for both CP titanium and 316 L stainless steel. For studying straightness of the hole the sample was sectioned between the holes and polished as explained earlier FIGURE 72.

A point was taken on the edge of the hole as an origin. Both X and Y coordinates were measured for different points along the edge of the hole. These points were plotted and a best fit line was drawn for CP titanium (FIGURE 73). Points which were farthest apart from this line on both the sides gave the error in straightness. Straightness was measured along the depth of the hole for a distance of 254 μm which in this case was twice the diameter (FIGURE 74). Similar plot was repeated for 316L stainless steel (FIGURE 75).

It can be seen that the spread of error in straightness was higher in 316L stainless steel compared to CP titanium. This could be due to strong built up edge formation near chisel edge in 316L stainless steel which could affect the geometry of the hole.

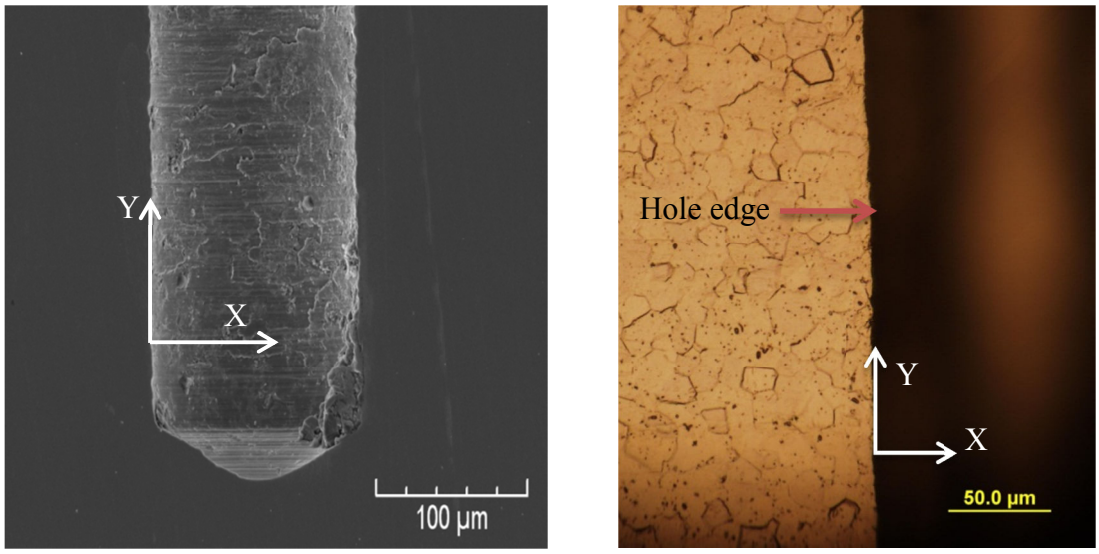

(a) (b)

FIGURE 72 Sectioned hole to measure straightness in CP titanium. Cutting speed: 20m/min, chip load: 0.05µm/flute. (a) Micrograph of hole section (b) Magnified view of hole edge.

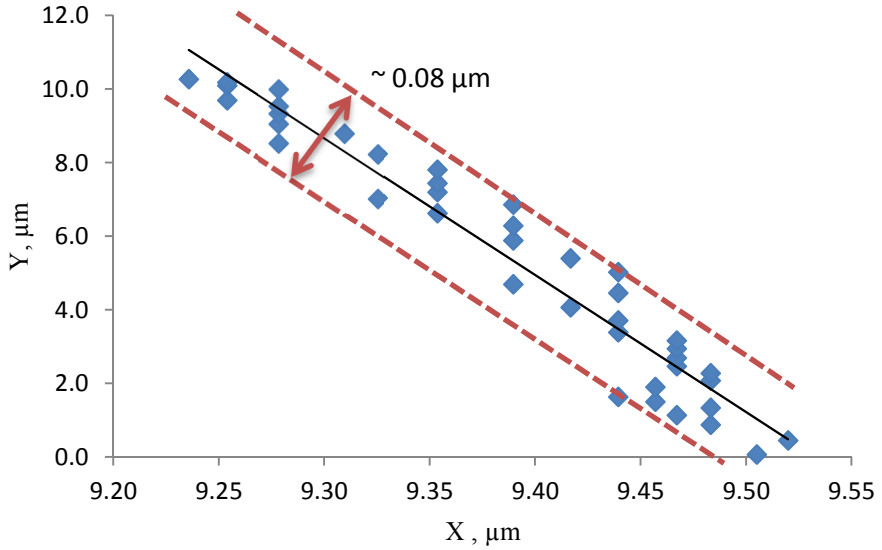

FIGURE 73 Hole straightness in drilling CP titanium. Cutting speed: 20m/min, chip load: 0.05µm/flute.

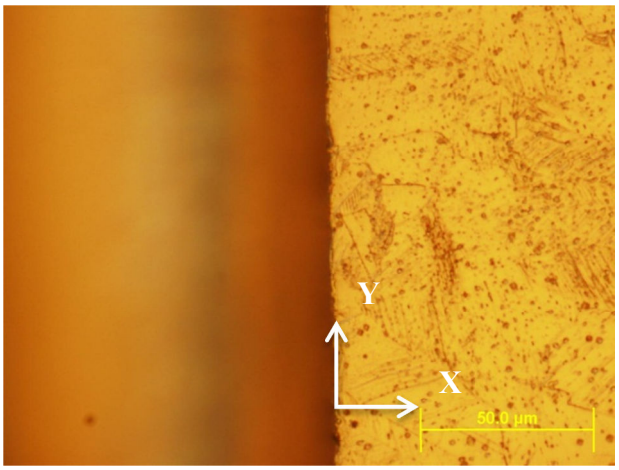

FIGURE 74 Edge of a sectioned hole to measure straightness in 316L stainless steel. Cutting speed: 14 m/min, chip load: 0.035µm/flute.

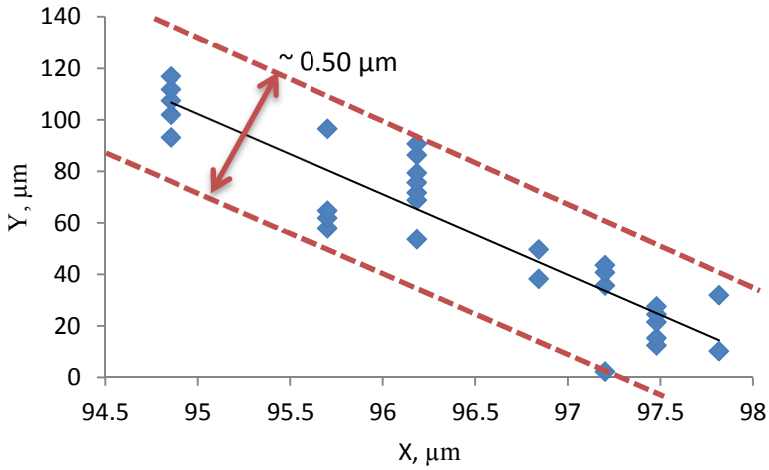

FIGURE 75 Hole straightness in drilling 316L stainless steel. Cutting speed: 14 m/min, chip load: 0.035µm/flute.

5. CONCLUSIONS

This research studied microdrilling of CP titanium, 316L stainless steel, aluminum 6061-T6, and PEEK plastic. It was found that:

1. Surface polishing was the key to successfully drill microholes. A rough surface deflected microdrill tip and caused positioning errors as well as premature tool failure.
2. Microholes of diameter 127 μm were successfully drilled on all materials at 10:1 aspect ratio using micromist and progressive pecking cycle. The selected parameters allowed at least 70 holes to be drilled with single tool on all tested materials.
3. Microdrill wear at the outer corner was more pronounced when drilling CP titanium but attrition wear at chisel edge was more significant for 316L stainless steel. Insignificant tool wear was found after drilling more than 150 holes on 6061-T6 aluminum and PEEK plastic.
4. The classical Taylor's equation for macro machining was applicable in microdrilling to rank tool performance and machinability of CP titanium and 316L stainless steel. For the same cutting speed of 20 m/min and comparable drilling distance of about 35 mm, CP titanium can be microdrilled 400% faster than 316L stainless steel since the chip load for the former is 0.1 μm/flute and that for the latter is 0.02 μm/flute. Also, AlTiN coated drills improved tool life by at least 122%.

5. Coated drills significantly improved hole quality. Hole position accuracy improved by 115%. Total variation in diameter decreased from 0.11% to 0.003% per mm of drilling distance.

Although, deep hole microdrilling was successful for all tested materials for a range of chip loads, productivity and cost should be optimized for AlTiN and other coating materials. Specific coating should be investigated for different materials such as CP titanium and Ni-Ti alloys. Another interesting direction for future research is to develop techniques to drill with minimum burr, or subsequent burr removal because burr formation at the entry or exit ends of a hole was often observed during the experiments.

REFERENCES

Allen D.; Almond H.; Logan P. (2000) A technical comparison of micro-electrodischarge machining, micro drilling and copper vapour laser machining for the fabrication of ink jet nozzles. *Proceedings SPIE*; Paris, France, 531-540.

Arrazola, P.J.; Garay, A.; Iriarte, L.M.; Armendia, M.; Marya, S.; Le Maître, F. (2009) Machinability of titanium alloys (Ti6Al4V and Ti555.3). *Journal of Materials Processing Technology*, 209(5): 2223–2230.

ASM Handbook (1990) *Properties and Selection: Irons, Steels, and High-Performance Alloys,*Vol.1, ASM International, Materials Park, OH, USA.

AZoM™, Pty.Ltd., Grade 316L – Properties, fabrication and applications, 10/20/2011, retrieved from: http://www.azom.com/Details.asp?ArticleID=2382.

BAM federal institute for material research and testing, surface technologies, 10/05/2011, retrieved from: http://www.bam.de/en/kompetenzen/fachabteilungen /abteilung_6/fg64/fg64_ag1e.htm

Boyer, R.; Welsch, G.; Collings, E. (1994) *Materials Properties Handbook: Titanium Alloys,* ASM International, Materials Park, OH, USA.

Chandrasekaran, H.; Johansson, J. O. (1994) Chip flow and notch wear mechanisms during the machining of high austenitic Stainless Steels. *CIRP Annals - Manufacturing Technology,* 43(1): 101-105.

Chern, G.L.; Lee, H.J. (2005) Using workpiece vibration cutting for micro-drilling. *The International Journal of Advanced Manufacturing Technology*, 27: 688-692.

Cheong, M .S., Cho, D. W., Ehmann, K.F. (1999) Identification and control for micro-drilling control and productivity enhancement. *International journal for machine tools and manufacture*, 39 (1): 1539-1561.

Chittipolu, S. (2009) Failure prediction and stress analysis of micro-cutting tools*,* Masters Thesis, *Texas A&M University*, College Station, TX, USA.

Dolinsek, S. (2003) Work-hardening in the drilling of austenitic stainless steels. *Journal of Materials Processing Technology,* 133(1-2): 63–70.

Dornfeld, D.; Kim, J.; Dechow, H.; Hewson, J.; Chen, L. (1999) Drilling burr formation in titanium alloy, Ti-6Al-4V. *CIRP Annals*, 48(1): 73-76.

Endrino, J.L.; Fox-Rabinovich, G.S.; Gey, C.; (2006) Hard AlTiN, AlCrN PVD coatings for machining of austenitic stainless steel. *Surface & Coatings Technology,* 200(24); 6840-6845.

Ezugwu, E.O.; Wang, Z. W. (1997) Titanium alloys and their machinability- a review. *Journal of Materials Processing Technology,* 68(3): 262-274.

GF AgieCharmilles, Wire Cut EDM, 10/20/2011, retrieved from: http://www.gfac.com /gfac /products/wire-cut- edm/general-purpose/cut-20-p.html?L=0

Ginting, A.; Che Haron, C. H.; Arshad H.(2004) Performance of carbide tools in green machining of Ti-6242S. *Pertanika Journal of Science and Technology,* 12(2): 101-112.

High Point Precision Products. Haas OM Series, 10/20/2011, retrieved from: http://www.highpointprecision.com/DS_OMSeries_US.pdf

Hung, N.P.; Zhong, C.H. (1996) Cumulative tool wear in machining metal matrix composites Part I: Modeling. *Journal of Materials Processing Technology*, 58(1):109-113.

Imran, M.; Mativenga, P.; Kannan, S.; Novovic, D. (2008) An experimental investigation of deep-hole microdrilling capability for a nickel-based superalloy. *Proceedings of the Institution of Mechanical Engineers, Part B: Journal of Engineering Manufacture*, 222 (12): 1589–1596.

Iwata, K.; Moriwaki, T.; Hoshi, T.; (1981) Basic study of high speed micro deep drilling. *Annals-Manufacturing Technology*, 30(1): 27–30.

Jiang, L.; Roos, Å.; Liu, P. (2007) The Influence of austenite grain size and its distribution on chip deformation and tool life during machining of AISI 304L. *Metallurgical and Materials Transactions A,* 28(11): 2415-2422.

Kajaria, S. (2009) Modeling of tool life and micro-mist flow for effective. Masters Thesis, *Texas A&M University*, College Station, TX, USA.

Klocke, F.; Gerschwiler, K.; Abouridouane, M. (2009) Size effects of micro drilling in steel . *Production Engineering*, 3 (1): 69-72.

Komanduri, R. (1982) Some clarifications on the mechanics of chip formation when machining titanium alloys. *Wear*, 76(1): 15-34.

Korkut, I.; Kasap, M.; Ciftci, I.; Seker, U. (2004) Determination of optimum cutting parameters during machining of AISI 304 austenitic stainless steel. *Materials and Design,* 25(4): 303-305.

Kudla, L. A. (2011) Fracture phenomena of microdrills in static and dynamic conditions. *Engineering Fracture Mechanics*, 78(1): 1-12.

Lee, K.; Stirn, B.; Dornfeld, D. A. (2002) Burr formation in micro-machining aluminum, 6061-T6 . *Initiatives of Precision Engineering at the Beginning of a Millennium*, Springer, USA.

Li, R.; Hegde, P.; Shih, A. J. (2007) High-throughput drilling of titanium alloys. *International Journal of Machine Tools and Manufacture*, 47(1): 63-74.

Lin, C.; Kang, S.; Ehmann, K. (1995) Helical micro-drill point design and grinding. *Journal of engineering for industry*, 45 (7-8): 277-287.

Mitsubishi materials corporation, Cutting Tool Materials, 10/20/2011, retrieved from: http://www.mitsubishicarbide.net/mmus/en/product/technical_information/information/sessaku.html

Muthukrishnan, N.; Davim, P. (2011) Influence of coolant in machinability of titanium Alloy (Ti-6Al-4V). *Journal of Surface Engineered Materials and Advanced Technology*, 1: 9-14.

Paro, J.; Hanninen, H.; Kauppinen, V.; (2001) Tool wear and machinability of X5 CrMnN 18 18 stainless steels. *Journal of Materials Processing Technology,* 119(1-3): 14-20.

Patil, R. Y. (2010) Cutting tool wear-mechanisms. *Journal of Engineering and Technology Management,* 2(1): 38-42.

Performance micro tool- solid carbide micro tools*,* products: performance micro tool, 10/20/2011, retrieved from: http://www.pmtnow.com/, Access date

Platt, D. (2003) *Engineering and High Performance Plastics* . Smithers Rapra Press., Akron, OH, USA.

POTOMAC leader in micro manufacturing solutions, metal: 160um diameter holes in stainless steel tubing, 10/20/2011, retrieved from: http://www.potomac-laser.com/metal-160-micron-diameter-holes-in-stainless-steel-tubing/

Rahim, E.A.; Sharif, S. (2006) Investigation on tool life and surface integrity when drilling Ti-6Al-4V and Ti-5Al-4V-Mo/Fe . *JSME International Journal Series C*, 49 (2): 340–345.

Rahman, M.; Ramakrishna, S.; Thoo, H.C. (1999) Machinability study of carbon/peek. *Machining Science and Technology,* 3(1): 49-59.

Ratner B.D.; Hoffman A.S.; Schoen F.J.; Lemons J.E. (2004) *Biomaterials Science, Second Edition: An Introduction to Materials in Medicine.* Elsevier Academic Press, San Diego, CA, USA.

Shao, H.; Liu, L.; Qu, H.L.; (2007) Machinability study on 3%Co–12%Cr stainless steel in milling. *Wear,* 263(1-6): 736-744.

Shaw, M.C.; Thurman, A.L.; Ahlgren, H.J. (1966) A plasticity problem involving plain strain and plane stress simultaneously: Groove formation in the machining of high-temperature alloys. *Journal of engineering for industry,* 88(2): 142-146.

Shioshaki, D. (2011) Modeling of tool wear and tool fracture in micromilling. Masters Thesis, *Texas A&M University*, College Station, TX, USA.

Shyu, T. L. (2000) Improvement of tool life and exit burr using variable feeds when drilling stainless steel with coated drills. *The International Journal of Advanced Manufacturing Technology,* 16(5): 308-313.

Simon, M.; Lagneau, C.; Moreno, J.; Lissac, M.; Dalard, F.; Grosgogeat, B. (2005) Corrosion resistance and biocompatibility of a new porous surface for titanium implants. *European Journal of Oral Sciences*, 113 (6): 537-545.

Sugawara, A.;Inagaki, K. (1982) Effect of workpiece structure on burr formation in micro-drilling. *Precision Engineering*, 4 (1): 9-14.

Tansel, I. N. (1998) Monitoring micro-drilling operations using neural networks. *Key Engineering Materials* , 138-140: 575-592.

Trent, E. (2000) *Metal Cutting.* Butterworth-Heineman, Boston, MA, USA.

Ueng, H.Y.; Guo, C.T.; Dittrich, K.H. (2006) Development of a hybrid coating process for deposition of diamond-like carbon films on microdrills. *Surface and Coatings Technology*, 200 (9): 2900-2908 .

Unist, Inc., Uni-MAX Coolubricator System, 10/19/2011, retrieved from: http://www.unist.com/machinecutting/MQL/Continuous_External/uniMAXcoolubricator.htm.

Williams, D. F. (1987) Advanced applications for materials implanted within the human body. *Materials Science and Technology*, 3 (10): 797-806.

X. Liu, R. E. (2004). The mechanics of machining at the microscale: assessment of current state of the science. *Journal of Manufacturing Science and Engineering,* 126(4), 666-678.

APPENDIX A

EQUIPMENT DETAILS

A.1 HAAS OM2 specifications:

- Five degrees of freedom
- Maximum spindle of 50,000 rpm
- Maximum feed rate 19.2 m/min

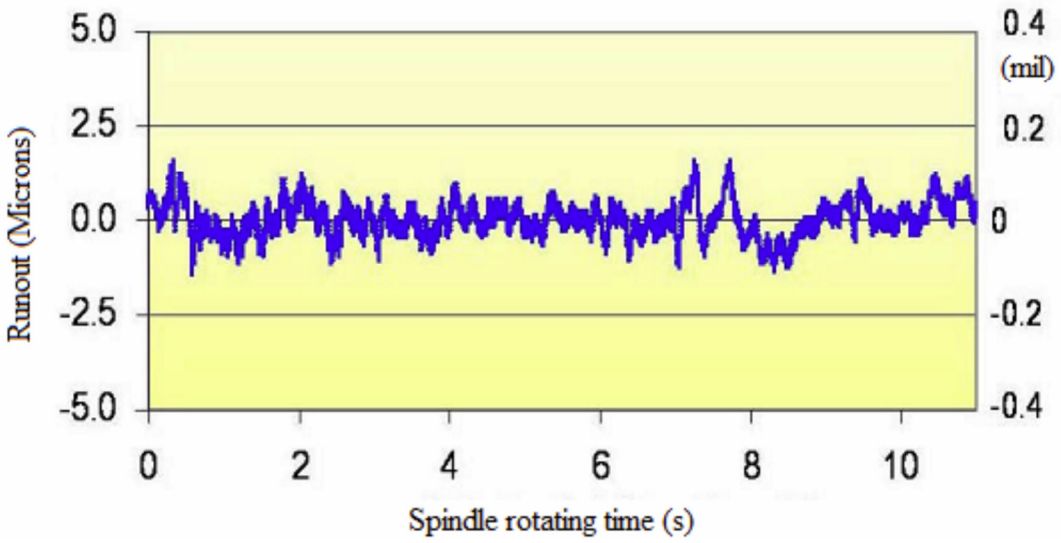

FIGURE A.1 Runout of HAAS OM2 air spindle at 10,000 rpm (after Kajaria, 2009).

FIGURE A.2 HAAS OM2 Office Milling Machine (after High Point Precision Products, 2011).

A.2 UNIST Cool Lubricator System

UNIST cool lubricator system is used to supply micro-mist during drilling. The micro fluidization system consists of a variable rate pulse generator which can produce infinite cycles of metering pump. This pulse generator allows for automatic, infinite repeat cycling of the lubricator pump from a single air source. The continuous output of lubricant can be controlled by 3 separate adjustments using an air metering screw, a pulse generator which can produce 5-200 pulse /minute and a 0.2-1.0 cc stroke liquid metering pump. It can be adjusted to deliver 0.1 to 3.0 drops of lubricant per cycle and the number of cycles can vary between 5 and 200 per minute. The system contains a standard 10-ounce oil reservoir which can hold more than 9000 drops of lubricant. Lubricant output is controlled by a knob on each metering pump. Air metering is done by a control screw which can be adjusted for density and distance of the spray. The spray has an included angle of approximate 11-18 degrees depending on the amount of air introduced. This provides flexibility in adjusting the area covered by the spray.

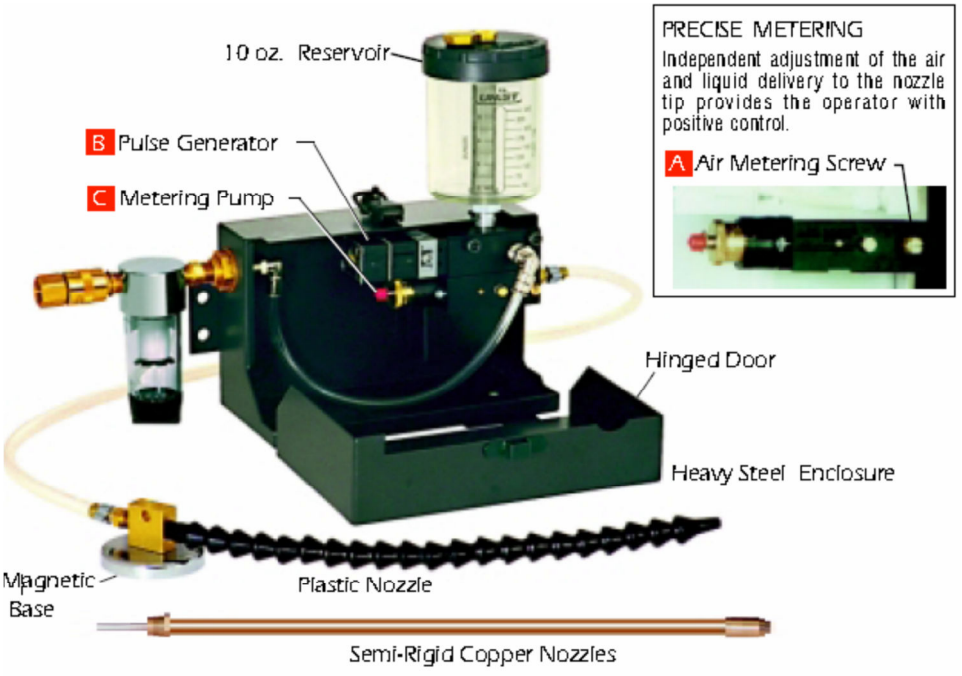

FIGURE A.3 Unist mist system (after Unist, 2011).

The lubricant used for the experiments is Coolube 2210 EP which is supplied by UNIST. The lubricant is compatible with titanium, aluminum, steel, stainless steel and many other materials. The lubricant is non-toxic, non-polluting, non-drying and non-staining. It is designed for long tool life. Some of the important properties of Coolube are:

- Low surface tension and high heat capacity
- Designed to eliminate burrs and rough surface finish
- Doesn't require high pressure pumps
- Viscosity index doesn't change much with temperature

A.3 Laser Displacement Sensor - Keyance LK-G1577

The Keyence laser systems allow the user to measure differentially over various surfaces ranging from glass like to highly dull metals. It is a 2D displacement system that has an emitter and a receptor, which are calibrated to measure with an accuracy of ±0.5% and resolution of 0.5μm. The laser system is used to investigate the stability of the spindle as well as measurement of distance between tool and workpiece. The latter information is used to position the tool with respect to the workpiece. Keyence uses software known as LK navigator to calibrate the laser intensity for different types of surfaces.

A.4 AgieCharmilles Wire EDM

The machine itself has capabilities to cut small pieces like the work material or larger samples if needed. The table size is 350 x 250 x 250 mm and can taper at 25 degrees as well. It uses wires of 0.15 to 0.30 mm so it has a reasonable small amount of cutout path, but more importantly it can cut pieces at under 0.25 microns. The high quality surface finish allows cutting of samples with minimal cutting tool residuals and is very efficient for the experiments that are needed in this research.

FIGURE A.4 AgieCharmilles Wire EDM (after Agie, 2011).

APPENDIX B

CNC CODE FOR MICRODRILLING

B.1 Spindle warm-up program:

```
O02026 (NSK 20 MIN SPINDLE WARM-UP)
M03 S10000
G04 P120.
M03 S20000
G04 P180.
M03 S25000
G04 P180.
M03 S30000
G04 P180.
M03 S35000
G04 P180.
M03 S40000
G04 P180.
M03 S50000
G04 P180.
M05
M30
```

B.2 Microdrilling macro :

```
(created 06/22/11)
(Start depth = B/#2)
(Hole depth = C/#3)
(Feed rate = J/#5)
(Tool diameter = D/#7)
(Retract height = A/#1)
(Number of holes = F/#9)
(#11= hole count)

#11= 0 (Sets hole count to zero)

WHILE [ #11 LT #9 ] DO1
#102= #2
#104= 2 * #7
(Temporary variables that do not alter original values)

WHILE [ #102 GT #3 ] DO2
(Pecking Loop Start)
#6= #102 - #104
(Current Peck Depth)
IF [ #6 LT #3 ] THEN #6= #3
(Sets Peck Depth to Final Depth if it overshoots)
```

```
G90 G01 Z [ #102 + 0.2 ] F50.
(Stands off 0.2 mm)
G01 Z#6 F#5
G01 Z#1 F100.
G04 P1.5 (Pauses one half second to cool and flush chips)

#102= #102 - #104
(Resets Hole Depth for next pass)
#8= -1.0 * #6 / #7
(Defines aspect ratio)
#104= #7 * [ -1.5 * #8 + 19.5 ] / 9
(Sets new peck increment)
END2
(Pecking Loop End)
G91 X [ #7 * 3 ] F200.
(MOVES INCREMENTAL DISTANCE IN X DIRECTION)
(NOT DEPENDENT UPON COORDINATES)
#11= #11 + 1

END1
M99
(RETURNS TO MAIN PROGRAM)
```

B3.Microdrilling main program:

```
(created 06/22/11)

N35 G00 G17 G21 G40 G90
(STANDARD START-UP SETTINGS)

N45 T1
(IDENTIFIES TOOLING)

N50 G54 G00 X1.5 Y-1. Z1.
(MOVES MACHINE TO STARTING COORDINATES)
(COORDINATES SET IN LINE G55 IN OFFSETS)
(MUST SET ZEROES ON UPPER LEFT CORNER OF PART)

N55 G43 H01
(CALLS OUT TOOL LENGTH COMPENSATION)

N60 S50000 M03
(SETS SPINDLE SPEED AND TURNS ON CLOCK-WISE)
```

```
N70 G65 P15 A1. B0. C-1.27 D0.127 J2. F20.
(G65 CALLS FOR MACRO)
(Retract height = A)
(Start depth = B)
(Hole depth = C)
(Tool diameter = D)
(Feed rate = J)
(Number of holes = F)

N75 G90 G54 X0. Y0. Z5.
(RETURNS TOOL TO START POSITION)

N80 M30
(ENDS PROGRAM)
%
```

APPENDIX C

TOOL WEAR DATA

TABLE C1 Tool wear while drilling 316Lstainless steel

No. of holes	Drill distance in mm		Mist_20m/min_0.02um/flute	Mist_20m/min_0.02um/flute	Mist_14m/min_0.02um/flute	Mist_14m/min_0.02um/flute	Mist_20m/min_0.035um/flute	Mist_14m/min_0.035um/flute
New tool								
10	12.70	10.0	5.66	9.00	7.08	9.78	12.86	11.96
20	25.40	20.0	7.98	11.32			16.34	12.86
30	38.10	30.0	7.98	16.21			22.38	15.18
40	50.80	40.0						19.04
50	63.50	50.0			9.52	13.51		
60	76.20	60.0			9.52	14.79		
70	88.90	70.0			9.52	14.79		
80	101.60	80.0			10.55	17.11		

TABLE C2 Tool wear while drilling CP titanium with chip load 0.05 µm/flute with 0.127 mm drill.

No. of holes	Mist_20m/min_0.05um/flute (T14_s50k_F 5mm/min_D0.127)	Mist_12m/min_0.05um/flute (T18_s30k_F 3mm/min_D0.127)
10	Radial Wear(um)	Wear(um)
20		
30	3.473	4.502
40	4.374	4.502
50		
60	9.777	6.175
70		6.689
80	10.934	8.233
85		
90		
100		8.233
110		

TABLE C3 Tool wear while drilling CP titanium with chip load 0.05 μm/flute with 0.1mm drill.

No. of holes	Mist_V 6m/min_0.05um/flute (T1_s20k_F 2mm/min_D0.100)	Mist_6m/min_0.05um/flute (T5_s20k_F 2mm/min_D0.100)
10	Wear(um)	Wear(um)
20		
30	3.345	4.116
40	5.789	5.660
50	8.104	6.689
60	8.876	6.689
70	8.876	
80	11.835	
85		
90		
100		
110		

TABLE C4 Tool wear while drilling CP titanium with chip load 0.1 µm/flute.

Number of holes	Mist_20m/min_0.1um/flute (T11_s50k_F 10mm/min_D0.127)	Mist_12.5m/min_0.1um/flute (T6_s40k_F 8mm/min_D0.100)
10	Wear(um)	
20		
30	2.701	3.731
40	5.274	5.146
50	5.274	6.303
60	5.274	6.303
70	6.818	6.303
80	6.818	6.303
85	7.847	7.590
90	7.847	8.748
100		
110	7.847	
	10.163	
	10.163	

TABLE C5 Tool wear while drilling CP titanium without mist coolant.

Number of holes	Air_V 12m/min_0.1um/flute (T3_s30k_F 6mm/min_D0.127)	Air_6m/min_0.05um/flute (T2_s20k_F 2mm/min_D0.100)	Air_5m/min_0.05um/flute (T4_s15k_F 1.5mm/min_D0.100)
	Wear(um)	Wear(um)	Wear(um)
10			
20	4.374		
30	5.660		7.461
40		8.876	9.262
50			
60			
70		11.320	
80			
85			
90			
100			
110			

APPENDIX D

RAW DATA FOR HOLE QUALITY MEASUREMENT

TABLE D1 Hole diameter while drilling CP titanium.

1st row	154.7804	3rd row	147.0284	6th row	147.6098
1st row	149.7416	3rd row	144.4444	6th row	141.2145
1st row	150.0646	3rd row	145.0904	6th row	146.3178
1st row	146.447	3rd row	147.1576	6th row	143.9922
1st row	147.4806	3rd row	146.5762	6th row	144.186
1st row	148.2558	3rd row	148.5142	6th row	142.4419
1st row	151.3566	3rd row	145.0904	6th row	146.2532
1st row	151.2274	3rd row	145.6718	6th row	143.3463
1st row	148.6434	3rd row	146.8346	6th row	144.3152
1st row	151.8734	3rd row	149.031		

TABLE D2 Hole diameter while drilling 316L stainless steel with AlTiN coated tool.

2nd row	148.0963	5th row	144.9319	7th row	146.1977
2nd row	146.1977	5th row	144.299	7th row	146.1977
2nd row	148.7292	5th row	146.1977	7th row	145.5648
2nd row	146.1977	5th row	144.9319	7th row	146.8306
2nd row	146.8306	5th row	147.4635	7th row	146.8306
2nd row	145.5648	5th row	144.9319	7th row	145.5648
2nd row	145.5648	5th row	148.7292	7th row	145.5648
2nd row	146.8306	5th row	148.0963	7th row	146.1977
2nd row	146.8306	5th row	146.8306	7th row	147.4635
2nd row	146.1977	5th row	149.3621	7th row	146.1977
2nd row	148.0963	5th row	147.4635	7th row	147.4635
2nd row	147.4635	5th row	146.1977	7th row	143.0332
2nd row	150.6279	5th row	147.4635	7th row	146.8306
2nd row	146.1977	5th row	148.7292	7th row	148.0963
2nd row	148.7292	5th row	148.0963	7th row	148.0963
2nd row	146.1977	5th row	147.4635	7th row	144.299
2nd row	148.0963	5th row	145.5648	7th row	145.5648
2nd row	146.8306	5th row	146.8306	7th row	145.5648
2nd row	147.4635	5th row	146.8306	7th row	145.5648
2nd row	146.8306	5th row	148.0963	7th row	145.5648

TABLE D3 Hole diameter while drilling 316L stainless steel with uncoated tool.

1st row	150.7599	2nd row	145.0828	3rd row	140.0364
1st row	142.5596	2nd row	144.452	3rd row	140.0364
1st row	148.8675	2nd row	143.8212	3rd row	141.298
1st row	143.1904	2nd row	143.8212	3rd row	140.6672
1st row	146.9752	2nd row	141.9288	3rd row	141.298
1st row	150.1291	2nd row	142.5596	3rd row	140.6672
1st row	145.0828	2nd row	142.5596	3rd row	138.144
1st row	148.8675	2nd row	139.4056	3rd row	141.9288
1st row	145.7136	2nd row	138.144	3rd row	137.5132
1st row	142.5596	2nd row	138.7748	3rd row	139.4056

VITA

Name: Sankalp Mohanty

Address: C/O Department of Industrial Engineering

Texas A&M University, College Station, TX 77843-3123

Email Address: sankalp.mohanty1@gmail.com

Education: B.Tech., Mechanical Engineering, National Institute of Technology, Tiruchirappalli, India, 2005

M.S., Industrial Engineering, Texas A&M University, 2011